Universidade de Aveiro Departamento de Química
Ano 2011/2012

CÂNDIDA MARÍLIA DAS NEVES DIAS

NANOPARTÍCULAS DE COBRE E DE ZINCO COMO ANTIMICROBIANOS

Dissertação apresentada à Universidade de Aveiro para cumprimento dos requisitos necessários à obtenção do grau de Mestre em Bioquímica, realizada sob a orientação científica do Doutor Nuno Faria, Investigador do Medical Research Council – Human Nutrition Research e do Prof. Doutor Brian Goodfellow, Professor Auxiliar do Departamento de Química da Universidade de Aveiro.

Universidade de Aveiro Departamento de Química
Ano 2011/2012

CÂNDIDA MARÍLIA DAS NEVES DIAS

COPPER- AND ZINC-BASED NANOPARTICLES AS ANTIMICROBIALS

o júri

presidente

Prof. Doutor Pedro Miguel Dimas Neves Domingues
professor auxiliar do Departamento de Química da Universidade de Aveiro

Doutor Nuno Jorge Rodrigues Faria
investigador do Medical Research Council-Human Nutrition Research

Prof. Doutor Tito Trindade
professor associado com agregação do Departamento de Química da Universidade de Aveiro

agradecimentos Agradeço a todas aqueles que me apoiaram durante este projecto, em especial aos meus pais por tornarem possível a minha ida para Cambridge, dando-me, em conjunto com a minha irmã, um apoio especial. Relativamente ao MRC HNR, agradeço profundamente ao Doutor Nuno Faria, com quem aprendi imensamente, por me ter aceitado e orientado neste projecto e pelo incrível apoio dado durante todo o seu desenvolvimento. Agradeço também à Doutora Sylvaine Bruggraber e à minha colega Kellie Hamill pela ajuda dada com os testes de determinação da actividade antimicrobiana. Um muito obrigado a todo o grupo pelo fantástico ambiente de trabalho que encontrei. Por último, agradeço ao Doutor Jonhathan Powell por me ter acolhido no seu grupo. No que toca a Universidade de Aveiro, um especial obrigado ao Prof. Doutor Brian Goodfellow, por todo o apoio dado durante este ano lectivo.

palavras-chave nanopartículas, cobre, zinco, antimicrobianos, bactérias, estabilidade, *E. Coli.*

resumo

Introdução: O aumento da resistência aos antimicrobianos atuais está a criar a necessidade para o desenvolvimento de novos agentes antimicrobianos, aos quais os micro-organismos não desenvolvam resistência facilmente. Nanopartículas parecem ser uma boa aposta nesta luta contra micro-organismos. De facto, tem-se verificado que diversos tipos de nanopartículas com base de metal, como prata, cobre e zinco, possuem atividade antimicrobiana. Apesar de a prata ter vindo a exibir maior atividade antimicrobiana, este elemento não faz parte da homeostase humana e apresenta algum potencial para citotoxicidade, sendo também mais caro que cobre e zinco. Estes, ainda que menos eficazes, são bons candidatos para a produção de baixo custo de nanopartículas com atividade antimicrobiana.

Objectivo: Desenvolver estratégias de síntese de baixo custo para a produção de nanopartículas de cobre e de zinco com actividade antimicrobiana.

Métodos: Síntese pelo aumento do pH de uma solução contendo cobre (II) ou zinco (II) e ligando(s), pela adição de uma base como hidróxido de sódio (NaOH). Modificações a este método foram feitas para a obtenção de diferentes fases minerais. As nanopartículas foram caracterizadas usando ICP-OES, DLS e XRD. A actividade antibacteriana foi determinada usando o método de micro-diluição em broth, usando placas de 96 poços.

Resultados e discussão: Nanopartículas de cobre (oxo-hidróxidos, óxidos, fosfatos) foram sintetizadas usando diversos ligandos e diferentes condições de síntese. Estas nanopartículas eram instáveis quando diluídas em broth. Apesar de um aumento da atividade antimicrobiana ter sido obtida, é necessário um aperfeiçoamento para que estes materiais sejam viáveis como antimicrobianos. Nanopartículas de zinco obtidas usando cisteína como ligando não inibiram o crescimento bacteriano.

Conclusão: Nanopartículas de diferentes composições e carga de superfície foram obtidas. Em alguns casos, houve um aumento da estabilidade e atividade antimicrobiana das nanopartículas de cobre em relação a trabalhos anteriores. As nanopartículas de zinco obtidas não inibiram o crescimento bacteriano.

keywords nanoparticles, copper, zinc, antimicrobials, bacteria, stability, *E. coli*

abstract

Introduction: The growing resistance to current antimicrobials is creating the need for novel antimicrobial agents, to which microorganisms will not easily develop resistance. Nanoparticles seem to be a valuable option in this fight against microorganisms and antimicrobial activity has been reported for several types of metal-based nanoparticles, such as silver, copper and zinc. Although silver has been shown to have higher antimicrobial activity, this element is not part of the homeostasis of humans and presents some potential for cytotoxicity. It is also more expensive than copper and zinc. These although less effective, are good candidates for the cheap production of nanoparticles with antimicrobial activity.

Aim: To develop cheap synthetic strategies for the production of copper and zinc nanoparticles with antimicrobial activity.

Methods: Synthesis by increasing the pH of a solution containing copper (II) or zinc (II) and ligand(s), by adding a base such as sodium hydroxide (NaOH). Modifications to this method were made in order to obtain nanoparticles of a different mineral phase. The nanoparticles were characterised using ICP-OES, DLS, and XRD. The antibacterial activity was tested using the method of microdilution in broth, using 96-well plates.

Results and discussion: Copper-based nanoparticles (oxo-hydroxides, oxides, phosphates) were synthesised using different ligands and different conditions of synthesis. These nanoparticles were unstable when diluted in broth. An increase in the antimicrobial activity was achieved, but further improvements are still required to make these materials viable antimicrobials. Zinc nanoparticles showed poor antibacterial activity.

Conclusion: Nanoparticles of different compositions and surface charge were obtained. There was improvement in the stability and antibacterial activity of copper based nanoparticles in relation to previous work. Zinc nanoparticles did not inhibit bacterial growth.

CONTENTS

FIGURES LIST

TABLES LIST

Abbreviations/acronyms

Ad – adipic acid

Car – carnitine

CFU – Colony Forming Units

Cit – citric acid

Cys - cysteine

C_{18}TAB - Octadecyltrimethylammonium bromide

DLS – Dynamic Light Scattering

FTIR – Fourier Transform Infra-red

Glr – glucuronic acid

GRAS – Generally Recognized as Safe

ICP-OES – Inductively Coupled Plasma - Optical Emission Spectrometry

MIC – Minimum Inhibitory Concentration

NAG – *N*-acetylglucosamine

NAM – *N*-acetylmuramic acid

OD – Optical Density

RI – Refractive Index

RND – Resistance-nodulation-cell Division

ROS – Reactive Oxygen Species

SDS – Sodium Dodecyl Sulphate

STEM – Scanning Transmission Electron Microscopy

Tart – tartaric acid

XRD – X-Ray Diffraction

1. Introduction

In the last century, antimicrobials have been developed and successfully used, however, their continuous usage led to the development of resistance by microorganisms. (e.g. bacterial resistance to antibiotics). Although most of the existing antibiotics can still fight drug-resistance bacteria, their effectiveness is decreasing [1]. Due to this problem, attempts have been made to develop new and effective antimicrobial agents, to which microorganisms will not develop resistance easily. Nanoparticles, due to their unique properties (e.g., large surface area to volume ratio), seem to be a valuable option as antimicrobials. In fact, silver nanoparticles have already been used and showed significant antimicrobial activity [2], but the cost of this metal limits its use. There are other cheaper metals which are known to have antimicrobial activity. For instance, copper has been used as a biocide for centuries, and, although its usage as an antimicrobial has decreased in the last few centuries, it is rising in prominence as an antimicrobial agent. The use of copper surfaces as self-sanitizing material is now encouraged, and many publications deal with the mechanistic aspects of contact-mediated killing by copper [3]. Zinc is another metal which has antimicrobial properties, and, for example, is added to many oral healthcare products [4]. The use of nanoparticles of copper or zinc may enhance the antimicrobial activity of these metals and their use is unlikely to result in development of resistance by bacteria because these elements are essential to their metabolism. In this way, nanotechnology seems to be useful in this battle against microbes. There are many different ways of producing metal nanoparticles, which depend largely on the type of nanoparticles to be produced. The production of nanoparticles can be done using chemical methods, which are typically cheaper than physical methods and can be readily scaled-up.

This project is part of an on-going programme to develop cheap synthetic strategies for the production of copper and zinc nanoparticles with antimicrobial activity on the same range as silver nanoparticles. Therefore, chemical approaches are being employed in this project for the production of nanoparticles. For this purpose, different conditions and ligands were tested, in order to produce a range of stable copper- and zinc-based nanoparticles. Subsequently, the antibacterial activity of the obtained nanoparticles was also tested.

2. Background

2.1. Bacteria

Bacteria are prokaryotes and are surrounded by a rigid cell wall composed of polysaccharides and peptides. Beneath the cell wall is the plasma membrane, which is a bilayer of phospholipids and associated proteins. The cell wall is readily penetrated by several molecules, but the plasma membrane provides the functional separation between the inside of the cell and its external environment. The genetic material is localized in a discrete region, the nucleoid, and is not separated from the surrounding cytoplasm by membranes. Ribosomes and inclusion bodies are scattered in the cytoplasmic matrix. They can also have flagella, which are used for locomotion [5].

The structure of the cell wall is unique in nature and is composed of disaccharide-pentapeptide subunits. The disaccharides *N*-acetylglucosamine (NAG) and *N*-acetylmuramic acid (NAM) are alternating sugars, with a four amino acid chain linked to the carboxyl group of NAM (Fig. 1). Polymers of these subunits crosslink one another via peptide bridges to form peptidoglycan sheets. Layers of these sheets are, in turn, crosslinked with one another to give a multi-layered, crosslinked structure of considerable strength [6].

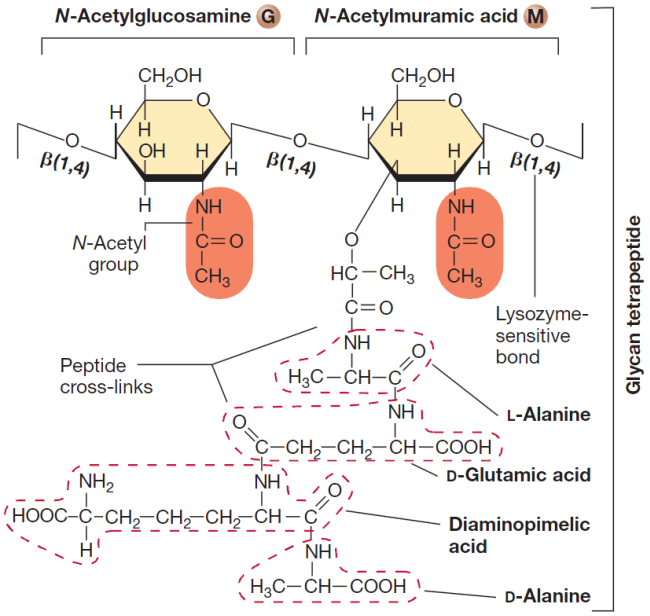

Fig. 1 – Structure of a subunit of peptidoglycan, containing N-acetylglucosamine (NAG), N-acetylmuramic acid (NAM), and four amino acids. The structure is the one found in most gram-negative bacteria. In some bacteria, other amino acids are present [7].

Bacteria can be divided in two major groups: gram-positive and gram-negative. This division results from the different responses of bacteria to the Gram-stain procedure. Gram-positive bacteria stain purple, whereas gram-negative bacteria are coloured pink or red by the technique. This different staining results from structural differences in the cell wall of both types of bacteria. The gram-positive cell wall consists of a single homogeneous peptidoglycan or murein layer. In contrast, the gram-negative cell wall is quite complex. It has a peptidoglycan layer surrounded by a thick outer membrane (Fig. 2) [8]. This outer membrane functions as the cell's initial barrier to the environment.

The components of the cell surface are comprised of macromolecules containing carboxylate, phosphate, and amino groups which are ionized as a function of the environmental pH, thereby conferring electrostatic charge to the cell surface. Bacterial cells possess a net negative electrostatic surface charge when cultivated at physiological pH values [9].

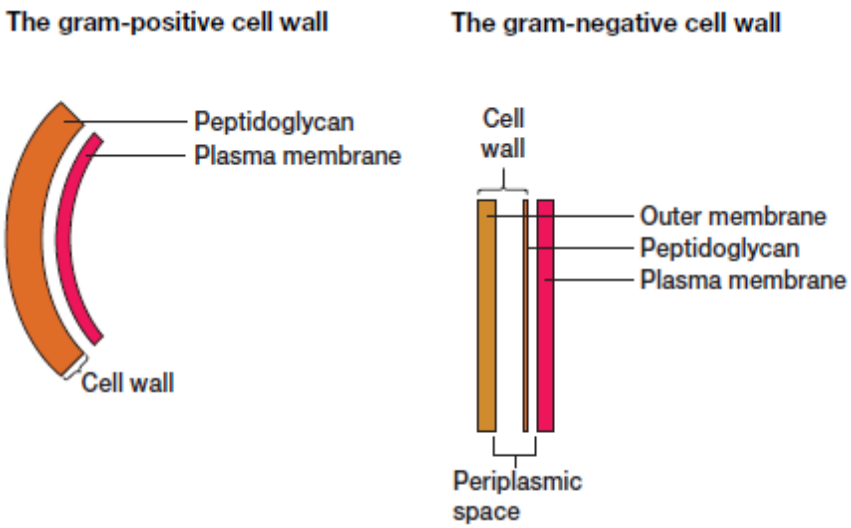

Fig. 2 – Structure of the cell wall from both gram-positive and gram-negative bacteria [8].

Bacteria need specific conditions to grow; they need nutrients to take energy from and to act as the cellular building components. They also need carbon, hydrogen, oxygen, nitrogen, sulphur, phosphorus, and other inorganic micronutrients. Growth can be defined as an increase in cellular components. This may result in the increase of the microorganism's size and/or number of cells. It is difficult to study the growth and reproduction of individual microorganisms, especially due to their small size and, thus, for studying the growth, normally the changes in the total population are followed [8]. The life of a bacterial cell can be seen as "feast or famine". This model comes up because, besides the ability of bacteria to consume virtually all readily metabolizable nutrients in the environment, they can also

persist for long periods of time under starvation conditions once the nutrients have been depleted [10].

For microbiological studies, there is a need to grow and maintain microorganisms in the laboratory, and this is only possible if suitable media are available. A culture medium is a solid or liquid preparation used to grow, transport and store microorganisms [8]. There is a classification for media types: defined media and complex media. In defined media, the exact composition is known in both a qualitative and a quantitative sense. However, the culture of many microorganisms does not require the knowledge of the exact composition of the medium. In these cases, complex media can be used. Complex media are made up of digests of microbial, animal or plant products. These digests are commercially available in dehydrated form and can be easily prepared [7]. Most heterotrophic bacteria would be routinely grown on such a medium. If a complex medium is in liquid form, it is called broth. When growing bacteria on a solid medium, a solidifying agent, such as agar, is added to the medium [11].

The growth of the population can be studied by analysing the growth curve of a microbial culture. When microorganisms are cultivated in liquid medium, they usually are grown in a batch culture or closed system. This means that no fresh medium is provided during incubation, leading to a decline in the concentration of nutrients and to an increase in the concentration of waste residues. Therefore the organisms cannot grow exponentially indefinitely [8]. The resulting growth curve of a microbial culture has four distinct phases: lag phase, exponential (log) phase, stationary phase, and death phase (Fig. 3). When microorganisms are inoculated into a fresh medium, usually the growth only starts after a period of time, the lag phase. The length of this period may vary, depending on the condition of the microorganisms and the conditions of growth. For example, this phase will be longer if the inoculum is from an old culture rather than young one. In the exponential phase, the microorganisms grow and divide at the maximum rate. The rate of exponential growth is constant and may vary greatly. It is influenced not only by the environment conditions and the nature of the culture medium but also by the genetic characteristics of the organism itself. The stationary phase results from the ceasing of the bacterial growth. This phase is usually reached by bacteria at a population level of around 10^6 cells per ml, but the final population size depends on several factors, such as nutrient availability and the type of microorganism. Generally, a microorganism culture enters the stationary phase due to the depletion of nutrients and/or the accumulation of waste residues that inhibit growth. The growth rate in this case is zero. The building up of toxic wastes and depletion of nutrients leads eventually to the death phase, where cells have lost their viability. The death of the population is constant like in the exponential phase, but typically the rate of death is much slower. In some cases cell death is accompanied by cell lysis. When cells fail to lyse, the

death rate may appear less pronounced when using turbidimetric assays [7, 8]. A fifth phase can be considered, the long-term stationary phase. After death, *E. coli* for example can be maintained in batch culture for longer periods of time without adding more nutrients. These can be done by adding distilled water to maintain the volume and osmolarity. Cultures can be maintained at densities of ~10^6 colony forming units (CFU) per ml for more than 5 years in these conditions. In this case, the growth and death are balanced and the growth rate is stationary [12].

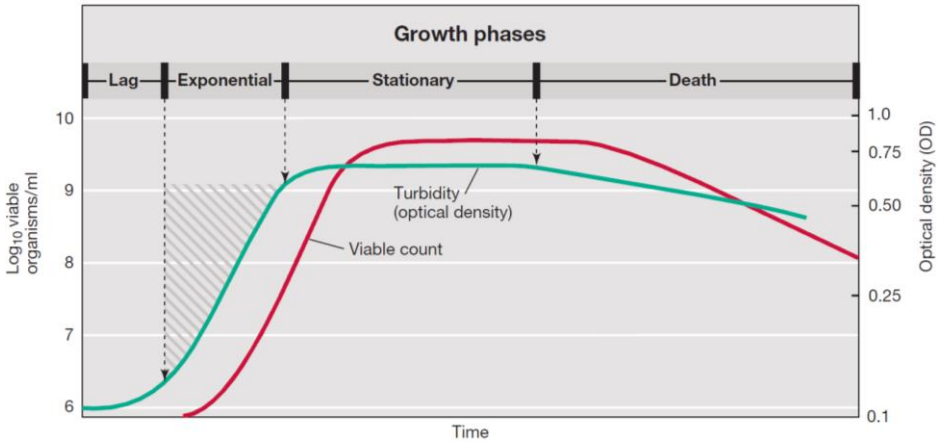

Fig. 3 – Typical growth curve for a bacterial population. A viable count measures the cells in the culture that are capable of reproducing. Optical density (turbidity), a quantitative measure of light scattering by a liquid culture, increases with the increase in cell number [7].

2.2. ANTIMICROBIALS

Antimicrobials are natural or synthetic chemicals that kill or inhibit the growth of microorganisms. Antibacterial agents can be classified as bactericidal, bacteriolytical, and bacteriostatic. Bactericidal agents kill the cell but do not destroy it. Thus, the total number of cells remains constant (Fig. 4A). Bactericidal agents can also be bacteriolytical, i.e. they can kill by cell lysis, leading to the release of the cytoplasmic contents. This means that not only the viable cell number decreases but also the total cell number (Fig. 4B). Bacteriostatic agents do not kill the organism and the number of viable cells remains constant (Fig. 4C) [7].

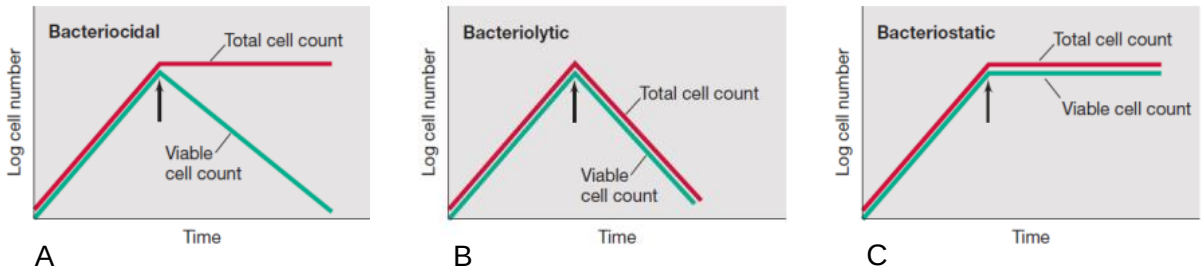

Fig. 4 – Curves of bacterial growth in the presence of bactericidal (A), bacteriolytical (B), and bacteriostatic (C) agents. The arrow represent the time at which the agent was added, during the exponential growth [7].

There are several possible strategies for antimicrobial therapeutics, but the most common against bacteria is the use of antibiotics. Different types of antibiotics have different targets, thus having different mechanisms of action. Although most antibiotics are effective at treating their target infections, some bacterial resistance has developed over the last decades. This poses as a serious problem in public health, as it results in treatment failure and it may also lead to infection control problems, either within healthcare institutions or the community [13]. Thus, there is a need to find other antibacterial therapeutics based on different mechanisms of action, to which bacterial resistance is less likely to be developed. Nanoparticles have shown antimicrobial activity, which has been reported over the past few years, and that makes them one possible option [13]. Nevertheless, before developing nanoparticulate strategies, it is important to understand the mechanism of action and of resistance to antibiotics.

There are four major modes of antibacterial action of antibiotics: (1) interference with cell wall synthesis; (2) inhibition of protein synthesis; (3) interference with nucleic acid synthesis; and (4) inhibition of a metabolic pathway [14].

Bacteria may develop resistance to antibacterial drugs through various mechanisms. Some species of bacteria are innately resistant to one or more classes of antimicrobial agents. A far more alarming problem, acquired resistance, is where initially susceptible populations of bacteria become resistant to an antibacterial agent and proliferate under the selective pressure of the use of that agent [13]. The mechanisms through which bacteria develop resistance to antimicrobials have their origins at the genetic level. The resistance can be a result of chromosomal mutation or inductive expression of a latent chromosomal gene or by exchange of genetic material through transformation (exchange of DNA), transduction (bacteriophage), or conjugation by plasmids (extrachromosomal DNA) [15]. Thus, normally susceptible populations of bacteria may become resistant to antimicrobial agents through mutation and selection, or by acquiring the genetic information that encodes the resistance (horizontal evolution) from other bacteria. Spontaneous mutation (Fig. 5) may cause resistance by: (1) changing the target protein to which the antibacterial agent binds or by modifying or eliminating the binding site; (2) by upregulating the production of enzymes that inactivate the antimicrobial agent; (3) downregulating or altering an outer membrane protein channel that the drug requires for cell entry; or (4) upregulating pumps that expel the drug from the cell [13]. Mutation and selection enable many bacterial species to adapt quickly to the introduction of antibacterial agents into their environment.

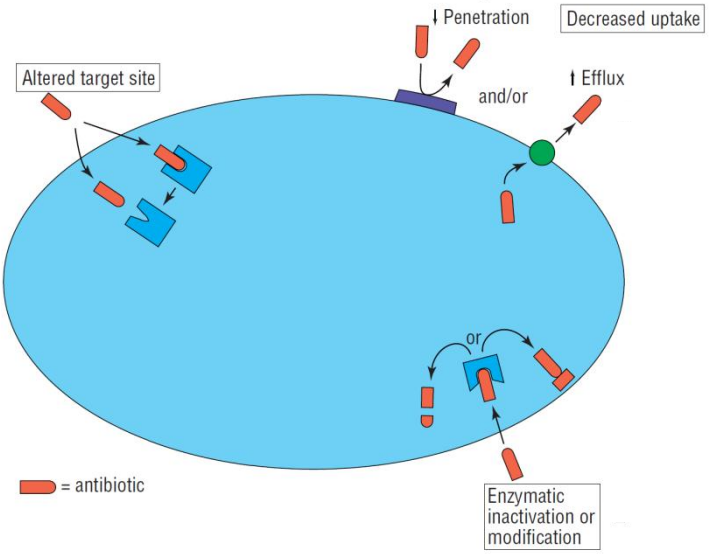

Fig. 5 - Main mechanisms by which spontaneous mutation results in antimicrobial resistance: altered target site, enzymatic inactivation or modification, decreased penetration, and increased efflux [16].

2.2.1. Nanoparticles as antimicrobials

Materials at the nanoscale are now seen as good antimicrobial agents due to their high surface area to volume ratio, thus having unique chemical and physical properties [17, 18]. Metallic nanoparticles are more promising with regards to antimicrobial activity due to their large surface area to volume ratio. Some nanoparticles of different metals display antibacterial activity and are used for various healthcare, hygiene and personal care purposes (e.g. silver, copper and zinc) [19, 20].

The interactions between metal nanoparticle and bacterium appear to be based on contact-mediated membrane lipid peroxidation by reactive oxygen species (ROS) production and, in the case of nanoparticles, are enhanced by a greater contact with the membrane due to their large surface area. The contact is facilitated by electrostatic forces between nanoparticles and bacteria [19]. Nanoparticles also cause the accumulation of envelope protein precursors, which seems to destabilize the outer cell wall and results in the collapse of the plasma membrane. This is probably due to the dissipation of the proton motive force, resulting in the depletion of intracellular ATP, which is needed for the translocation of newly synthesized bacterial envelope membrane proteins by preprotein translocase [21]. Nanoparticles can also be taken up by the bacterium. Once they are internalized they tend to react with sulphur-containing proteins as well as with phosphorus-containing compounds

such as DNA [17]. The antibacterial action of the nanoparticles can also be due to the release of ions by the nanoparticle. These ions can then pass the bacterial cell wall and reach the cytoplasm, where they will induce the production of ROS and interact with cellular components, such as proteins and DNA [18]. The bactericidal properties of nanoparticles are size dependent as shown by a study on the determination of the effect of silver nanoparticles with sizes between 1-100 nm on gram-negative bacteria. In this case, only the particles with a diameter between ~1-10 nm presented a direct interaction with bacteria. Also, it has been shown that silver nanoparticles of smaller size show a stronger antibacterial activity possibly due to their higher surface area to volume ratio [17]. Since nanoparticles interact mostly with the cell membrane, causing its disruption, bacteria are unlikely to develop mechanisms of resistance for the nanoparticles.

Silver nanoparticles, in particular, have shown to be efficacious against bacteria, viruses and other microorganism. It has been shown that silver nanoparticles can have a bacterial MIC as low as 6 ppm [22]. Thus, silver nanoparticles have been applied in a wide range of applications from disinfecting medical devices and home appliances to water treatment. Additionally, silver nanoparticles have been used in the preparation of silver nanocomposite fibers, in which the nanoparticles are incorporated inside the fabric [2]. There are some disadvantages associated to the use of silver nanoparticles as antimicrobials: (1) they are unstable under light and heat conditions; (2) they can interact with Cl^- ions in aqueous medium, which makes the Ag^+ ions lose antibacterial activity; (3) silver is a noble metal and is very expensive [23]. Also, silver nanoparticles have been shown to be cytotoxic and genotoxic for several human cell lines, and it has been demonstrated that silver nanoparticles induce apoptosis in fibroblast cells via the mitochondrial pathway. This may be due to the disruption of the mitochondrial respiratory chain by the nanoparticles, leading to production of reactive oxygen species and interruption of ATP synthesis, which in turn cause DNA damage [24]. In humans, the long-term exposure to silver compounds can cause irreversible skin discoloration or Argyria. The exposure limit to soluble silver recommended by the Health and Safety Executive is 0.01 $mg.m^{-3}$ [25].

Similarly to silver, copper and zinc nanoparticles also show antimicrobial activity. These elements are part of the homeostasis of eukaryotic organisms and therefore, in principle, these are likely to be safer than silver nanoparticles. The exposure limit to fumes of copper and zinc by the Health and Safety Executive is 1 $mg.m^{-3}$ for both [25]. However, copper and zinc nanoparticles appear to have lower antimicrobial activity than silver nanoparticles, but their lower toxicity and their lower cost may offset this disadvantage.

2.3. COPPER

Copper is a transition metal with partially filled *d* orbitals and is the strongest Lewis acid in Group IB of the periodic table, which gives copper the ability to mediate electron transport, accepting and donating electrons. Copper exists primarily in one of two oxidation states: the oxidized Cu(II) cupric form and the reduced Cu(I) cuprous form. Cu(I) and Cu(II) are the most effective monovalent and divalent ions, respectively, for binding to organic molecules and possess almost equal tendencies to form complexes with many organic ligands [26]. Cu(I) is a closed shell $3d^{10}$ transition metal ion and hence diamagnetic. As a soft Lewis acid, it tends to bind to soft bases such has thiols, hydrides, alkyl groups, cyanide, and phosphines. Cu(II) has a $3d^{9}$ configuration and is paramagnetic. As an intermediate Lewis acid it forms complexes with additional ligands to Cu(I), including sulphate and nitrate [27]. Copper is usually bound to proteins via cysteine, methionine, or histidine amino acid side chains [28].

2.3.1. Copper uses

Human civilization has been using copper for some millennia. Copper was always used in a medical way at different levels: for the treatment of headaches, burns, intestinal worms, and ear infections and for hygiene in general. Copper can be used as an alternative to antibiotics, using copper surfaces in hygiene-sensitive areas. For instance, the idea of using copper vessels to render drinkable water has been revived as a low-cost alternative for developing countries [3]. It seems to be a good alternative to antibiotics, because, in contrast to the highly resistant microbes that have evolved to antibiotics in less than 50 years of use, tolerant microbes to copper are extremely rare, a surprising fact, given copper's ubiquitous presence. This may be due to the essentiality of copper to most microorganisms. Viruses do not have tolerance and repair mechanisms as bacteria and fungi and thus are highly susceptible to copper induced damage [29].

However, copper is not appropriate for use for systemic applications (e.g. oral, intravenous), mainly since once copper is ingested it readily interacts with transport proteins as well as small molecular weight ligands, making it unavailable as an antimicrobial for these applications. Furthermore, in cases where no copper excretion pathways are available, the unligated free copper in the body may be involved in diseases pathogenesis, such as in Alzheimer's disease [29].

2.3.2. Homeostasis in bacteria

Although essential to the correct function of eukaryotic and prokaryotic cells, high concentrations of copper are toxic. Copper is therefore an essential and a toxic element at the same time, and the viability of cells depends on a perfect regulation of transport, storage and distribution of this metal. Usefully, for antibacterial applications, the tolerance of eukaryotic cells is generally greater than that of prokaryotic. This may be due to the existence of metallothioneins (cytoplasmic metal-binding proteins), that can protect cells against the toxic effects of copper by chelating this heavy metal. Genes encoding metallothioneins occur in animals, higher plants, and eukaryotic micro-organisms but only in some prokaryotes [30], such as Synechococcus (Cyanobacteria), Enterobacteriacea, and Gammaproteobacteria (Proteobacteria) and Mycobacterium (Actinobacteria) [31].

Copper ions are essential for bacteria but can cause a number of toxic cellular effects if levels of free ions are not controlled. Thus, bacteria must achieve precise copper homeostasis to avoid copper-mediated toxicity whilst maintaining a supply of copper for copper-requiring proteins. Bacteria developed a range of mechanisms to protect themselves from the toxic effects of copper ions in low concentrations: extracellular sequestration of copper ions, relative impermeability of the outer and inner bacterial membranes to copper ions, metallothionein-like copper-scavenging proteins in the cytoplasm and periplasm, and active extrusion of copper from the cell [3]. The way in which bacteria meet the conflicting demands imposed by copper varies depending upon environmental conditions, their adopted ecological niche, and phylogeny.

Thus, copper homeostatic systems have been studied in great detail. *Escherichia coli*, which is a gram negative bacterium and a facultative aerobe, is particularly well studied. It lives in the digestive tract of warm-blooded animals. The concentration of copper can be high in the digestive tract, particularly in the stomach and duodenum, but even there it should not exceed 10 µM. However, it has been shown that under acidic anaerobic conditions, which prevail on that part of the digestive tract, copper becomes much more toxic. Thus, intestinal bacteria have elaborated mechanisms for copper homeostasis as an adaption to their specific ecological niche, the animal gut [32]. Copper enters the bacterial cell through an unknown importer (Fig. 6). The responses of *E. coli* to elevated copper levels primarily involve the chromosomally-encoded cue and cus systems. The cus system only confers copper-tolerance under extreme copper stress while the cue system is the primary copper homeostasis [32]. As extracellular copper levels increase, CueR mediates production of a copper-exporting P_{1B}-type ATPase CopA at the cytoplasmic membrane and a periplasmic multicopper oxidase CueO – these three proteins constitute the cue system [27].

Although these proteins apparently clear the cytosol of excess of copper, this is retained within the periplasm and thus may serve as a compartmentalized store [32]. If copper levels keep increasing, expression of the cusCFBA operon is induced by the CusR/S two-component sensory system, which detects excess of copper in the periplasm, mediating export of copper across the outer membrane [27]. The cus system is particularly important in providing copper-tolerance under anaerobic conditions [32]. Some *E. coli* strains also harbor the plasmid-borne pco system which involves seven genes, providing further copper-resistance. The mechanism of copper detoxification provided by this system involves the multi-copper oxidase PcoA and its putative partner PcoC, both of which are exported to the periplasm [32].

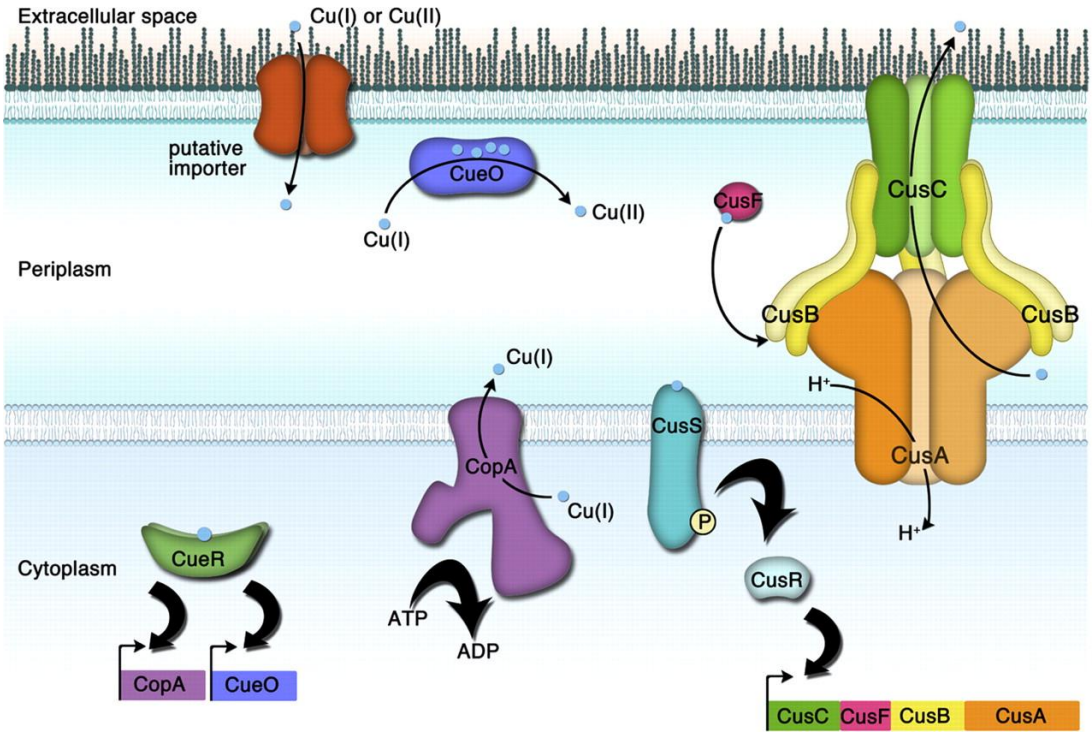

Fig. 6 - Copper homeostasis mechanisms in *E. coli*. The most relevant homeostatic systems are shown. CopA is a Cu(I)-translocating P-type ATPase, CueO a multi-copper oxidase, and CusCFBA a four-component copper efflux pump (regulated by the system CusRS) [33].

2.4. ZINC

Zinc is the first element in group 12 of the periodic table. It has a complete *d* subshell and the divalent cation is the only naturally occurring oxidation state and has no redox activity under physiological conditions. Its relative stability, ability to co-ordinate 4 or sometimes 6 ligands, and its acid Lewis properties may be fundamental to the biological role of zinc [34]. In fact, zinc is the second most abundant trace element in the body, thus being

one of the most important trace elements related to health and disease. This element is present in all cells and is a requirement for the normal functions of cells, tissues and organs of the body. It catalyses enzyme activity, contributes to protein structure, and regulates gene expression [35].

Zinc (II) is a strong intracellular Lewis acid and is predominantly coordinated to proteins via either sulphur “thiol” moieties of cysteine residues or the amino “imidazole” ligands of histidine residues [36]. Because of its ability to interact with thiols and block essential reactions in the cell, high concentrations of zinc are toxic. Among its many applications, zinc materials can also be used as antimicrobials. Some enzyme systems can be inhibited by zinc, such as glycolytic enzymes in streptococci. Also, Zn^{2+} is a well-known sulfhydryl reactive agent and many of its antimicrobial actions may be caused by reaction with sulfhydryl groups. Due to these antimicrobial properties, zinc is added to many oral healthcare products. Usually, zinc is considered more of a bacteriostatic agent rather than a bactericidal one. However, it can be used along with other bactericidal agents to increase their power [4].

2.4.1. Homeostasis in bacteria

Prokaryotic organisms do not possess organelles, i.e. sub-cellular compartments, thus the major mechanisms that maintain cellular Zn(II) concentrations are limited to the highly regulated processes of Zn(II) import, metal sequestration by metallo-chaperones and Zn(II) export across the cytoplasmic membrane (Fig. 7) [36].

One of the primary mechanisms of Zn(II) import is the ZnuABC, which is a high affinity Zn(II) uptake system. This type of transporters usually has two transmembrane proteins that form a pore in the membrane allowing the transport of specific substrate from one side of the membrane to the other. On the cytosolic membrane face of this pore are one or two ATP-binding regions that act to provide the energy for substrate transport from ATP hydrolysis. The Znu proteins of *E. coli* belong to a family of uniquely bacterial divalent metal ion ABC transport systems that are dependent upon an extra-cytoplasmic metal-binding protein [37]. The ZnuABC system is regulated by Zur, which is a member of the Fur family of bacterial metal-responsive regulators and can sense sub-femtomolar concentration of cytosolic Zn(II) [38]. In its native state, Zur forms a dimer, which in the presence of excess Zn(II) binds to a regulatory sequence that is located within the central znu operator region and prevents the binding and activity of RNA polymerase. This Zur dimer is only active in the reduced form [39]. The first binds Zn(II) very tightly and is functionally analogous to the Zn(II)-binding site in Fur, whereas Zn(II) is more readily exchanged in the second site in the

Zn(II) metallo-regulatory proteins SmtB from Synechococcus. Zur proteins seem to be widespread among gram-negative, gram-positive and cyanobacteria [36]. There is a group of porins in *E. coli*, which form a cylindrical, fluid-filled channels in the outer membrane of cells that allow selective hydrophilic solutes of up to 600 Da, including divalent metal cations such as Zn(II), to diffuse across into the periplasmic space. Zn(II) may then be imported into the cytosol of cells such as *E. coli* as neutral metal phosphate via the constitutively expressed inorganic phosphate uptake system (Pit) [40].

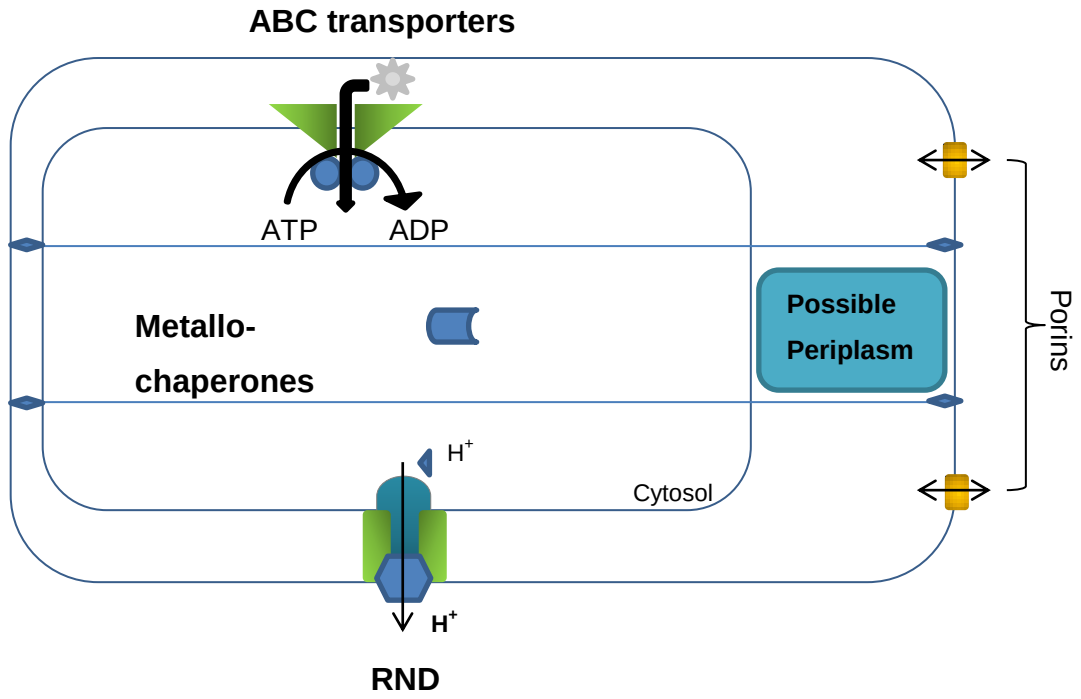

Fig. 7 – Protein families involved in prokaryotic Zn(II) trafficking: ABC transporters, metallo-chaperones, porins and RND [41].

Chaperones act to escort or usher interactive entities through the potentially hostile environments in which they find themselves. The primary function of the chaperones is to protect, preventing unfavourable interactions between the entity and the environment [36]. A family of soluble metal-binding proteins, known as metallo-chaperones are thought to facilitate the intracellular tracking of metal ions [42].

The export of the zinc can be made by different high and low-affinity exporters. One example of such exporters is the resistance-nodulation-cell division (RND) protein family, which exports excessive cations. The RND protein family was first described as a related group of bacterial transport proteins involved in heavy metal resistance (*R. metallidurans*), nodulation (*Mesorhizobium loti*) and cell division (*E. coli*). The first member of this family to be identified was the CzcA protein from *R. metallidurans* [36]. This β-proteobacterium

contains two large plasmids involved in the heavy metal resistance. One of them, increased the MICs of Zn^{2+} by 50 fold [43].

Zinc-uptake can occur at the different levels of transporter synthesis and activity. One example is the zinc-binding protein-dependent transport systems, which were firstly identified in cyanobacteria and in pathogenic streptococci [44]. These bacterial metal transporters belong to the cluster 9 family of ABC transporters, which mainly transport zinc and manganese and which have been found in nearly all bacterial species. This high-affinity zinc-uptake system consists of the periplasmic binding protein ZnuA, the membrane permease ZnuB, and the ATPase ZnuC [45]. Most of the system of membrane transport mechanisms are controlled at the level of transcription and are mediated by metal-responsive regulators, which modulate expression of genes in response to respective substrate concentrations. Hence, the cellular level of loosely bound, labile Zn(II) is sustained at close to required levels in conditions of either metal ion limitation or excess [36].

2.5. NANOPARTICLES

2.5.1. Properties

Nanoparticles are generally defined as clusters of atoms in the size range of 1-100 nm and they show distinct properties of their bulk equivalents. They usually contain 20-15 000 atoms and can be produced from different materials in different shapes such as spheres, rods, wires and tubes (Fig. 8) [46].

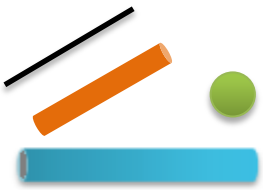

Fig. 8 – Possible shapes of nanoparticles: spheres, rods, wires and tubes.

Some properties of nanoparticles remain unchanged from their bulk material equivalents. However, many other properties change as particle size decreases. A nanoparticle may have similar properties of their bulk equivalent and as well of their molecular precursors, due to its small size, therefore high surface area, and size-dependent properties (classical vs. quantum mechanics) [47].

The chemical composition of the particles will affect their physicochemical properties and the core and the surface may be different. To determine nanoparticle composition, there are many techniques which can be used. Raman Spectroscopy, Inductively Coupled Plasma

- Optical Emission Spectrometry (ICP-OES), X-Ray Diffraction (XRD; for crystalline samples), and Fourier-Transform Infrared Spectroscopy (FTIR) are examples of such techniques [47].

Size is the key parameter for nanoparticles but it is not constant and is affected by the surrounding environment. For example, the size in the dry state may be very different from the one in a solvent, and different solvents impact size differently [48]. Although nanoparticles do not generally have a spherical shape, their size is usually defined as the diameter of a sphere [49].

The particle size distribution (PSD), i.e. the range of sizes of particles within a sample, gives an indication of the aggregation/agglomeration state of the nanoparticles [47]. There are several techniques which can be used to evaluate the PSD: Electron Microscopy (TEM and SEM), and Dynamic Light Scattering (DLS) are examples of such techniques. Electron Microscopy is more adequate for samples in the dry state because it is not influenced by solvent effects. DLS is a more adequate technique for solution studies, since it takes into account the environment [47]. Further details will be given in how to use DLS (Section 2.6.1).

Nanoparticles present some limitations often related to their small size. Of particular importance is their instability over longer storage periods as they tend to agglomerate. This agglomeration reduces the high surface area to volume ratio, which may lead to the loss of their properties [50]. This formation of agglomerates is partly driven by van der Waals interactions. Agglomerations can also be formed due to increasing the particle concentration or changing the pH or ionic strength of the solvent [47]. This tendency for agglomeration can be explained by the difference in the thermodynamics of bulk materials and nanoparticles [51]. The free energy of the system (ΔG) is dependent on the material surface energy (ΔG_s) and the free energy per unit volume (ΔG_v):

$$\Delta G = 4\pi r^2 \Delta G_s - \frac{4}{3}\pi r^3 \Delta G_v$$

In nanoparticles, ΔG_s is high and ΔG_v is low, which makes the system free energy greater for a nanoparticle than for the bulk material of identical chemical composition. Thus, in order to reduce the system free energy, nanoparticles tend to agglomerate. Also, this higher system free energy affects many properties of the material, such as melting points and the crystallographic structure of nanoparticles [47]. This difference in thermodynamic properties is mainly due to the nanoparticle's high radius of curvature and high surface area and surface free energy [49].

2.5.2. Synthesis

The synthesis of metallic nanoparticles can be divided into two alternative methods: the “bottom-up” approach and the “top-down” approach (Fig. 9). “Bottom-up”, can refer to self-assembly, i.e. the construction of a structure atom-by-atom, molecule-by-molecule, or cluster-by-cluster, in which the nanostructured building blocks are firstly formed and then assembled into the final material using chemical or biological procedure(s) for synthesis [52]. The formation of nanoparticles from atoms goes through two processes: (1) formation of primary particles and (2) agglomeration between the newly formed primary particles, which allow the formation of nanostructures [53]. This approach has an advantage of enhancing the possibility of obtaining metallic nanoparticles with comparatively lesser defects and more homogeneous chemical composition(s). In the “top-down” approach, the starting material is reduced in size using physical or chemical means. However, this approach has the disadvantage of producing structures with some imperfections in their surface, which can have a significant impact on physical properties and surface chemistry [52].

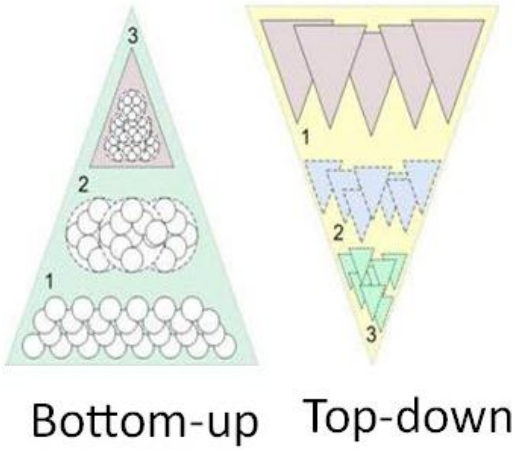

Fig. 9 – Diagram of how bottom-up and top-down approaches are processed [54].

The preparation of metal nanoparticles can also be categorized as a physical or a chemical approach. Physical strategies utilize methods such as inert gas condensation or laser ablation. With the inert gas condensation (IGC) method, a resistive source is used to evaporate the material at a low pressure of a non-reactive gas. Collisions among the material molecules lead to homogeneous nucleation and growth of nanoparticles, which can be collected onto a cold surface. Laser ablation is another physical method that involves the generation of nanoparticles by laser ablating a solid target that lies in a gaseous or a liquid environment and the nanoparticles are collected in the form of nanopowder or a colloidal solution [55]. One disadvantage of most of the physical processes is that the production rate of nanoparticles is quite low and also that these processes are highly expensive [56]. They

also lead to an enormous consumption of energy to maintain the high pressure and temperature used in the synthesis processes [52]. Chemical strategies rely on the metal ions in solution in conditions that allow the formation of small metal cluster or aggregates. The nanoparticles can be stabilized by using surfactants or ligands.

The production of copper and zinc nanoparticles can use either chemical or physical methods. However, most synthesis strategies for copper nanoparticles production rely on chemical methods. The application of the nanoparticles has to be taken into account when choosing the method of synthesis. For instance, when producing nanoparticles for biomedical applications (e.g., antimicrobial), the end product has to be as less toxic as possible for human cells.

2.5.3. Mechanisms of antimicrobial action

One of the antimicrobial mechanisms of action of nanoparticles is the perforation of the cell wall. In fact, copper oxide (CuO; Cu(II)) nanoparticles (1-10 nm) have shown antibacterial activity against *E. coli* and *S. aureus* and the interactions between nanoparticles and bacteria resulted in perforation of the cell wall. They also can show some selectivity, since that, in this case, the effect was more pronounced against the gram-negative organisms (*E. coli*). Also, the effect did not depend on the acquisition of resistance against antibiotics (studies were carried out on both antibiotic resistant and non-resistant strains of gram-negative bacteria). The higher effect on gram-negative bacteria may be due to the higher interaction between cell wall and nanoparticles by electrostatic forces [57].

Zerovalent copper nanoparticles (Cu^0) of 12 nm have been synthesized, using inert gas condensation, and their antibacterial activity was tested. The test was carried out against *E. coli* and it was observed that there was a reduction in CFUs (colony forming units) with increasing copper nanoparticle concentration in the growth medium. Also, as the surface of the bacteria was visualized by scanning electron microscopy, it was observed that after the interaction between bacteria and copper nanoparticles, the surface of the bacteria had some cavities and pits. These results were attributed to the opposite charges of bacterial cell wall (negative) and copper ions released from nanoparticles (positive) leading to adhesion between them. More copper ions might have been allowed to enter the bacteria due to the fact that *E. coli* are gram-negative bacteria [58].

Copper nanoparticle antibacterial activity may also be due to penetration inside bacteria, where they are likely to produce damage by interacting with phosphorus and sulphur containing compounds, such as deoxyribonucleic acid (DNA), because they have high affinity with such compounds [58]. The antibacterial mechanism of copper nanoparticles has been attributed to the fact that Cu^{2+} ions leached from nanoparticles are absorbed by

bacteria when the nanoparticle concentration is high enough. Copper ions are absorbed onto the bacterial cell surface, damaging the cell membrane by solidifying protein structure or altering enzyme function [59]. Cu^{2+} ions entering cells combine strongly with intracellular amino acids and proteases, resulting in degeneration that leads ultimately to the denaturation of proteins [23]. Under physiological conditions, the intracellular enzyme activity of bacteria treated with copper nanoparticles is believed to increase, suggesting that permeability of the cell membrane also increased, resulting in bacterial injury. From these results, it is believed that the binding of copper ions to the bacterial cell surface plays an important role in the bactericidal activity [60].

The study of the effect of ZnO nanofluids against *E. coli* showed they have bacteriostatic activity against these bacteria. The antibacterial activity increased with increasing particle concentration and decreasing particle size. Scanning electron microscopy (SEM) analysis of the bacteria before and after treatment with ZnO nanofluids showed that the presence of ZnO particles causes damages to the membrane wall of the bacteria. Such damage may be partly due to direct interaction between ZnO nanoparticles and the bacterial surface. Therefore ROS generated by ZnO particles could be part of the mechanism for damaging bacteria [61]. Another study of the toxicological impact of ZnO nanoparticles against *E. coli* has been carried out. *E. coli* cells were damaged and the cell contents may have leaked out. It was also observed that there was cellular internalization of these nanoparticles and cell wall disorganization [62].

Although most of the time ZnO nanoparticles seem to be only bacteriostatic, a study of *Campylobacter jejuni* showed that ZnO has a bactericidal effect. The results showed that *C. jejuni* was extremely sensitive to treatment with ZnO nanoparticles of ~30 nm. It was possible to see that cell morphology, membrane integrity, and gene expression in these bacteria were affected by ZnO nanoparticles. A dramatic change in the cell morphology was revealed, by showing the dominance of coccoid forms in the treated cells while the untreated remained spiral. In addition to this change in structure, ZnO nanoparticles resulted in the formation of irregular cell surfaces and “bubbles” in the membrane, an increase in membrane permeability, and a substantial increase in oxidative stress gene expression. This resulted in the inhibition of cell growth and eventually in cell death [63].

2.6. CHARACTERISATION TECHNIQUES

2.6.1. Dynamic Light Scattering

Dynamic light scattering (DLS) is a technique used to measuring the size of particles, typically in the sub-micron region. DLS is based on the scattering of light by moving

particles, i.e. it measures Brownian motion and relates it to the size of particles. Brownian motion is the random movement of particles due to the bombardment by the solvent molecules that surround them. The larger the particles, the slower the Brownian motion will be. Smaller particles are 'kicked' further by the solvent molecules and move more rapidly .

The velocity of the Brownian motion is defined by the translational diffusion coefficient (D) and that is what is measured in DLS. If the particles are spherical and do not interact, their radius can be calculated from the diffusion coefficient by the Stokes-Einstein equation:

$$D = \frac{kT}{6\pi\eta R}$$

Where *k* is the Boltzmann's constant, *T* is the absolute temperature, *η* is the viscosity, and R the radius of the scatterers [65]. The translational diffusion coefficient will depend not only on the size of the particle "core", but also on any surface structure, as well as the concentration and type of ions in the medium. The measurement of D is carried out by measuring the rate at which the intensity of the scattered light fluctuates when detected using a suitable optical arrangement. DLS works by having particles (for example in a cuvette), which are illuminated by a laser and then a screen is used to view the sample cell . The end result is then a size distribution by volume (Fig. 10).

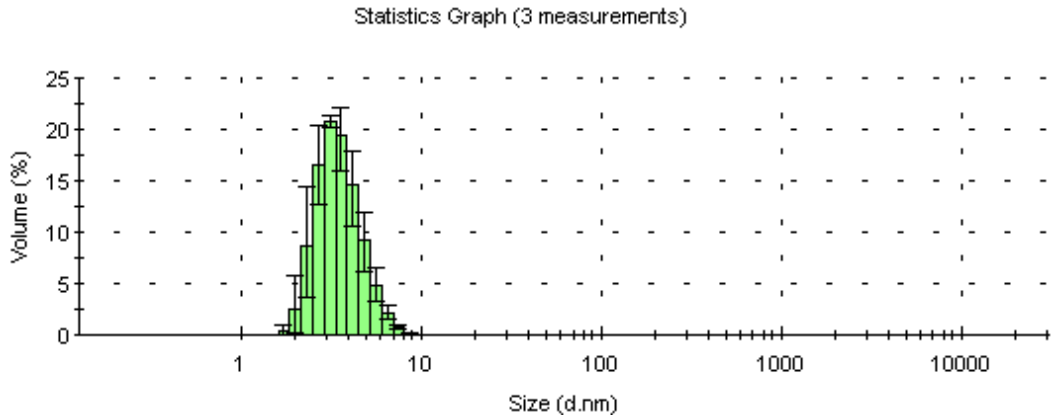

Fig. 10 – Size distribution graph obtained in for copper nanoparticles produced in the current project (n=3). In this case, the size distribution is reported in terms of volume percentage.

2.6.2. Zeta potential

The zeta potential (ζ potential) is the electrostatic potential on the surface of a particle. Although particles may be electrically charged, the charge on the surface of each particle is counterbalanced by ions of opposite charge in the surrounding solution [66]. Thus, the liquid layer surrounding the particle has two regions; an inner region (Stern layer) where

the ions are strongly bound and an outer (diffuse) region where they are less firmly associated. When the charges on the particle surface are attached the diffuse layer stretches out for some distance from the particle surface (Fig. 11). The surface that separates the bound charge from the diffuse charge around the particle marks where the solution and the particle move in opposite directions when an external field is applied. The electrostatic potential at this boundary (surface of hydrodynamic shear) is the zeta potential [66].

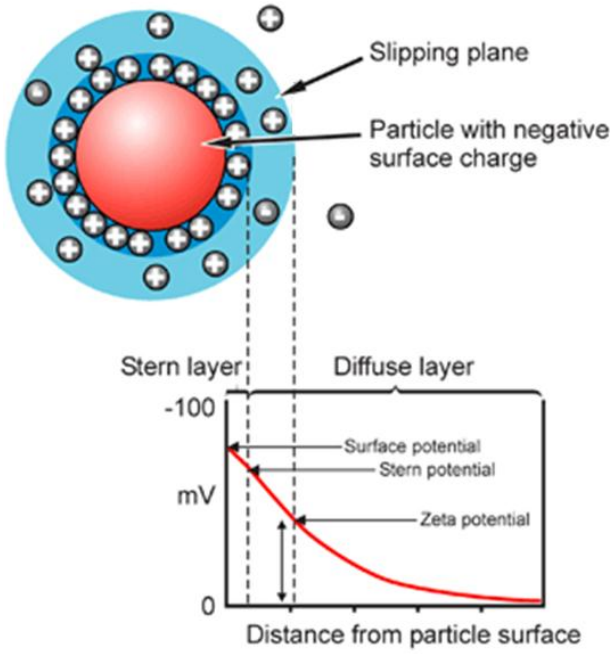

Fig. 11 – Distribution of charge around a negatively charged particle [67].

The magnitude of the zeta potential gives an indication of the potential stability of the colloidal system. If all the particles in suspension have a large negative or positive zeta potential then they will tend to repel each other and there will be no tendency for the particles to agglomerate [66]. Thus, the knowledge of the zeta potential can be used to optimize the formulations of suspensions.

A consequence of the existence of electrical charges on the surface of particles is that they interact with an applied field. When an electric field is applied across an electrolyte, charged particles are attracted towards the electrode of opposite charge. The particles move with constant velocity depending on the strength of the electric field or voltage gradient, the dielectric constant of the medium, the viscosity and the zeta potential. The velocity of a particle in a unit electric field is referred to as its electrophoretic mobility. Zeta potential is related to the electrophoretic mobility by the Henry equation:

$$U_E = \frac{2\,\varepsilon\,\zeta\,f(\kappa a)}{3\eta}$$

Where U_E = electrophoretic mobility, ζ = zeta potential, ε = dielectric constant, η = viscosity, and $f(\kappa a)$ = Henry's function .

2.6.3. Inductively Coupled Plasma – Optical Emission Spectrometry

Optical emission spectrometry (OES), also known as atomic emission spectrometry (AES), is a versatile, powerful, and sensitive method for elemental analysis. It involves nonradiative excitation of atoms or ions, followed by the emission of a photon that is collected by a detection system (Fig. 12). Although less sensitive than atomic spectrometry techniques coupled with mass spectrometers, OES is widely used because of its lower cost, reduced interferences, and sensitivity for many elements in the parts-per-billion range. The most commonly used atom cell for OES is the Inductively Coupled Plasma (ICP) [68]. ICP generates excited ions or atoms that emit electromagnetic radiation at wavelengths characteristic for certain elements. The concentration of the elements can be determined by the intensity of emission [69].

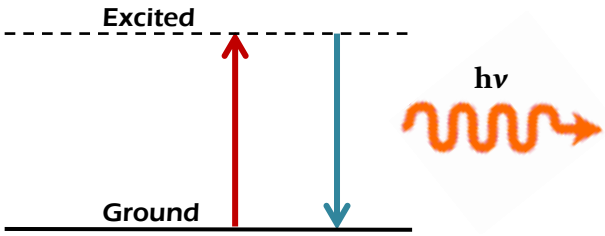

Fig. 12 – Emission of radiation upon relaxation from an excited state.

Inductively Coupled Plasma – Optical Emission Spectrometry is one of the several techniques available in analytical atomic spectroscopy. It utilizes plasma, which is an electrically neutral, highly ionized gas that consists of ions electrons, and atoms, as the atomization and excitation source. The energy that maintains the analytical plasma is derived from an electric or magnetic field, unlike in atomic absorption techniques there is no combustion, i.e. it is not a flame. Most analytical plasmas operate with pure argon or helium and are characterized by their temperature (assures that most samples are completely atomized), as well as their electron and ion densities. Analytical plasmas can range in temperature from 600 to 8000 K. ICP-OES is a total elemental technique, and one of its limitations is that it does not identify the oxidation state of the element [69].

2.6.4. X-ray diffraction

X-ray diffraction (XRD) is an important technique for the identification, quantification, and characterisation of minerals. It can provide information on phase composition, chemical composition, and the crystal structure of the material under analysis [70].

Solids can be divided into two categories: amorphous and crystalline. In an amorphous solid the atoms are arranged in a random way. In a crystal the atoms are arranged in a regular pattern, and there is a volume element that by repetition in three dimensions describes the crystal, i.e. a unit cell [71]. A macroscopic crystal then consists of a three dimensional, ordered arrangement of such unit cells and the geometry and structure of a crystalline solid determines the X-ray diffraction pattern.

The unit cell has the dimensions *a*, *b* and, *c* along the axes *x*, *y*, and *z*. For determining absolute distances, the geometry of the unit cell, i.e. the lengths of the cell dimensions *a*, *b*, and *c* and the angles between the axes must be known [70].

When an X-ray beam hits an atom, the electrons around the atoms start to oscillate with the same frequency as the incoming beam. In almost all directions there will be a destructive interference, i.e. the combining waves are out of phase and there is no resultant energy leaving the solid sample. However, the atoms in a crystal are arranged in a regular pattern, and in a very few directions there will be a constructive interference. The waves will be in phase an there will be well defined X-ray beams leaving the sample at various directions [72]. The interference pattern can be described by Bragg's law (Fig. 13):

$$n\lambda = 2d \sin\theta$$

Where λ is the wavelength of the radiation, *n* is an integer number, θ is the angle between the lattice planes and the incident beam, and *d* is the distance of the lattice planes for which the peak occurs [70].

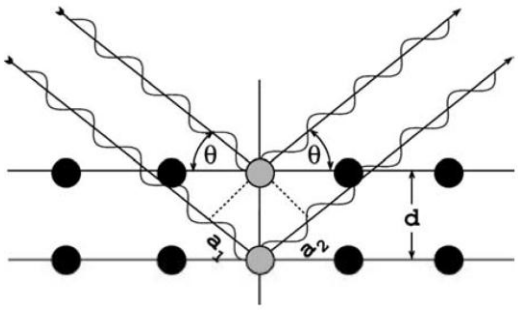

Fig. 13 – Geometric derivation of Bragg's law: constructive Interference of reflected waves [70].

Amorphous materials have short-range order. Since the “quality” of diffraction effects in XRD depends strongly on the strict and undisturbed periodicity of atoms, any kind of deviation from the ideal order will show in the X-ray diagram. This results in the loss of distinct XRD peaks [70].

2.6.5. Antimicrobial activity assays

For susceptibility tests to determine accurately the antimicrobial activity of a certain agent, standardization has to be achieved. The bacterial growth conditions must be optimized in a way that the inhibition of growth can be only linked to the presence of the antimicrobial agent and not to nutrient limitations, temperature or other environmental conditions [6].

One possible method for the determination of antimicrobial activity is the disc-diffusion assay. In this technique, discs containing known amounts of the antimicrobial agent are placed on a petri plate containing an agar medium previously inoculated with the test microorganism. The agent diffuses from the disc into the agar establishing a gradient. After incubation, the microorganisms will only grow beyond the point where the minimum inhibitory concentration (MIC), i.e. the lowest amount of agent that inhibits the growth of a test organism, is reached, but they do not grow closer to the disc where the amount of agent is higher. A zone of inhibition is created with a diameter proportional to the amount of antimicrobial agent added to the disc, the solubility of the agent, the diffusion coefficient, and the overall effectiveness of the agent [7]. The diameter of the zone of inhibition is then correlated to MICs obtained by broth or agar dilution [6]. The method presents several advantages, such as being easy to perform, cost effective, and easily adapted. However, this method is not suitable for tests with nanoparticles, since the diffusion of the nanoparticles is unknown.

The antimicrobial activity of a certain agent can be measured by determining its MIC [7]. The MIC can be determined by dilution methods. In this type of tests the visible growth of microorganisms is tested on a series of agar plates (agar dilution) or in broth (broth dilution) containing dilutions of the antimicrobial agent [73].

The agar dilution test consists in the in the inoculation of different agar plates containing various amounts of agent. After incubation, the plates are examined for growth and the MIC is the lowest concentration of the agent in agar that completely inhibits visible growth. This method has also been used for the determination of antibacterial activity of both copper and zinc nanoparticles [74, 75]. This is a highly sensitive method and is also easily adapted, but it also is labour intensive and very costly.

In broth dilution tests, the MIC is determined by making a sequence of decreasing concentrations of the agent in broth, which was inoculated with the test organism. Broth dilution tests can be divided into two categories: microdilution and macrodilution. The tests have the same basis and the only difference is the volume of broth in which the test is performed (0.05 to 0.1 mL and >1 mL, respectively). After incubation, the suspensions are tested for visible growth (turbidity) [7]. This method has been used for the determination of the antibacterial activity of both copper [57] and zinc [76] nanoparticles. The main advantages of this method are the generation of a quantitative result (MIC) and high throughput of results. However, the MIC value obtained is not accurate, since that this method only measures the total cell number and not the viable cells. When bacteria are killed, they remain in suspension and are accounted for the total cell number, which will have influence in the turbidity of the suspension. Thus, this method can be a good screening assay, but for more accurate results the method of agar dilution shall be carried out.

3. MATERIALS AND METHODS

3.1. MATERIALS

Copper (II) chloride dihydrate ($CuCl_2.2H_2O$; ≥ 99 %), D-glucuronic acid ($C_6H_{10}O_7$; ≥ 98 %), copper (II) acetate monohydrate ($Cu(CO_2CH_3)_2 \cdot H_2O$; ≥ 98 %), L-tartaric acid (Tart; 99.5%), Adipic acid (Ad; 99%), L-cysteine (≥ 97 %), citric acid (≥ 99.5 %), sodium phosphate tribasic (Na_3PO_4; ≥ 94 %), sodium dodecyl sulphate (SDS; 99%), octadecyltrimethylammonium bromide ($CH_3(CH_2)_{17}N(CH_3)_3Br$), and zinc (II) chloride ($ZnCl_2$; ≥ 99 %) from Sigma were used. Sodium hydroxide (NaOH; 99.4%) from Calbiochem and DL-carnitine hydrochloride ($C_7H_{15}NO_3 \cdot HCl$; 99%) from Acros were also used.

3.2. METHODS

3.2.1. Synthesis

3.2.1.1. Synthesis of ligand-modified copper hydroxide nanoparticles

The basis of the method consisted in the preparation of a copper and ligands solution at low pH to which a base was added, such as sodium hydroxide (NaOH). $Cu(OH)_2$, CuOH Glr, CuOH TartGlr, CuOH SDS, CuOH C_{18}TAB, CuOH Car[1], were prepared using the salt copper chloride ($CuCl_2$), whereas CuOH TartAd synthesis used copper acetate ($Cu(CO_2CH_3)_2$). All were prepared as described in patent WO/2008/096130.

3.2.1.2. C_{18}TAB modification of ligand-modified copper hydroxide nanoparticles

Octadecyltrimethylammonium bromide (C_{18}TAB) was added into a suspension containing CuOH SDS in order to prepare copper nanoparticles coated with C_{18}TAB. The same procedure was used to prepare CuOH Tar nanoparticles coated with C_{18}TAB.

3.2.1.3. Heat treatment of ligand-modified copper hydroxide nanoparticles

[1] This is an internal nomenclature, as the exact compositional formula was not determined.

Copper (II) chloride was added into sub-boiling water (90-100^{o}C). The same procedure as the one described on patent WO/2008/096130 was followed and the sub-boiling conditions were maintained. Tartaric acid was added as a ligand at different pHs.

3.2.1.4. Synthesis of ligand-modified copper oxo-phosphates nanoparticles

$Cu_3(PO_4)_2$ and $CuPO_4$ Cit were prepared using the salt copper (II) chloride ($CuCl_2$) and Na_3PO_4 was used for the synthesis. The same procedure as the one described on patent WO/2008/096130.

3.2.1.5. Synthesis of ligand-modified zinc oxide nanoparticles

$Zn(OH)_2$, and ZnOH Cys were prepared using the salt zinc (II) chloride ($ZnCl_2$). All were prepared as described in patent WO/2008/096130.

3.2.2. Characterisation of phase distribution

Several samples were recovered at different pHs. A study on the phase distribution was carried out for all these samples. The soluble, nanoparticulate, and precipitate phases of copper in suspension were determined using inductively coupled plasma optical emission spectrometry (ICP-OES; JY 2000, Horiba). The samples were centrifuged (13 000 rpm, 5 minutes) in order to remove the precipitate copper, i.e. agglomerated, thus enabling the measurement of the copper in the supernatant. To obtain the soluble fraction, samples were ultra-filtered using a membrane of 3 KDa. Once the concentrations were obtained, the following calculations were done in order to obtain the copper or zinc phase distribution:

$$\text{Soluble copper } (\%) = \frac{\text{Cu}_{\text{soluble}}}{\text{Cu}_{\text{total}}} \times 100$$

$$\text{Precipitated copper } (\%) = \frac{\text{Cu}_{\text{total}} - \text{Cu}_{\text{supernatant}}}{\text{Cu}_{\text{total}}} \times 100$$

$$\text{Nanoparticulated copper } (\%) = 100 - \text{Soluble Cu } (\%) - \text{Precipitated Cu } (\%)$$

The same procedure was carried out for zinc suspensions.

3.2.3. ICP-OES

Before determining the concentrations of total, supernatant, and soluble fractions by ICP-OES, each sample was diluted using 5% HNO_3 for the complete dissolution of the copper or zinc, since that the analyte needs to be soluble for the analysis to take place. These dilutions were made in order to obtain concentrations within the calibration curve (Cu: 0-100 ppm; Appendix 1). The samples were then analysed by ICP-OES (JY2000, Horiba Jobin Yvon), at a wavelength of 325 nm for copper and nm for zinc.

3.2.4. Determination of particle size and zeta potential

Both the particle size and zeta potential were determined by Dynamic Light Scattering (DLS; Zetasizer, Malvern Instruments) immediately after the particles had been synthesised. For the particle size distribution determination, the sample was placed into a low volume disposable sizing cuvette. The measurements were carried out for refractive index (RI) of 1.85, which is the refractive index for particles of this composition. For the zeta potential measurements a disposable zeta potential cell was used. The sample was placed carefully into this cell, avoiding the formation of bubbles. The same RI for the material as in the particle size measurements was used. The measurements for both particle sizing and zeta potential were carried out at a temperature of 25^{o}C, using water as dispersant (viscosity=0.8872; RI=1.330; dielectric constant=78.5). It is important to define the medium in which the material is dispersed, because the composition of the disperse phase will have an impact on the particle size and zeta potential, as it is on the nature of the particle surface. The data analysis was carried out by using DTS software (Version 4.1; Malvern Instruments).

3.2.5. XRD

3.2.5.1. Sample preparation

The suspensions were first oven dried at 50^{o}C. The suspensions containing agglomerated particles were first centrifuged (3855 rpm, 20 min.) and the supernatant was discarded. After completely dry, the material was milled.

3.2.5.2. Analysis

The analyses by XRD were carried out at the Earth and Environmental Department, University of Leeds. The unmodified and ligand-modified Cu(II) oxo-hydroxide, oxide and phosphate, and Zn(II) oxo-hydroxide materials were mixed with ethanol and pipetted onto a low background silicon holder. The diffraction data was collected with a Philips PW1050 Powder Diffractometer using Cu K alpha radiation and a Ge secondary monochromator. The scanning range was 5-70 deg 2 theta at a speed of 0.8 deg/min and a step size of 0.01 deg. TRACES software with the ICDD (international centre for diffraction data) database was used to process the data.

3.2.6. Antibacterial activity tests

The nanoparticle suspensions were tested against *Escherichia coli* NCTC11100. Bacteria were grown overnight at 37^{o}C in sterile broth (Iso-sensitest broth, Oxoid). The tests were carried out in a 96-well plate, with different amounts of bacteria (decimal dilutions of an initial culture; 10^{-1}, 10^{-2}, 10^{-3}, 10^{-4}, and 10^{-5}) and different concentrations of copper- or zinc-based particles (25, 50, and 100 ppm of either copper or zinc). A turbidimetric assay was used to determine the inhibition of bacterial growth. This method relies on the scattering of light caused by the bacterial cell surface, which presents a high refractive index. The reduction of transmitted light can be then measured by optical density and related to relative bacterial growth. The bacterial growth was carried out at 37^{o}C and the measurements were taken at 595 nm with a plate reader (Multiskan RC 351, Labsystems), at 0, 2, 4, and 6 hours.

The inhibition percentage for the bacterial growth presented throughout this dissertation corresponds to the one at 100 ppm of copper or zinc, 10^{-2} bacterial dilution, and 6 hours. The inhibition at 100 ppm was chosen because this is the best inhibition, due to the higher concentration. The 10^{-2} amount of bacteria is also the best one because with this amount the growth does not reach a plateau (for the 10^{-1} it does). The time chosen was 6h due to the linear growth observed at that time, which does not happen before. Refer to Appendix 2 for the standard growth curves.

4. Results and discussion

4.1. Copper

Copper, when in solution (i.e. in ionic form), acts as a Lewis acid, being an electron pair acceptor. Thus, when copper (II) chloride ($CuCl_2$) is dissolved in water the resulting solution has a low pH:

$$CuCl_2 \cdot 2H_2O\ (s) \rightarrow Cu^{2+}(aq) + 2Cl^-(aq) + 2H_2O\ (l) \quad (2)$$

$$Cu(H_2O)_n^{2+} + H_2O \rightarrow Cu(H_2O)_{n-1}(OH)^{1+} + H_3O^+ \quad (3)$$

As a control experiment for the production of unmodified copper oxo-hydroxides, the pH of a solution of copper (40 mM) was adjusted drop-wise with NaOH. Initially, copper remained soluble at very acidic pH's, but as the pH was raised (>pH4), copper started to precipitate (Fig. 14). This precipitation is due to the formation of unmodified copper oxo-hydroxide particles, which are insoluble, and, for example, $Cu(OH)_2$ is formed according equation 3:

$$Cu^{2+}(aq) + 2OH^-(aq) \rightarrow Cu(OH)_2(s) \quad (4)$$

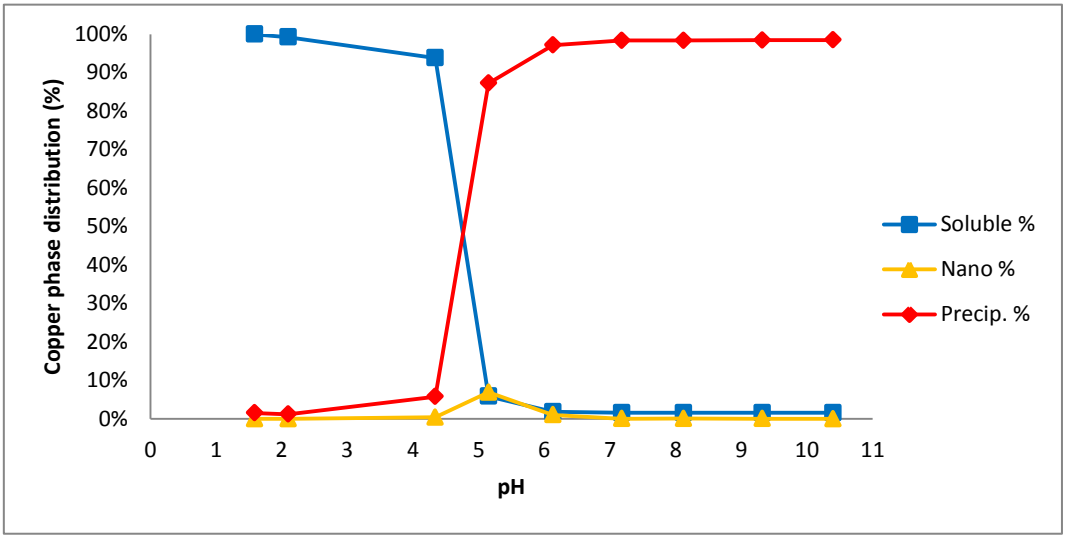

Fig. 14 – Copper phase distribution (%) with varying pH during the synthesis of copper oxo-hydroxide ([Cu]=40 mM).

A mineral phase is a mineral system with homogenous physical and chemical properties, i.e. a system where the composition and tridimensional arrangement are uniform.

The mineral phase of the obtained particles was paratacamite ($Cu_2Cl(OH)_3$; trigonal-rhombohedral), as determined by XRD in the previous work [77]. The agglomeration of the copper oxo-hydroxide particles has to be controlled in order to produce smaller particles, i.e. to produce nanoparticles.

4.1.1. Ligand effect

Previous work at MRC-HNR [77], showed it is possible to obtain modified copper oxo-hydroxide nanoparticles with sizes between 3-5 nm, using tartaric acid and adipic acid as ligands (Fig. 15). Tartaric acid is a natural occurring dicarboxylic acid with two proton donor centers, two carboxylic and two hydroxyl groups (pKa=3.03; pKa=4.37 [78]). Adipic acid is also a dicarboxylic acid with the same proton donor centres (pKa=4.44; pKa=5.44 [78]). These two ligands act as dispersive agents, avoiding the excessive agglomeration of the particles and thus allowing the control of the particle size. However, these nanoparticles were labile and dissolved partially in bacterial broth (medium used in the antimicrobial assay). Thus, the current work is focused on the development of copper nanoparticles with different ligand combinations to make them more stable. As for the previous work [77] safety was a key determinant in the choice of ligands. To ensure this, almost all ligands tested were dietary ligands, i.e. typically present in a normal diet. Low cost was an additional advantage of using dietary ligands, which would, in principle, lead to low manufacturing costs. Furthermore, all ligands were GRAS (Generally Recognized as Safe) as it further ensured a good safety profile for the resulting materials.

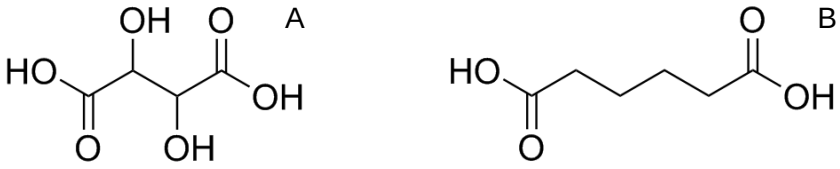

Fig. 15 – Structures of tartaric acid (A) and adipic acid (B).

Glucuronic acid is a carboxylic acid, with a structure similar to glucose (Fig. 16) and has a pKa of 3.18 [78]. The interaction with copper should also be via the carboxylic group and the several –OH groups would lead to a higher stabilization [79]. Thus, this ligand was tested to attempt a higher stabilization of the nanoparticles. The concentrations used in this case were 40 mM of copper (II) and 40 mM of glucuronic acid and the same method was followed. The copper phase distribution was studied (Fig. 17). At pH 2, before NaOH had been added, all copper was soluble. However, approximately at pH 5, there was a

substantial precipitation. The yield on the production of nanoparticles was very low and it was concluded that this ligand alone is ineffective in the production of nanoparticles.

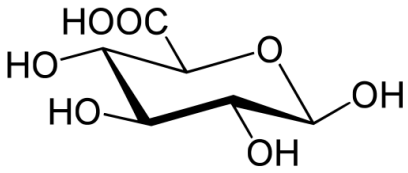

Fig. 16 – Structure of glucuronic acid

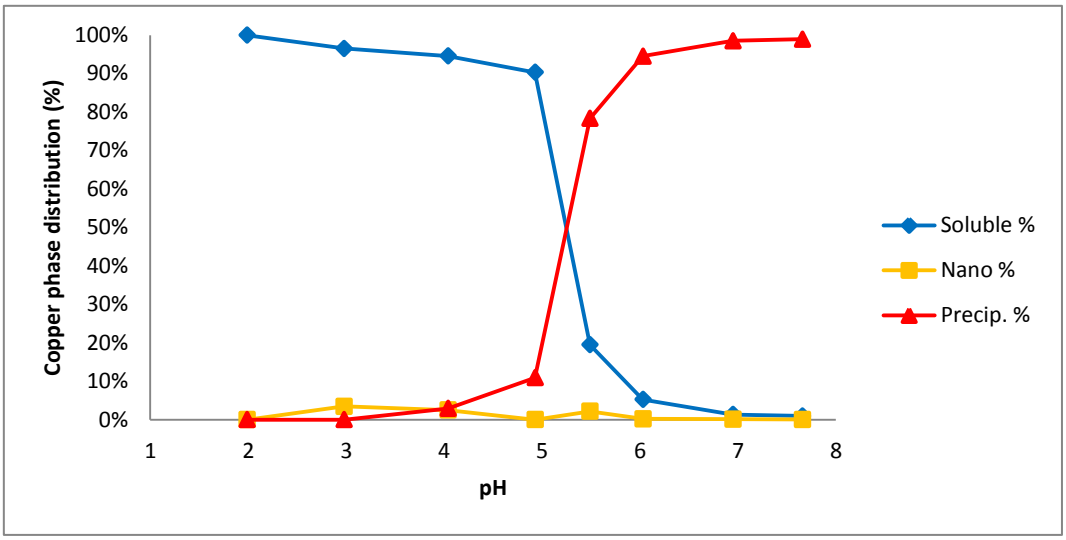

Fig. 17 - Copper phase distribution (%) with varying pH during the synthesis of copper (II) oxo-hydroxide ([Cu]=40 mM) in the presence of glucuronic acid (40 mM).

The use of glucuronic acid as a ligand did not lead to the formation of copper oxo-hydroxide nanoparticles. To further disperse these particles, tartaric acid (20 mM) was used along with glucuronic acid (20 mM), using a 40 mM solution of copper (II). The copper phase distribution obtained during this synthesis (Fig. 18) shows that a great amount of nanoparticles were formed (95.5%, pH 9.2). The particle size varied according to pH. At pH 6 (Fig. 19A) the mean size of the particles was 1.4 nm and at pH 10 it was 2.6 (Fig. 19B). Next, the effect of dilution in broth on the copper phase distribution was studied (Fig. 20). There was a partial dissolution of the nanoparticles at all concentrations. In fact, only ~50% of the copper remained nanoparticulate. This shows that the obtained nanoparticles were not stable. Nevertheless, these nanoparticles were tested against *E. coli* (Fig. 21). Although the nanoparticles produced a greater inhibition (57.8%) than a copper (II) chloride solution

(41.0%), the bactericidal action was still below intended. These results may be due to the partial dissolution of the nanoparticles when in broth.

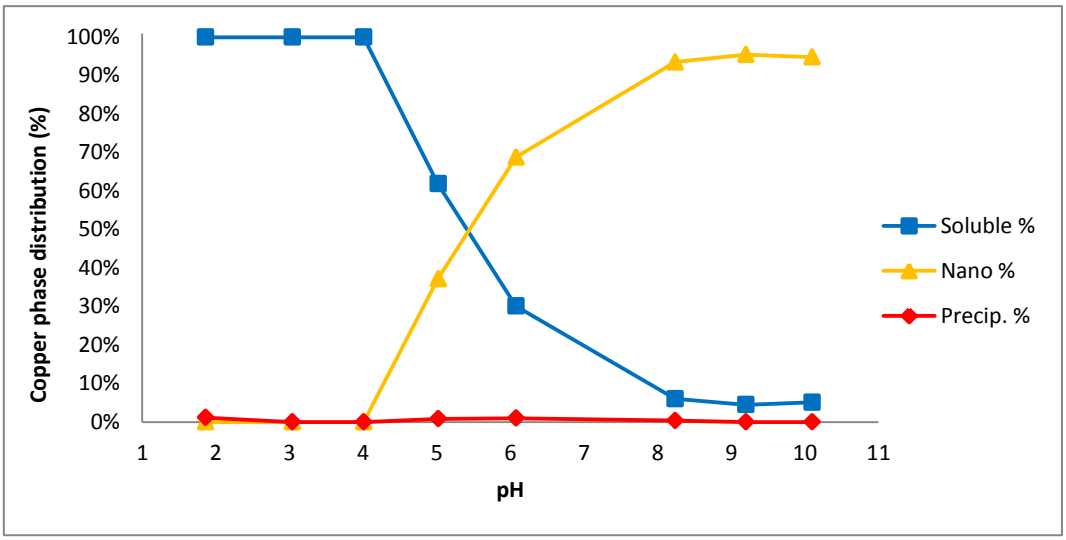

Fig. 18 - Copper phase distribution (%) with varying pH during the synthesis of copper (II) oxo-hydroxide ([Cu]=40 mM) in the presence of tartaric acid (20 mM) and glucuronic acid (20 mM).

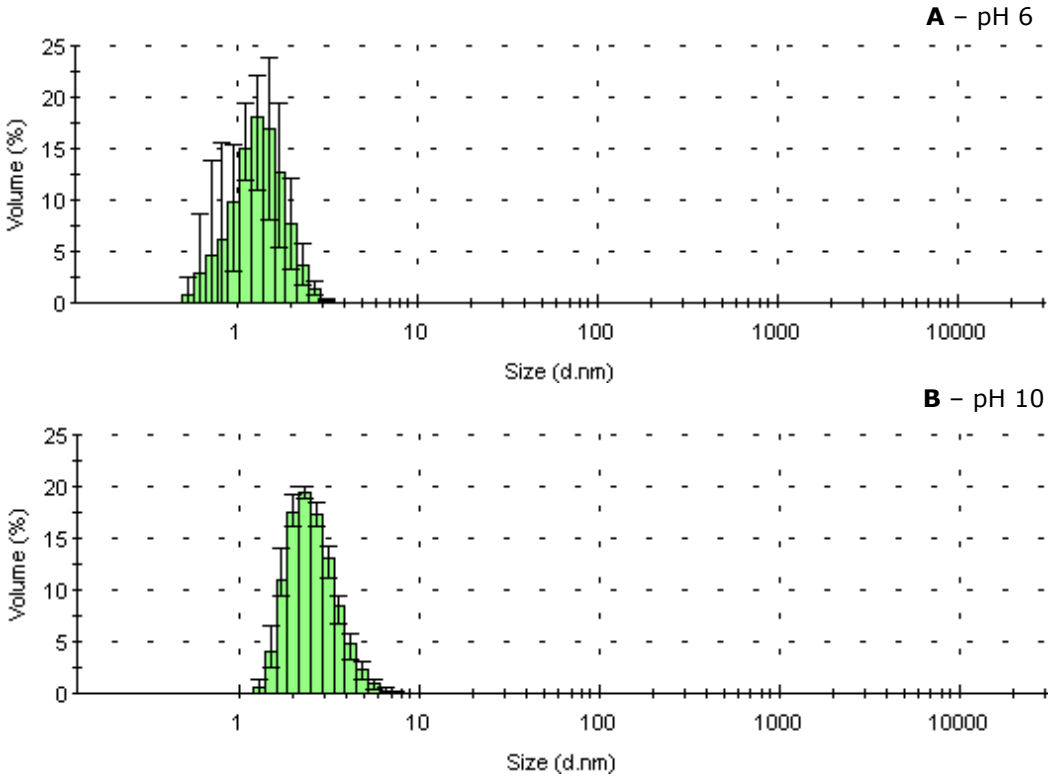

Fig. 19 - Particle size distribution at various pH's during the synthesis of copper oxo-hydroxide ([Cu]=20 mM) in the presence of tartaric acid (20 mM) and glucuronic acid. (A) pH 6; (B) pH 10.

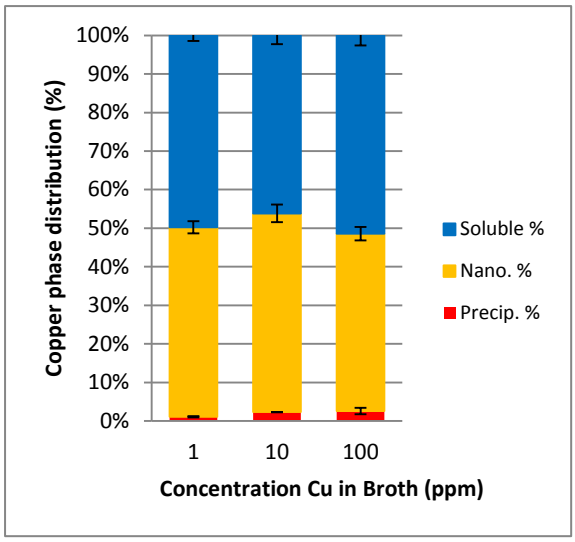

Fig. 20 - Copper phase distribution (%) of CuOH TartGlr diluted in broth at concentrations 1, 10 and 100 ppm.

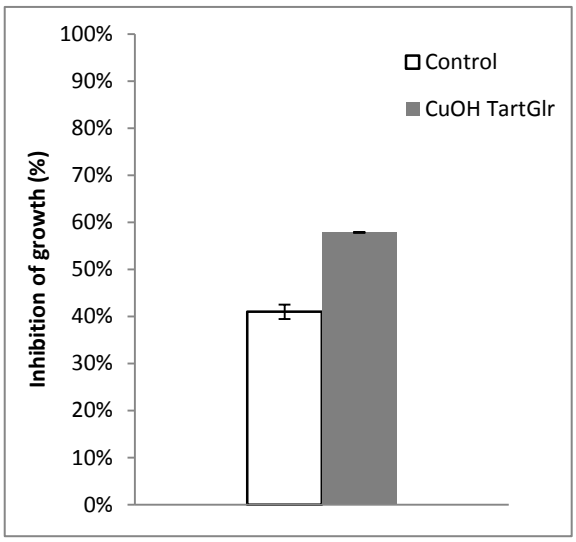

Fig. 21 – Inhibition of growth of *E. coli* by CuOH TartGlr nanoparticles at 6h, 100 ppm of copper, and 10^{-2} bacterial dilution. The white column represents the results for control (40 mM solution of copper chloride) and the grey one for the suspension.

4.1.1.1. Other ligands

Other ligands were tested for the production of copper oxo-hydroxide nanoparticles, such as cysteine, histidine, phenylalanine, tryptophan, alanine, and maltol. None of this ligands resulted in the production of a high yield of nanoparticles. However, the use of these ligands allowed a better understanding on how the production of copper oxo-hydroxide nanoparticles works. For example, the use of ligands with a high affinity to copper, such as cysteine and histidine, did not result in the production of copper oxo-hydroxide nanoparticles. They may work on the production of nanoparticles of a different mineral phase, but they do not seem to work for paratacamite related phases. For the sake of conciseness, these experimental data has not been reported in this Thesis.

4.1.2. Increasing stability

4.1.2.1. Copper salt

Copper chloride was replaced by copper acetate to test the effect of using a different copper salt. This should lead to the production of a different mineral phase other than paratacamite ($Cu_2Cl(OH)_3$) due to the replacement of chloride ions by acetate. When copper oxo-hydroxide is produced using copper acetate, the copper phase distribution at increasing pH varies according to Fig. 22. The precipitation occurs at a pH between 5 and 6.

Nanoparticles were produced at pH 6.2 but as the pH increased these nanoparticles agglomerated and at pH 7 most of the copper was precipitated. These particles were also characterized by XRD (Fig. 23), showing that there was a significant agreement with the XRD pattern for copper (II) hydroxide ($Cu(OH)_2$). This informed that due to the absence of chloride in this experiment, the mineral phase paratacamite ($Cu_2Cl(OH)_3$) was not obtained. Instead, $Cu(OH)_2$ was obtained, however, some of the peaks could not be identified. They may correspond to other mineral phases formed during the synthesis.

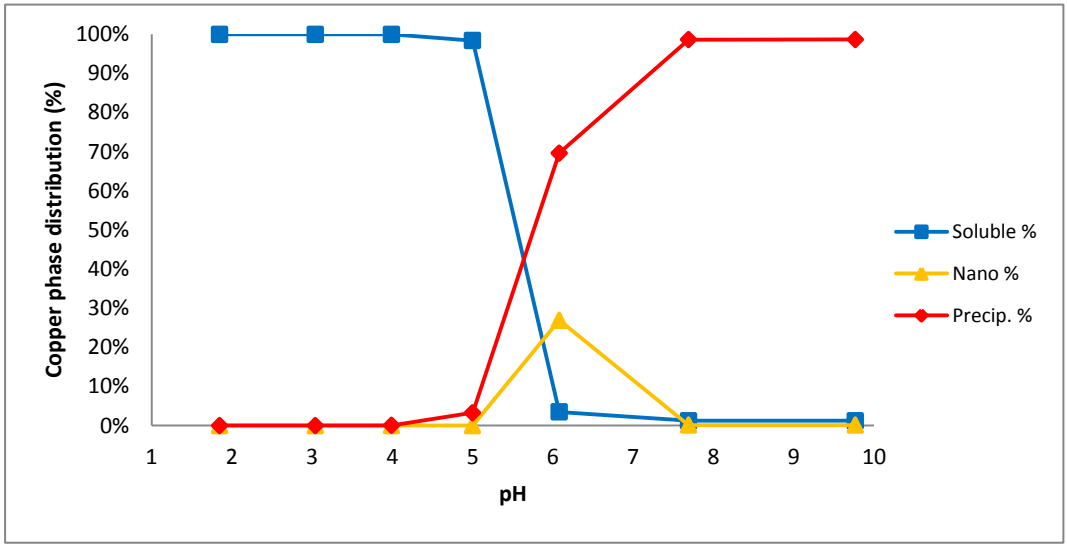

Fig. 22 - Copper phase distribution (%) with varying pH during the synthesis of copper oxo-hydroxide ([Cu]=40 mM) using a different copper salt.

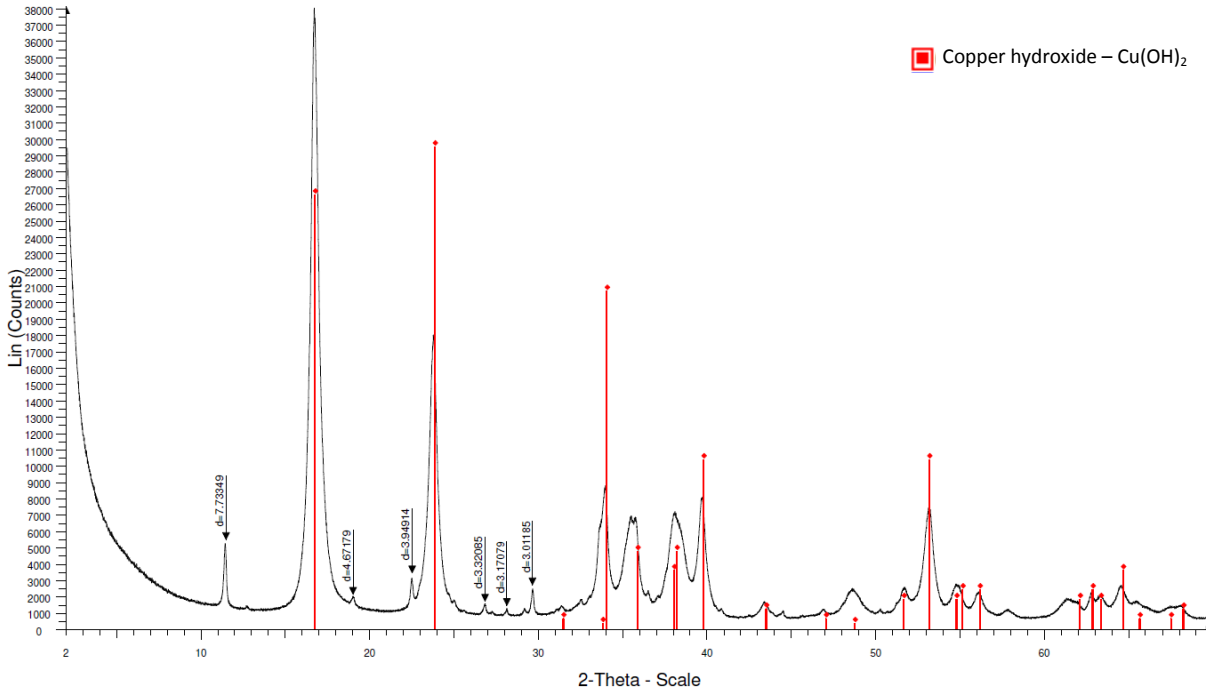

Fig. 23 – XRD characterization of copper oxo-hydroxide particles using a different copper salt. The lines in red represent the XRD reference for copper (II) hydroxide ($Cu(OH)_2$).

Next, to produce modified copper (II) hydroxide nanoparticles, tartaric acid and adipic acid (20 mM each), which were previously shown to be good dispersive agents for the production of copper oxo-hydroxide nanoparticles, were added to a solution containing 40 mM of copper acetate. Here, the highest amount of nanoparticles (77%) was obtained at pH 8 (Fig. 24). In this synthesis the level of precipitation remained constant throughout the synthesis (~15%). The analysis of the particle size distribution at pH 7 showed that the nanoparticles had an approximate mean size of 2 nm (Fig. 25A) but at pH 8 they were larger, they had an approximate mean size of 4.5 nm (Fig. 25B). The mean size of the nanoparticles increased with pH, which may have made them more stable. The characterization of these particles by XRD showed that a significant fraction of sodium acetate hydrate was obtained in this synthesis ($C_2H_3NaO_2 \cdot 3H_2O$), since some of the peaks match the XRD reference for this mineral phase (Fig. 26). Again it was not possible to identify a pattern for a copper mineral phase, which may mean that an amorphous material was produced, due to the integration of the ligands in the particle structure. It was also not possible to identify some of the peaks. The antibacterial activity of this material against *E. coli* was tested (Fig. 27), presented more than 50% of inhibition in relation to copper free media, but, when compared to the control (copper (II) acetate solution) at the same concentration, the results were equivalent, which indicates that the nanoparticles did not have a greater effect than copper in solution. This may have been due to the solubilisation of the nanoparticles when in broth, meaning that the problem of the instability of the nanoparticles was not overcome by using a different source of copper.

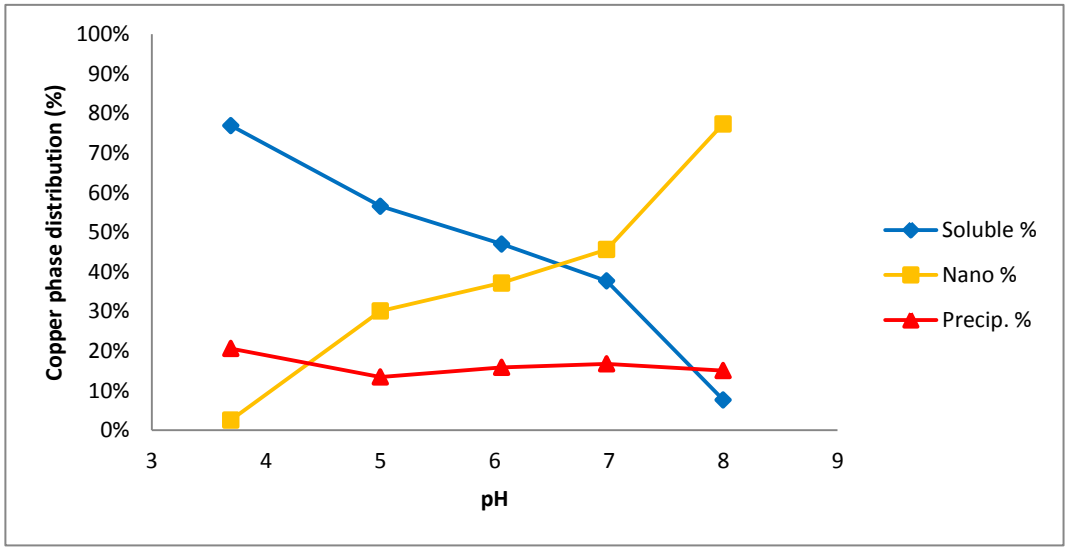

Fig. 24 - Copper phase distribution (%) with varying pH during the synthesis of copper oxo-hydroxide ([Cu]=40 mM) using a different copper salt and in the presence of tartaric acid (20 mM) and adipic acid (20 mM).

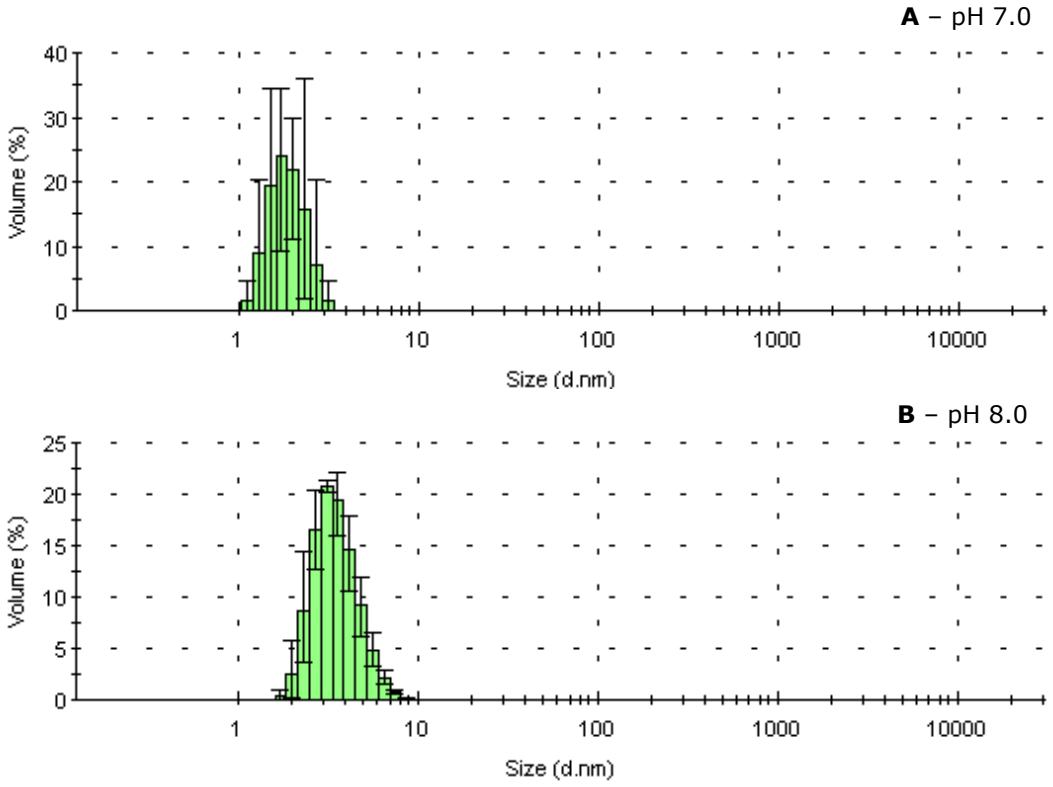

Fig. 25 - Particle size distribution at various pH's during the synthesis of copper oxo-hydroxide ([Cu]=40 mM) in the presence of tartaric acid (20 mM) and adipic acid (20mM) (A) 7.0; (B) pH 8.0.

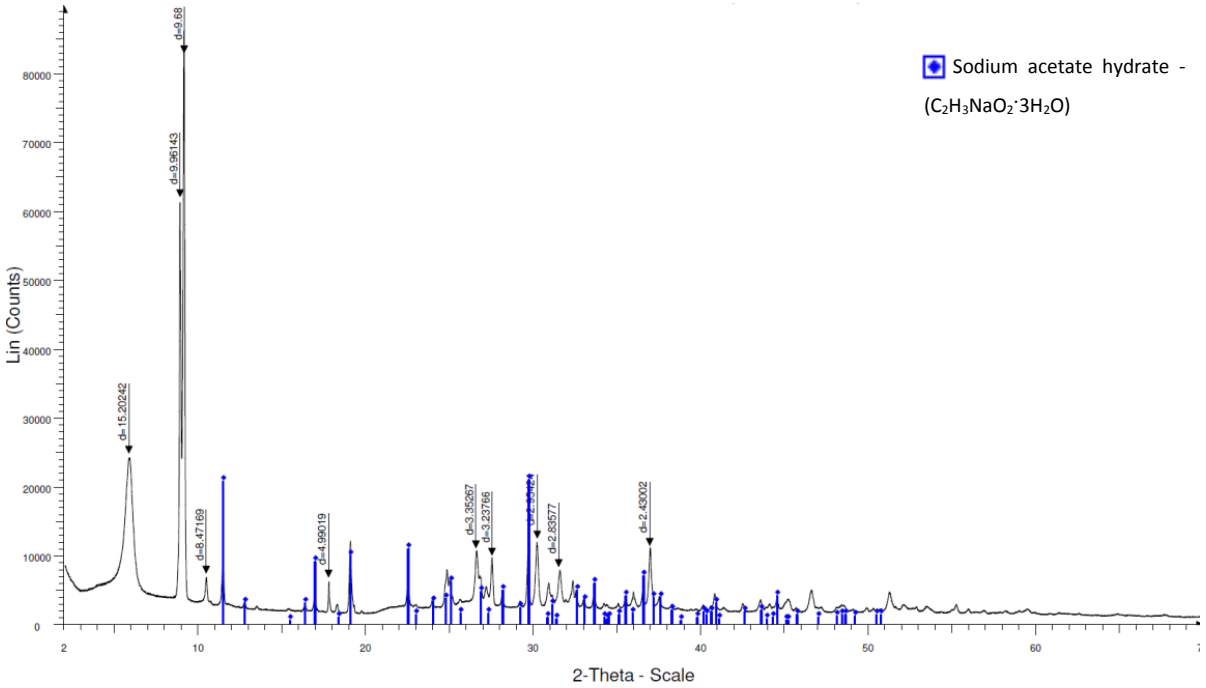

Fig. 26 – XRD characterization of copper oxide nanoparticles. The lines in blue represent the XRD reference for Sodium acetate hydrate ($C_2H_3NaO_2 \cdot 3H_2O$).

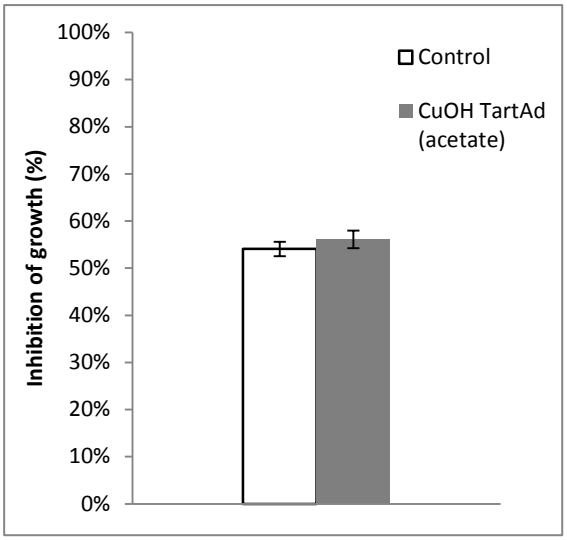

Fig. 27 – Inhibition of growth of *E. coli* by CuOH Tart Ad nanoparticles synthesised using a different copper salt (copper (II) acetate) at 6h, 100 ppm of copper, and 10^{-2} bacterial dilution. The white column represents the results for control (40 mM solution of copper (II) acetate) and the grey one for the suspension.

4.1.2.2. Copper oxides

Modified copper oxide (CuO) nanoparticles have been reported to show antibacterial activity [80]. CuO nanoparticles have also shown great cytotoxicity for eukaryotic cells which has been hypothesized to be due to a 'Trojan-horse' effect, i.e. once they reach the lysosomes, they solubilize due to the lower pH inside them, leading to the release of copper ions inside the cell [81]. However, the aim of this project is to produce nanoparticles that interact with the cell membrane rather than penetrating it. Oxide based nanoparticles may be more stable, due to the nature of the mineral phase. So CuO nanoparticles were produced at high temperatures and this mineral phase was identified during the synthesis by the observation of the suspension colour, which should be black rather than blue [82].

As a control experiment for the production of copper oxides, a 40 mM copper (II) solution was added to water at sub-boiling temperature and then the pH was gradually increased. Before adding NaOH, 60% of the copper was soluble (Fig. 28). There were also a nanoparticulate fraction (30%) and some precipitate (10%). As NaOH was added, there was a substantial precipitation and all the copper was precipitated. This precipitate was then characterized by XRD (Fig. 29), which showed that the mineral phase of the obtained particles is tenorite, a phase chemically constituted of nearly pure copper (II) oxide (CuO) [83]. Halite (NaCl) was also found but this was expected, since the copper salt used was copper (II) chloride and the base was NaOH.

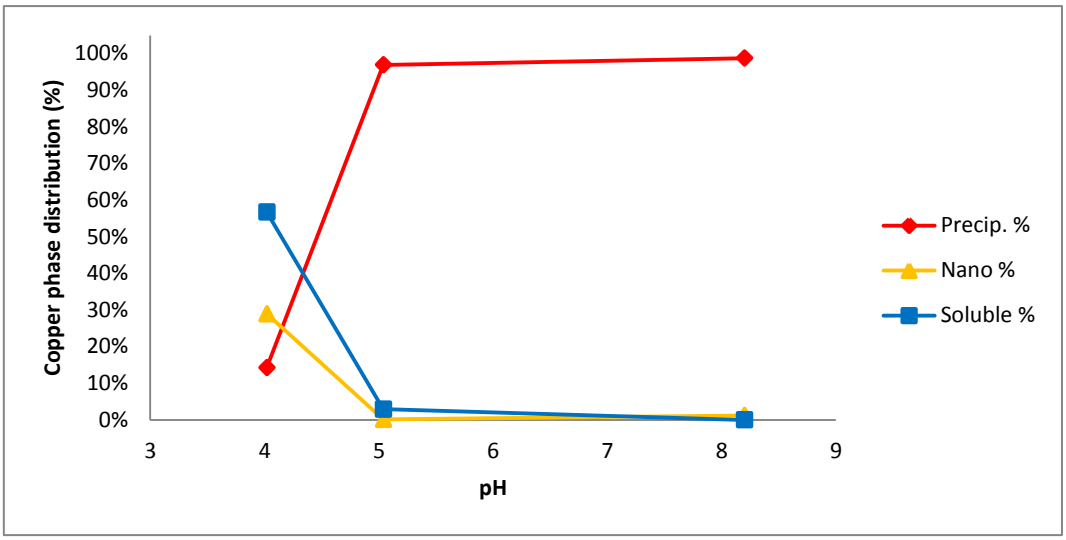

Fig. 28 - Copper phase distribution (%) with varying pH during the synthesis of copper oxide ([Cu]=40 mM) under heating.

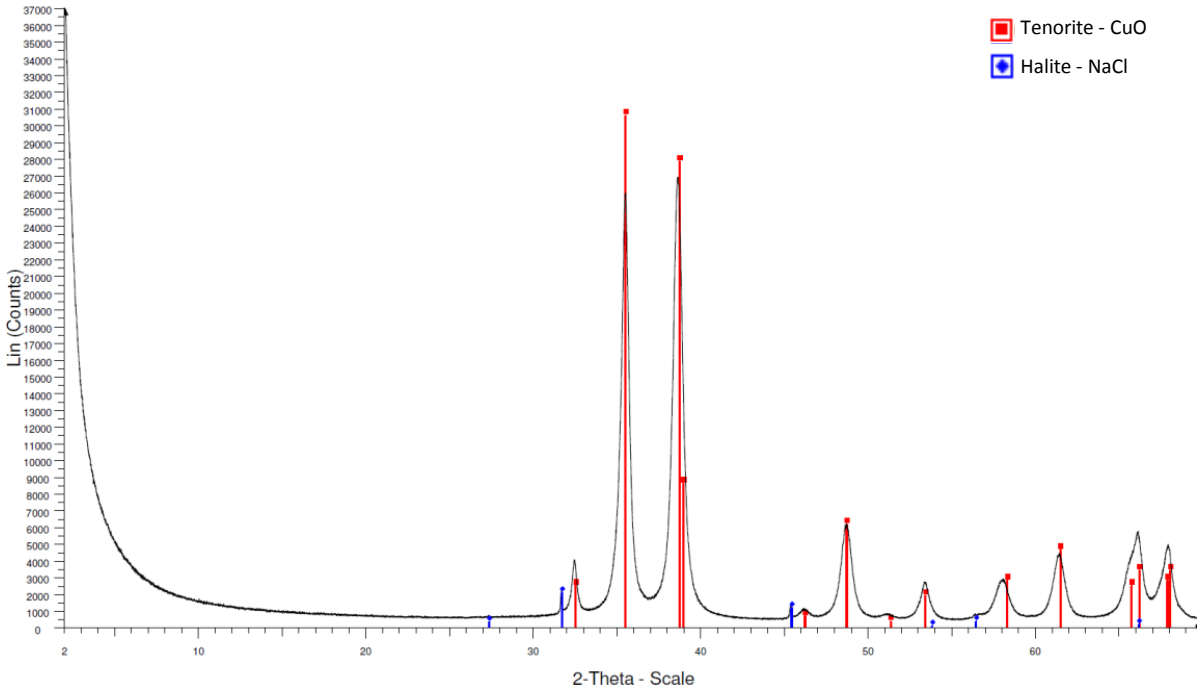

Fig. 29 – XRD characterization of copper oxide particles. The lines in red represent the XRD reference for Tenorite (CuO) and the blue ones for Halite (NaCl).

For the production of copper oxide nanoparticles, tartaric acid was used as a ligand, since it has been shown to be a good dispersive agent for copper. A solution of copper (II) was added to sub-boiling water with a final concentration of 40 mM. Then, a solution containing tartaric acid was also added (final concentration=40mM) and NaOH was added drop-wise. The copper phase distribution was studied (Fig. 30) and also the progression of

colour was observed as it can be informative of mineral phases. At low pH most of the copper was soluble. When the pH was raised to pH 2.4, there was some precipitation and the amount of soluble and precipitate copper was roughly the same. By this time, the colour of the suspension was light blue. However, as the pH was raised, nanoparticles started to form and the suspension turned into a clear dark blue. The highest amount of nanoparticles was obtained at pH 10.0 and at this pH the suspension turned into dark green which may be due to a mixture of copper oxo-hydroxide and CuO particles. Then at pH 12.4 a substantial precipitation occurred and the colour turned into dark brown, possibly due to a further mineral phase change. Overall, CuO particles appear to have been formed, but they were not nano-sized.

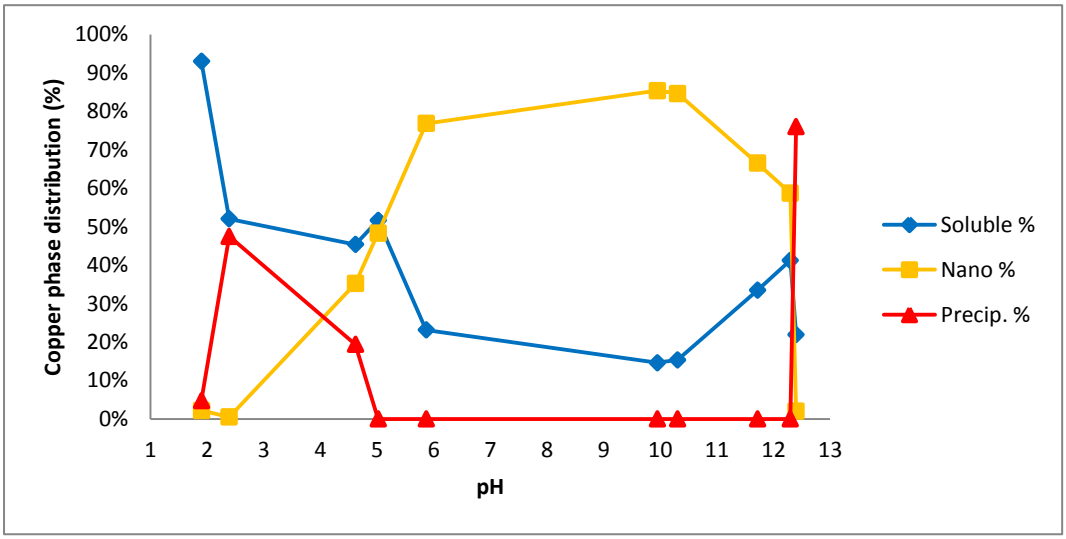

Fig. 30 – Copper phase distribution (%) with varying pH during the synthesis of copper oxide ([Cu]=40 mM) in the presence of tartaric acid (40 mM) under heating.

The previous synthesis resulted in the production of large copper oxide particles and, to tackle this effect, the concentration of tartaric acid was increased to 80 mM. With this increase on the concentration of tartaric acid, its dispersive power should be higher and thus nanoparticles could be produced. Before adding any NaOH, at pH 1.7, most copper was soluble but when the pH was raised to 2.8, there was a substantial precipitation (Fig. 31), similarly to what happened in the previous experiment. At pH 4.8, nanoparticles were present and their amount kept rising for higher pHs. The suspension turned into clear dark blue and remained with this colour till the end of the titration. Thus, such a high concentration of tartaric acid did not allow the production of CuO nanoparticles and only copper oxo-hydroxide nanoparticles were produced.

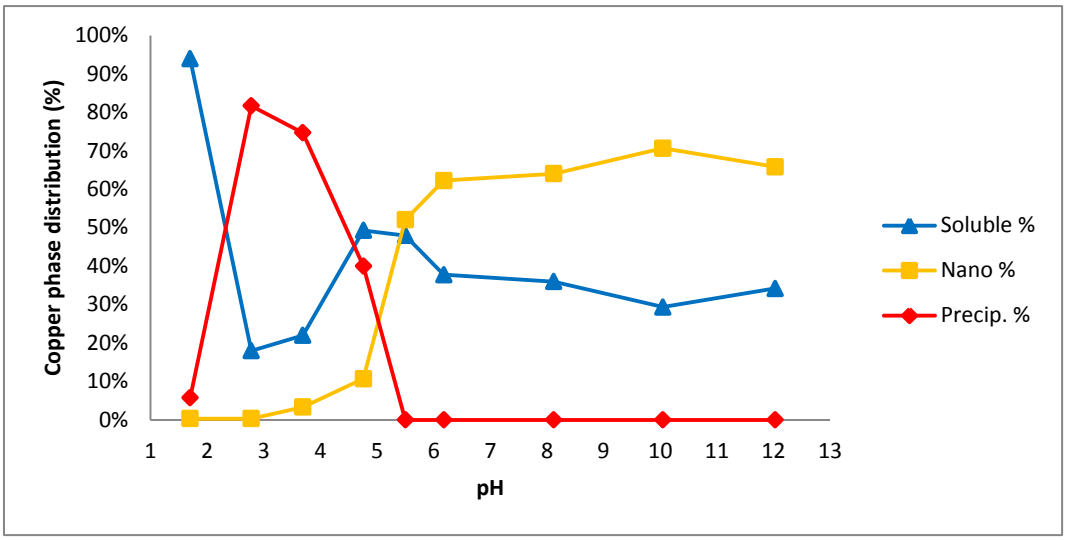

Fig. 31 – Copper phase distribution (%) with varying pH during the synthesis of copper oxide ([Cu]=40 mM) in the presence of tartaric acid (80 mM) under heating.

To test the effect of adding tartaric acid after CuO particles appeared to be already formed without any ligand, a 40 mM copper (II) solution was added to water at sub-boiling temperature and at high pH. After adding tartaric acid to this suspension (final concentration=20 mM), the copper remained precipitate (Fig. 32). The characterization of these particles by XRD shows that tenorite (CuO) was also produced, since most of the peaks obtained match with those of the pattern of this mineral phase (Fig. 33). This means that even in the presence of tartaric acid, CuO is formed and that the ligand is not integrated in the particle structure.

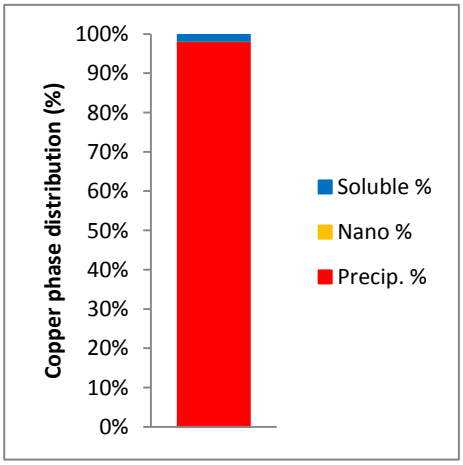

Fig. 32 – Copper phase distribution (%) during the synthesis of copper oxide nanoparticles ([Cu]=40 mM) in the presence of tartaric acid (20 mM) under heating.

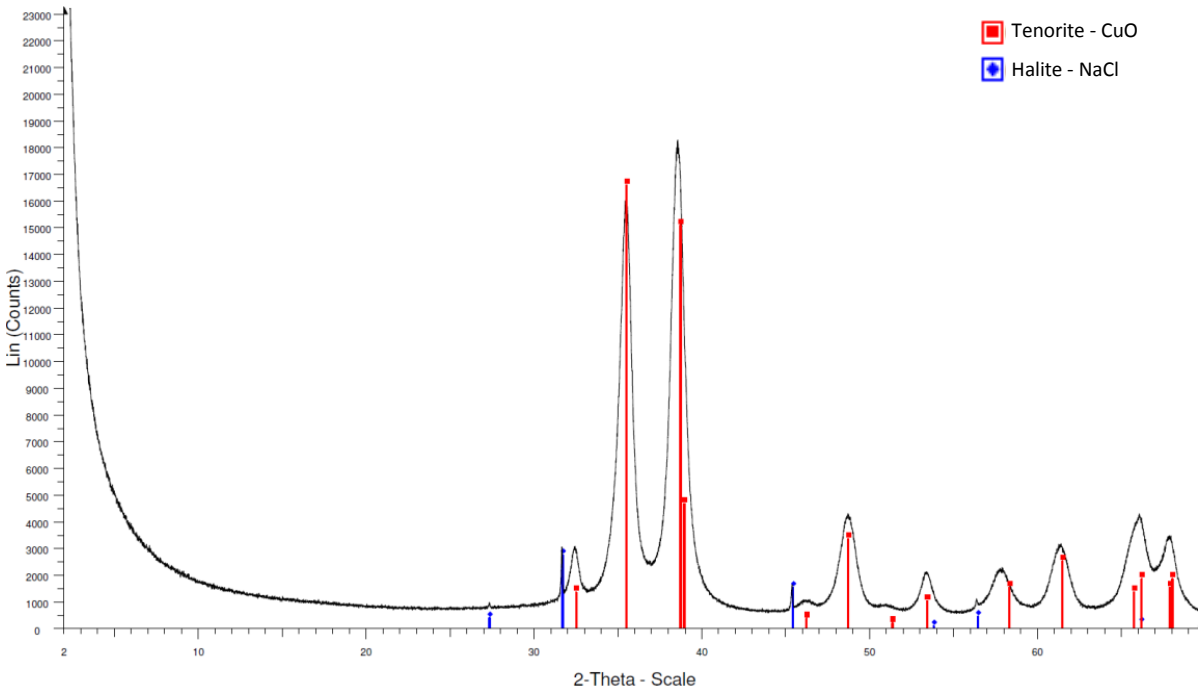

Fig. 33 – XRD characterization of copper oxide particles modified with tartaric acid. The lines in red represent the XRD reference for Tenorite (CuO) and the blue ones for Halite (NaCl).

Cysteine (Fig. 34) is a neutral amino acid (pKa=1.92 – COOH; pKa=8.37 – SH; pKa=10.70 $–NH_3^+$ [78]) and is one of the two sulphur-containing amino acids. This amino acid has a high affinity for copper and forms complexes with this metal through the thiol group [84]. Due to its structure features, it can also lead to the production of nanoparticles. This ligand was also added to a suspension of CuO particles. Nanoparticles were obtained and the yield was 86.6% (Fig. 35). When this suspension was diluted in broth, a higher percentage of the copper remained nanoparticulate when comparing to the previous suspensions (Fig. 36). These nanoparticles are more stable than the ones previously synthesised but there is still a great dissolution of the nanoparticles. This suspension was also tested against *E. coli*. The results revealed to be worse than the copper (II) chloride solution and any other previous results, since an inhibition of only 16.3% was obtained (Fig. **37**). Although these nanoparticles were more stable than the previous ones, they did not show relevant antimicrobial activity.

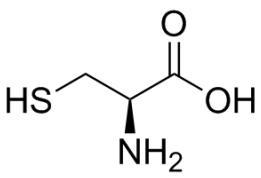

Fig. 34 – Structure of cysteine.

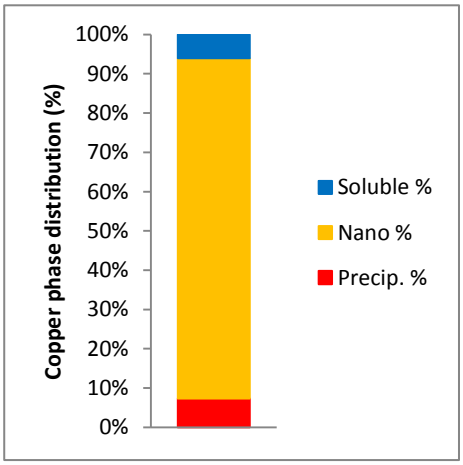

Fig. 35 - Copper phase distribution (%) during the synthesis of copper oxide nanoparticles ([Cu]=40 mM) in the presence of cysteine (40 mM) under heating.

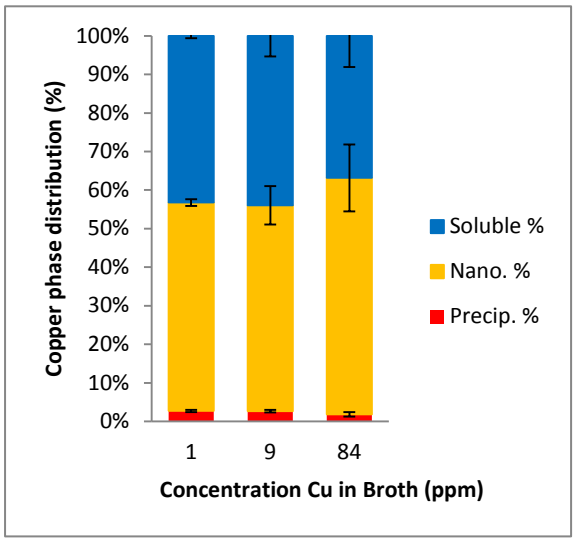

Fig. 36 - Copper phase distribution (%) of CuO Cys diluted in broth at concentrations 1, 9 and 84 ppm.

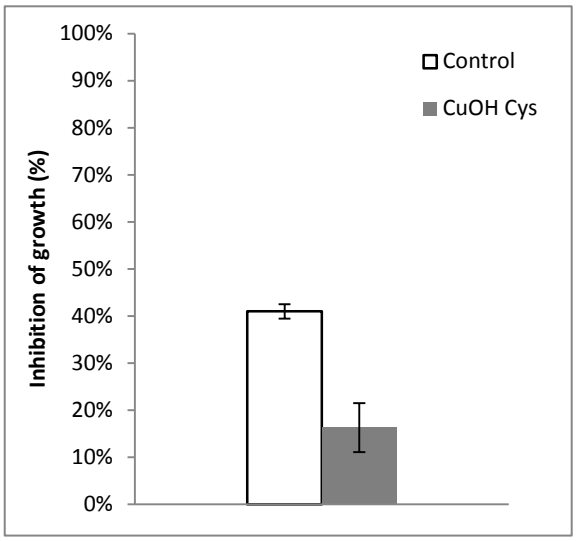

Fig. 37 – Inhibition of growth of *E. coli* by CuO Cys nanoparticles at 6h, 100 ppm of copper, and 10^{-2} bacterial dilution. The white column represents the results for control (40 mM solution of copper (II) chloride) and the grey one for the suspension.

4.1.2.3. Copper phosphates

Another possible way to obtain nanoparticles of a different mineral phase is by substituting the –OH groups for other groups such as $-PO_4^{3-}$. By increasing the pH of a solution containing 40 mM with Na_3PO_4, the copper precipitates at around pH 4 (Fig. 38). The copper remains agglomerated till pH 10. The characterization of these particles by XRD shows that a great part of the peaks obtained matches with the XRD pattern of a mixture of

two copper hydrogen phosphate hydrate mineral phases: $Cu_4H(PO_4)_3{\cdot}3H_2O$ and $CuHPO_4{\cdot}H_2O$ (Fig. 39). Thus, the use of Na_3PO_4 resulted in the production of unmodified copper phosphates of two different compositions.

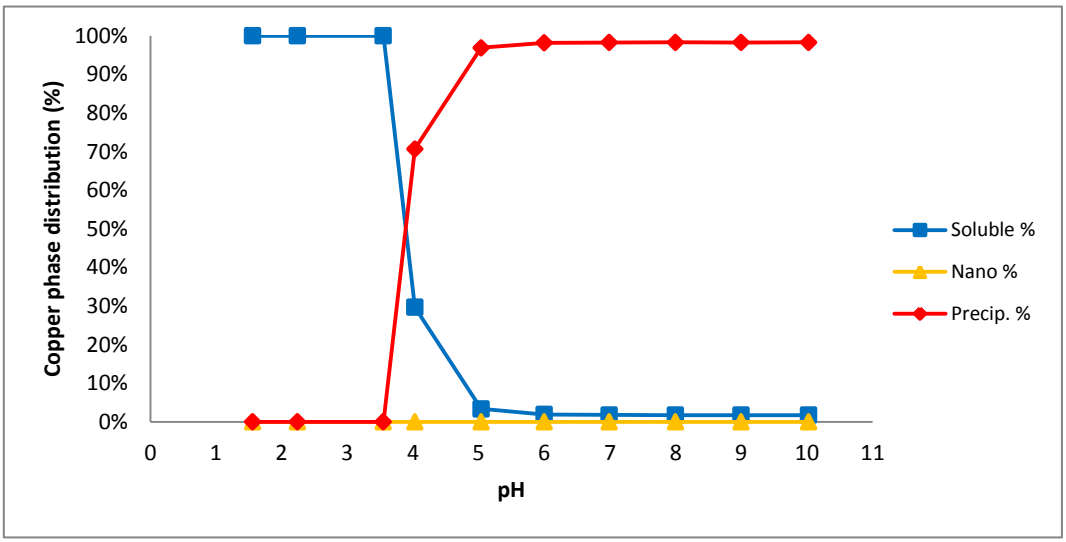

Fig. 38 – Copper phase distribution (%) with varying pH during the synthesis of copper phosphate ([Cu]=40 mM).

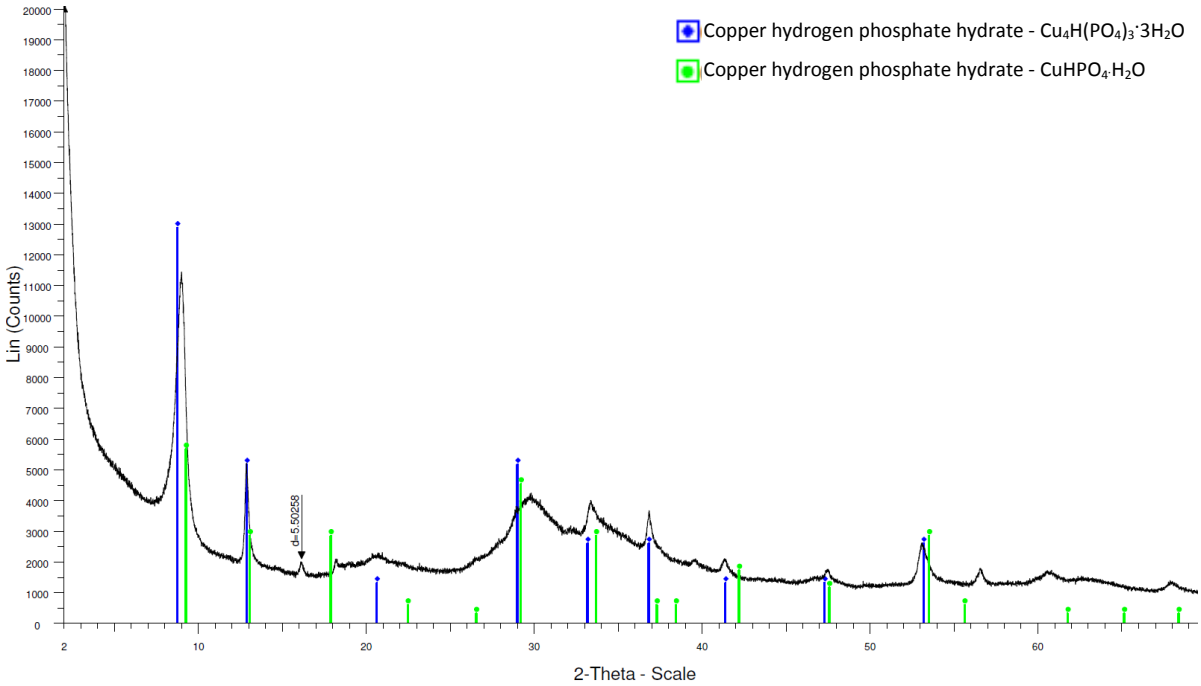

Fig. 39 – XRD characterization of unmodified copper phosphate particles. The lines in blue represent the XRD reference for $Cu_4H(PO_4)_3{\cdot}3H_2O$ and the green ones for $CuHPO_4{\cdot}H_2O$.

Citric acid is a symmetric tricarboxylic acid (Fig. 40) and is naturally occurring (pKa=3.13; pKa=4.76; pKa=6.40 [78]). This weak organic acid has been previously used for the production of copper oxo-hydroxide nanoparticles [77]. Thus, it was used for the

production of copper phosphate nanoparticles. As the pH was increased nanoparticles started to form (Fig. 41). The highest amount of nanoparticles (63.6%) was obtained for pH 9.28. At pH 6.1, the mean particle size was 1.0 nm (Fig. 42). The characterization of these nanoparticles by XRD is shown on Fig. 43. The only identified peaks corresponded to halite (NaCl). The XRD pattern was compared with the XRD references of several copper phosphate phases (cornetite - $Cu_3(PO_4)(OH)_3$; libethenite - $Cu_2(PO_4)(OH)$; ludjibaite - $Cu_5(PO_4)_2(OH)_4$; pseudomalachite - $Cu_5(PO_4)_2(OH)_4$; reichenbachite - $Cu_5(PO_4)_2(OH)_4$), but the peaks could not be identified. These unidentified peaks are broad, which may indicate that we are in the presence of an amorphous phase, possibly due to the integration of the ligand in the particle structure. Although the yield on the production of nanoparticles was not high, the copper phase distribution of these nanoparticles at pH 6 when diluted in broth was still tested (Fig. 43). Only a small portion of nanoparticles dissolved because to start with there was only 57% of nanoparticulate copper. The results of the antimicrobial activity test show that a higher inhibition of the bacterial growth was also obtained (Fig. 44). Although, a better result was obtained, these nanoparticles also did not show a complete efficacy on the inhibition of bacterial growth (Fig. 45).

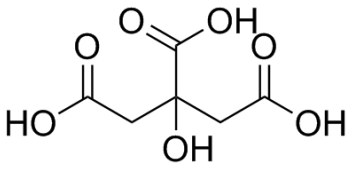

Fig. 40 – Structure of citric acid.

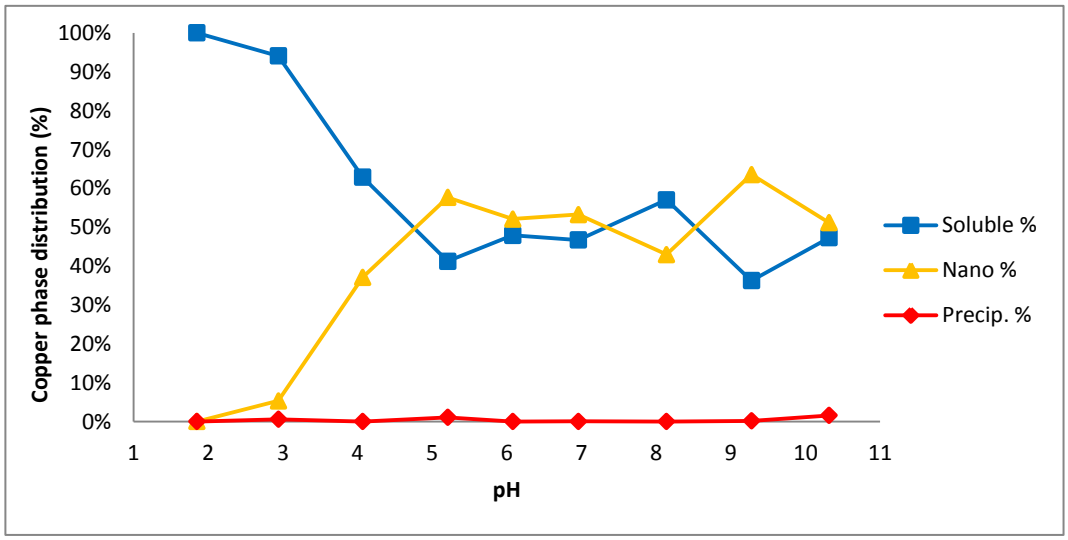

Fig. 41 – Copper phase distribution (%) with varying pH during the synthesis of copper phosphate nanoparticles ([Cu]=40 mM) in the presence of citric acid (40mM).

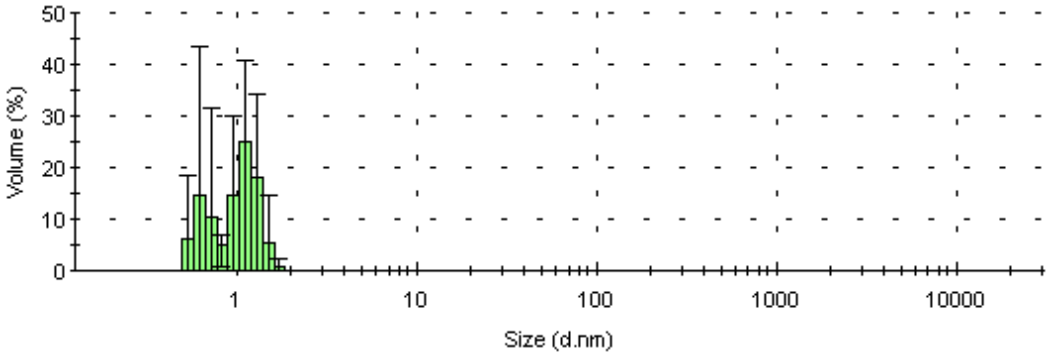

Fig. 42 - Particle size distribution at pH 6 during the synthesis of copper phosphates ([Cu]=40 mM) in the presence of citric acid (20 mM).

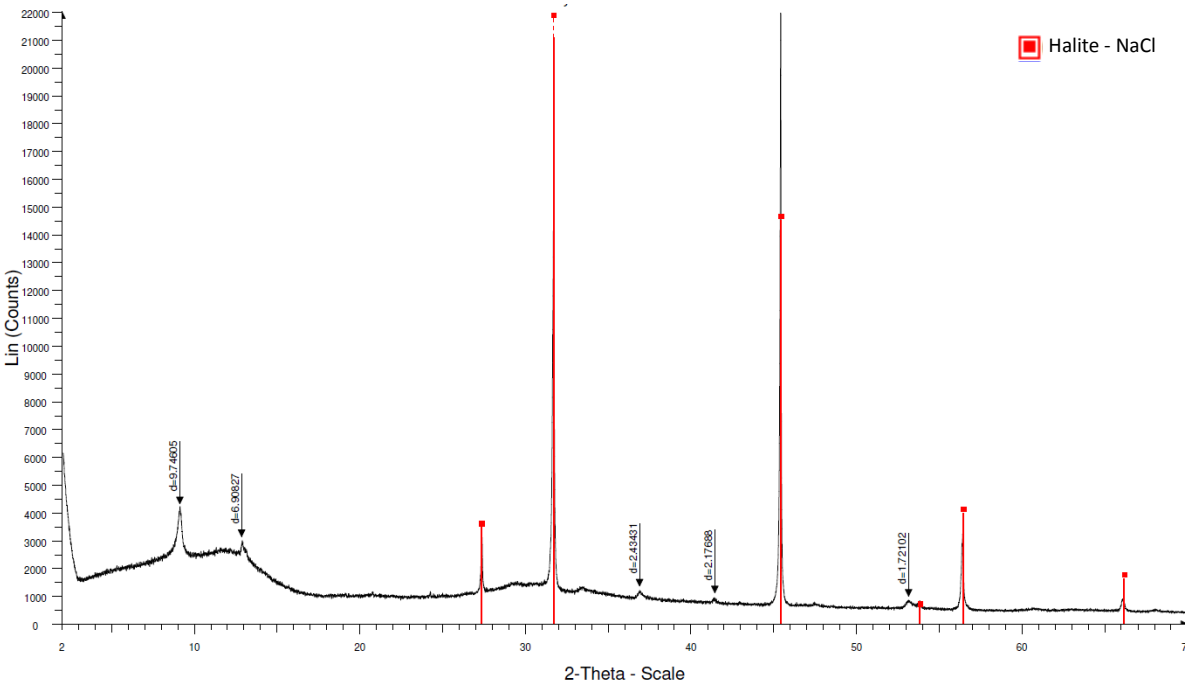

Fig. 43 – XRD characterization of $CuPO_4$ Cit nanoparticles. The lines in red represent the XRD reference for Halite (NaCl).

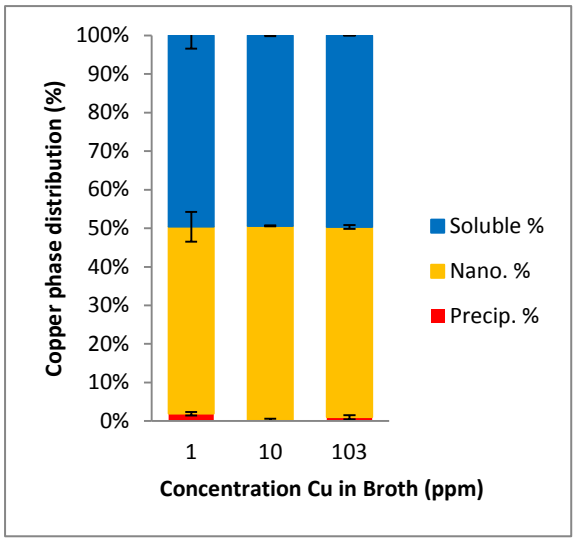

Fig. 44 - Copper phase distribution (%) of $CuPO_4$ Cit diluted in broth at concentrations 1, 10 and 103 ppm.

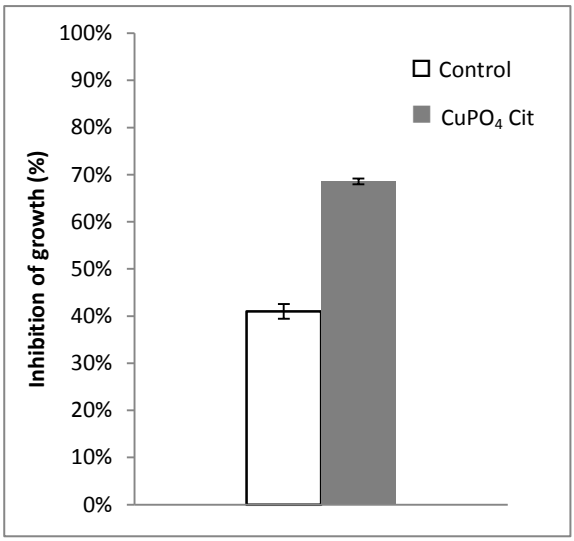

Fig. 45 – Inhibition of growth of *E. coli* by $CuPO_4$ Cit nanoparticles at 6h, 100 ppm of copper, and 10^{-2} bacterial dilution. The white column represents the results for control (40 mM solution of copper (II) chloride) and the grey one for the suspension.

4.1.3. Lamellar structures

Another way of producing and stabilizing nanoparticles is by using surfactant structures, namely lamellar structures. In fact, surfactants may act as stabilizers, capping agents, and/or a template, thus controlling size, growth and/or agglomeration of nanoparticles [85]. There are different types of surfactants, and they can vary in charge. An example of an anionic surfactant is sodium dodecyl sulphate (SDS) and an example of a cationic one is octadecyltrimethylammonium bromide (C_{18}TAB).

4.1.3.1. Negatively charged

SDS (Fig. 46) has also been used as a dispersive agent for the production of metal-based nanoparticles [86, 87]. It can act as a dispersive agent due to its hydrophobic chain, preventing the particles from agglomerating. Thus, 20 mM of copper (II) and 10 mM of SDS (a concentration slightly above its critical micelle concentration, which is 7-8 mM in water [55]) was used in the synthesis. The copper phase distribution during the synthesis can be seen on Fig. 47. With this method, nanoparticles were not formed and a substantial precipitation occurred at pH 5. The particle size distribution was determined by dynamic light scattering, confirmed that the particles were not in true nano range (pH 6.9; Fig. 48), i.e. were larger than 100 nm.

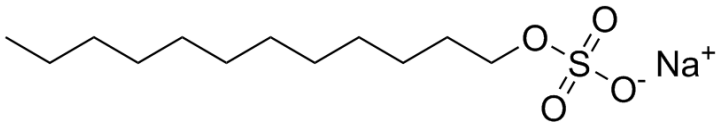

Fig. 46 – Structure of sodium dodecyl sulphate (SDS).

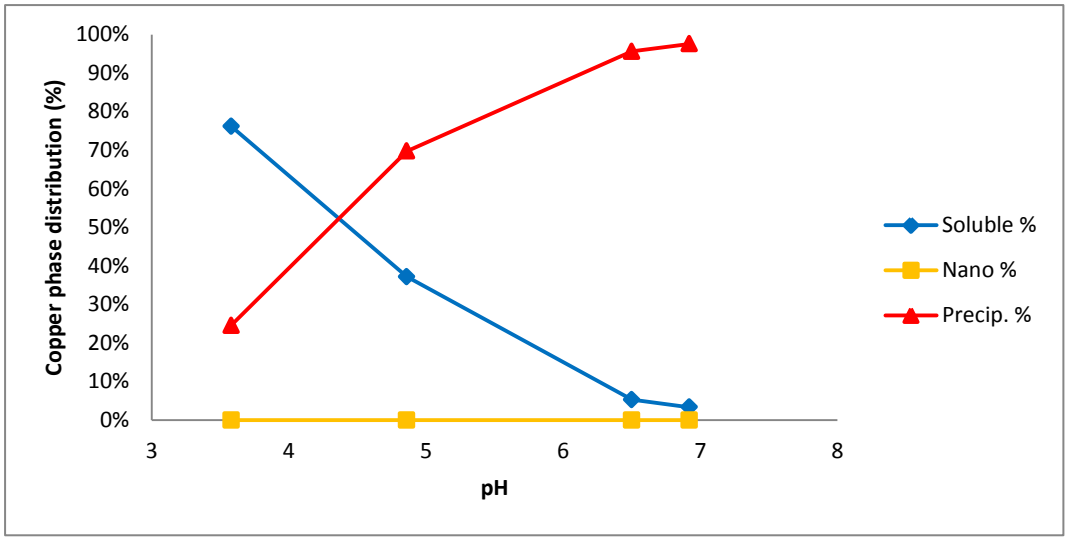

Fig. 47 - Copper phase distribution (%) with varying pH during the synthesis of copper oxo-hydroxide ([Cu]=20 mM) in the presence of SDS (10 mM).

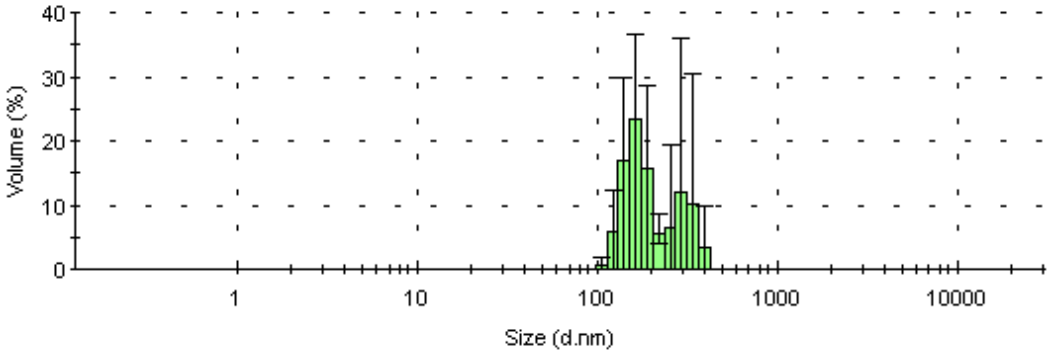

Fig. 48 - Particle size distribution at pH 6.9 during the synthesis of copper oxo-hydroxide ([Cu]=20 mM) in the presence of SDS (10 mM).

The pH at which SDS is added may have an effect on the production of nanoparticles and, to test this parameter, this surfactant was added at pH 6.5 after the copper oxo-hydroxide particles had already been produced. When SDS was added, the pH changed from 6.5 to 6.9, but other than that, the results were almost the same as for the previous experiment: even after adding SDS, the particles were large (Fig. 49). Also, it is possible to see that on the previous experiment the ligand did not have influence on the precipitation of the copper, since the precipitation occurred at about the same pH. By observing the particle size before adding SDS, it is possible to see that there were two populations of particles, both of them with sizes higher than 100 nm (Fig. 50A). After adding SDS, the particle size was still higher than 100 nm, but apparently some of the particles diminished in size (Fig. **50**B). At a higher pH (7.7) the results were the same, which means that the increasing in the pH did not have a great effect on the particle size (Fig. 50C). Thus, the addition of SDS at a higher pH, after copper oxo-hydroxide particles were formed, did not lead to the production

of nanoparticles. In this case SDS did not act as a dipersant, probably due to the formation of large micelles.

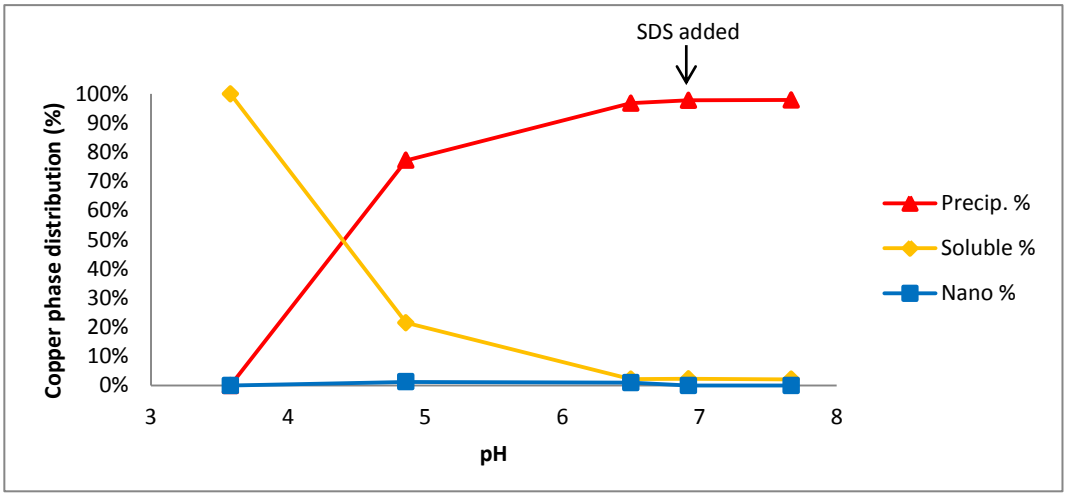

Fig. 49 - Copper phase distribution (%) with varying pH during the synthesis of copper oxo-hydroxide ([Cu]=20 mM) to which SDS (10 mM) was added at pH 6.5.

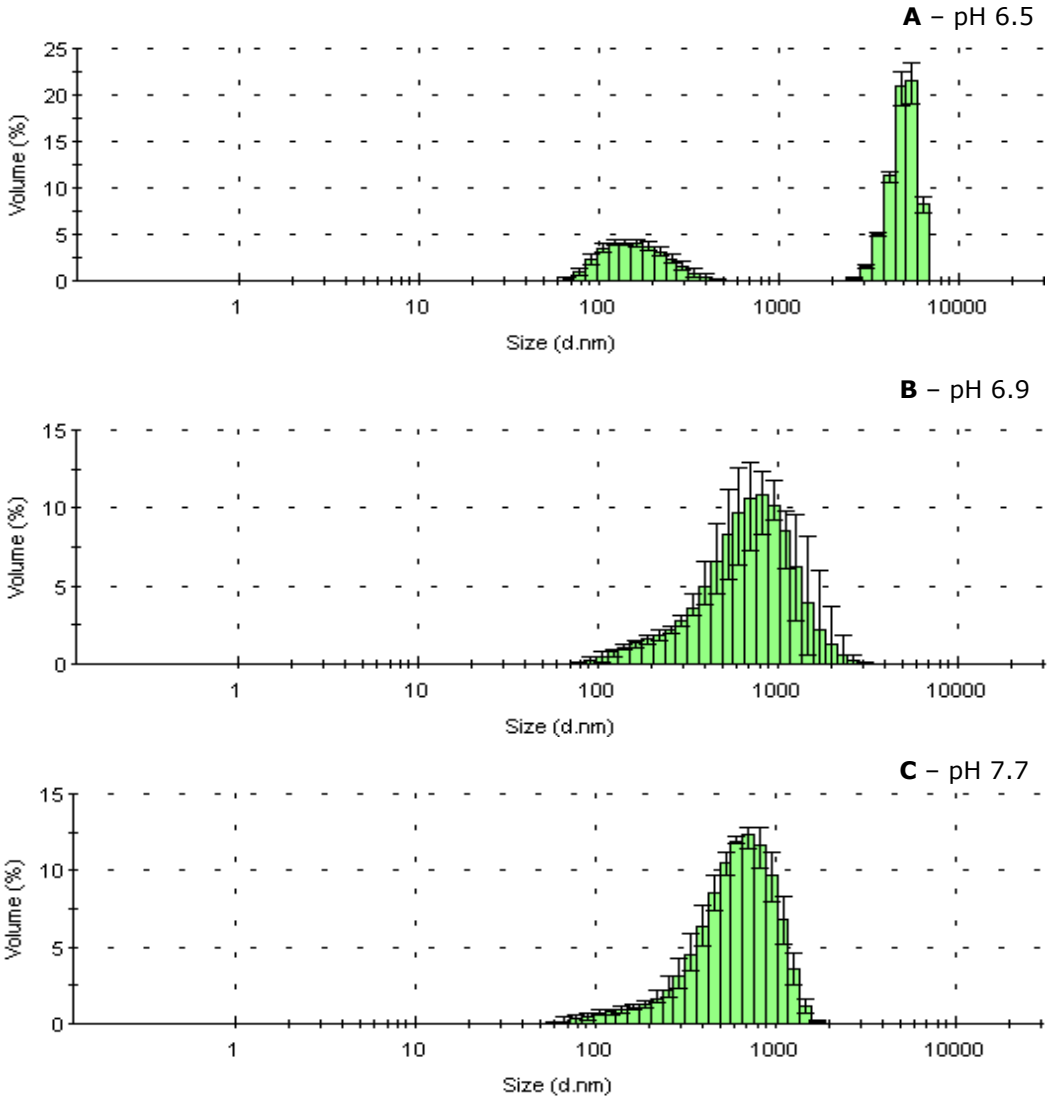

Fig. 50 - Particle size distribution at various pH's during the synthesis of copper oxo-hydroxide ([Cu]=20 mM) to which SDS (10 mM) was added at pH 6.5. (A) pH 6.5 (-SDS); (B) pH 6.9 (+SDS); (C) pH 7.7 (+SDS).

4.1.3.2. Positively charged

Octadecyltrimethylammonium bromide (C_{18}TAB; Fig. 51) was also tested to produce copper nanoparticles. It is a cationic surfactant and it was added to the suspension previously prepared (Cu + SDS, pH 7.7) with a final concentration of 10 mM. This surfactant was added in order to act as a dispersive agent and coat the particles, making them positively charged rather than negatively, which may result in a higher interaction between the nanoparticles and the bacterial membrane. However, particle size remained over 100 nm (Fig. 52), which means that the addition of this ligand did not have a pronounced effect on particle size and that the two surfactants together did not dispersed the particles, possibly due to charge neutralization.

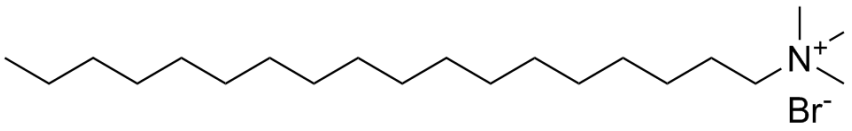

Fig. 51 - Octadecyl trimethyl ammonium bromide (C_{18}TAB).

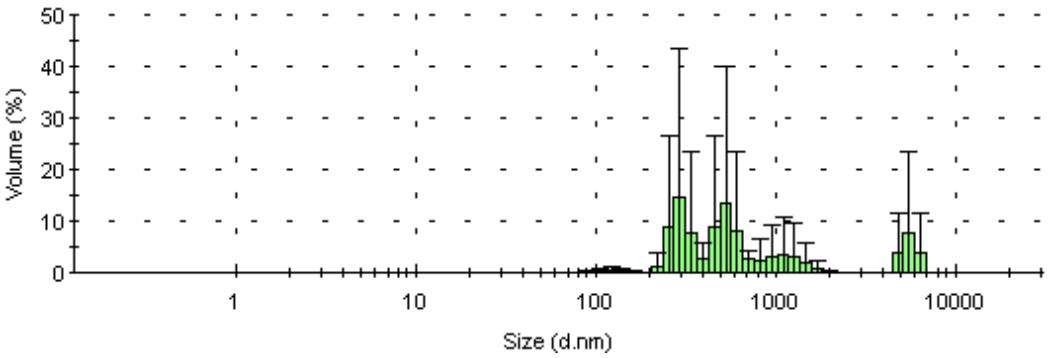

Fig. 52 - Particle size distribution at pH 7.4 during the synthesis of copper oxo-hydroxide ([Cu]=20 mM) to which SDS (10 mM) was added at pH 6.5 and C_{18}TAB (10 mM) was added at pH 7.

To determine if oxo-hydroxide particles could be produced using tartaric acid as a ligand as previously were further dispersed by the addition of C_{18}TAB, another experiment was carried out. NaOH was added to a 20 mM copper (II) and 10 mM tartaric acid solution and, at pH 6.4, C_{18}TAB was added (10 mM). Before adding C_{18}TAB there were polydisperse population of particles, some of them with sizes below 100 nm (Fig. 53A). However, with the addition of C_{18}TAB, all particles had sizes over 100 nm (Fig. 53B). It seems that C_{18}TAB induced the nanoparticles that were present to agglomerate, instead of acting as a dispersive agent.

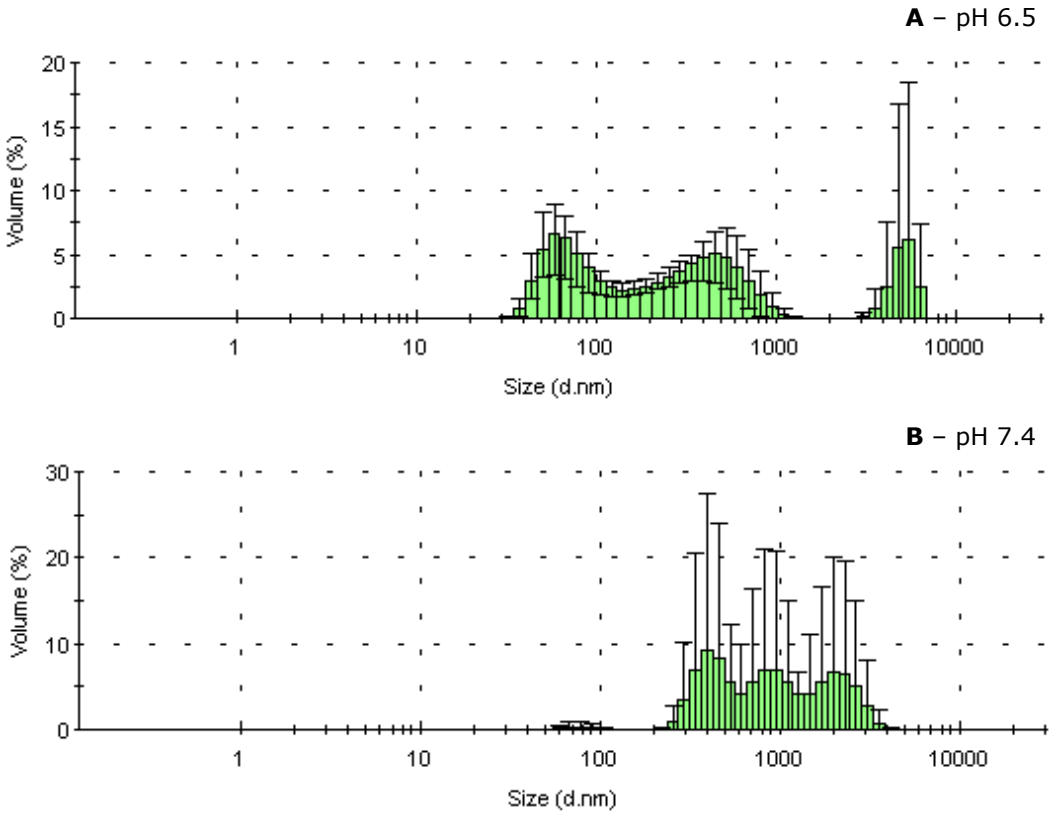

Fig. 53 - Particle size distribution at various pH's during the synthesis of copper oxo-hydroxide ([Cu]=20 mM) in the presence of tartaric acid (10 mM), to which C_{18}TAB (10 mM) was added at pH 6.4. (A) pH 6.4 (-C_{18}TAB); (B) pH 7.4 (+C_{18}TAB).

4.1.4. Positively charged nanoparticles

The surface charge of the nanoparticles may have an influence on their interaction with the bacterial membranes. The bacterial membranes present a net negative electrostatic surface charge [88] and positively charged nanoparticles may have a greater interaction with bacteria. So far, the nanoparticles obtained should have a negatively charged surface. The zeta potential can be measured for particles with a very high refractive index (e.g. gold) down to 2 nm. The oxo-hydroxides of transition metals are not as refractive and, typically, the measurements can only be performed for particles with 10-15 nm or greater. Thus, it was not possible to measure the potential of the nanoparticles previously prepared, since they were too small. However, it was possible to measure the zeta potential for CuOH TartAd. The method for the production of the nanoparticles was the same as the one used in previous work [77]. Note that these particles were recovered at pH 6, since that at this pH the particles are partly agglomerated thus enabling the zeta potential measurement. The mean zeta potential obtained was -14.6 mV (Fig. 54), which confirms that this type of nanoparticles are negatively charged. This may have led to a lower interaction between nanoparticles and bacterium cell wall. The zeta potential indicates also the level of stability of

the nanoparticles and, in this case, it indicates that the nanoparticles are quiet unstable, since that the higher the zeta potential, the more stable are the particles.

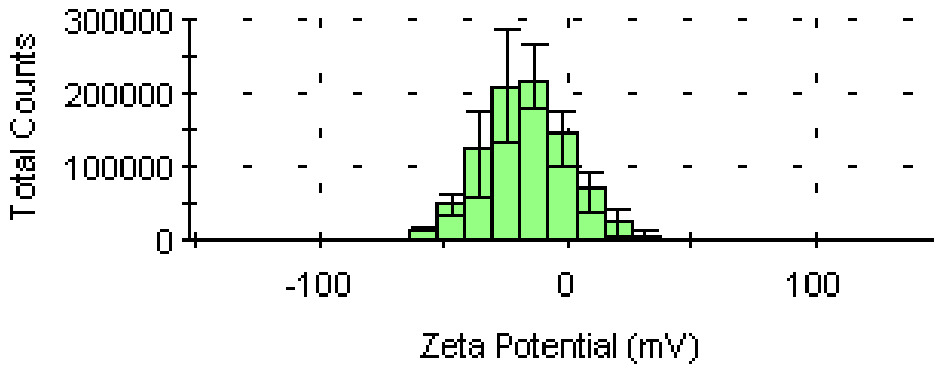

Fig. 54 – Zeta potential distribution at pH 6 of CuOH TartAd, using water as dispersant.

In order to obtain positively charged nanoparticles, carnitine (Fig. 55) was used as a ligand. At physiological pH, carnitine is a zwitterion (pka=3.80 [78]), i.e. the molecule is neutral, but it presents a positive and a negative charge at different sites. The expected interaction between carnitine and copper should be via the carboxylic group (negatively charged), while the amine group should be oriented to the outside of the particles, giving a positive charge to the surface of the particle. Since carnitine shares some functional groups with tartaric acid, it may also act as a dispersive agent, allowing the production of nanoparticles. Thus, the effect of this ligand on the production of copper oxo-hydroxide nanoparticles was tested. A solution containing 20 mM of copper (II) and 20 mM of carnitine was prepared and its pH was increased by adding NaOH. The copper phase distribution as the pH was increased (Fig. 56) shows that from pH 6.5 there was a substantial precipitation. According to these data, nanoparticles were not formed during this synthesis. The particle size distribution was determined and for pH 6.5 the particles had a mean size of 124 nm (Fig. 57). The obtained particles are not in the so called nano-range but they are submicron. The zeta potential of these nanoparticles was also determined. At pH 6.5 the particles had a mean zeta potential of 39.1 mV (Fig. 58) which indicates that the surface of the nanoparticles is positively charged. These particles were also characterized by XRD (Fig. 59). The mineral phase obtained in this case was the same as the one obtained for unmodified copper oxo-hydroxides, paratacamite ($Cu_2Cl(OH)_3$). This may indicate that the carnitine does not make part of the structure of the particles, but it is coating them. A study on the copper phase distribution when these particles were diluted in broth shows that a part of the submicron particles decrease size, they became nanoparticulate, and that a part of these particles solubilised (Fig. 60). Thus, the problem with instability of the particles

obtained so far was not overcome by using this ligand. Also, even though the particles were larger, a partial solubilisation occurred. Nevertheless, their antimicrobial activity was tested. The results show that the particles led to a 68% inhibition of the bacterial growth (Fig. 61) and, although quite a substantial improvement in relation to the previous one was achieved, the bactericidal effect is still insufficient. The positive charge of the particles may have led to a higher interaction with the bacterial membrane but the antimicrobial activity was not much higher than the ones before.

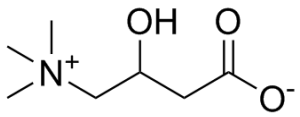

Fig. 55 – Structure of carnitine.

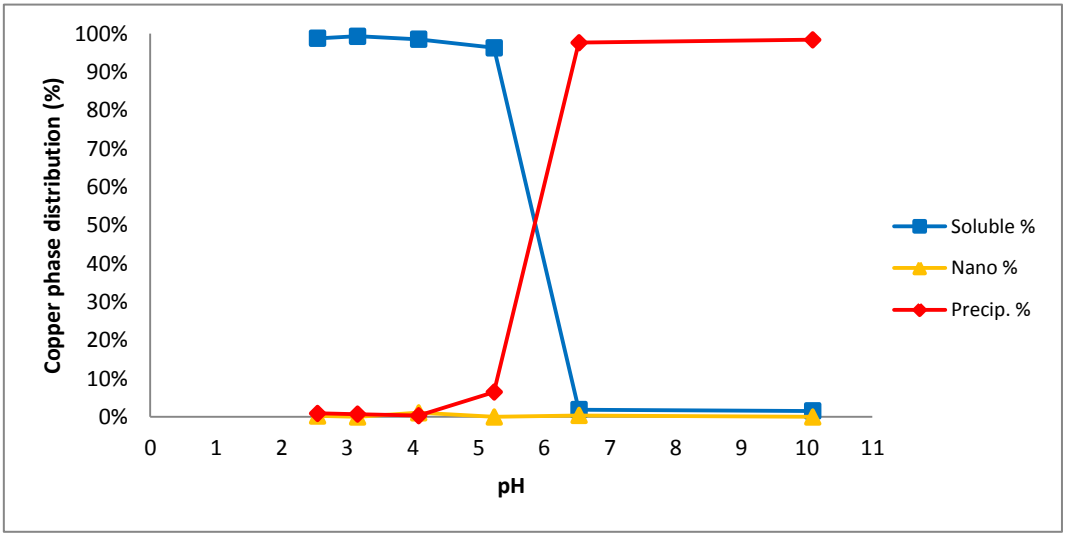

Fig. 56 - Copper phase distribution (%) with varying pH during the synthesis of copper oxo-hydroxide ([Cu]=20 mM) in the presence of carnitine (20 mM).

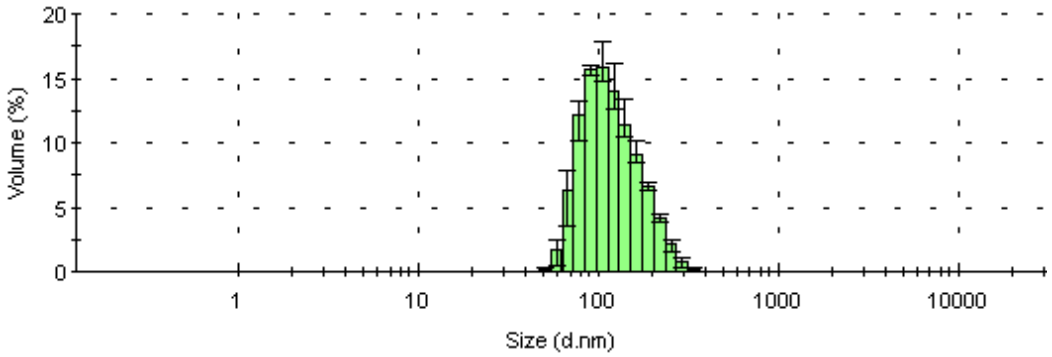

Fig. 57 - Particle size distribution at pH 6.5 during the synthesis of copper oxo-hydroxide ([Cu]=20 mM) in the presence of carnitine (20 mM).

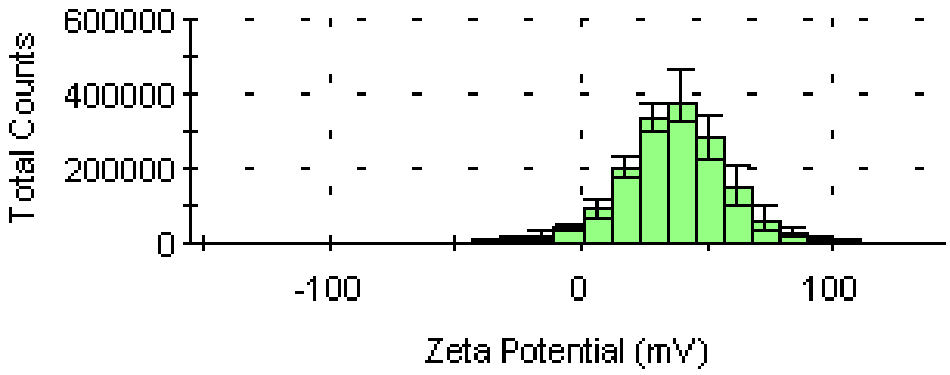

Fig. 58 – Zeta potential distribution at pH 6.5 during the synthesis of copper oxo-hydroxide ([Cu]=20 mM) in the presence of carnitine (20 mM).

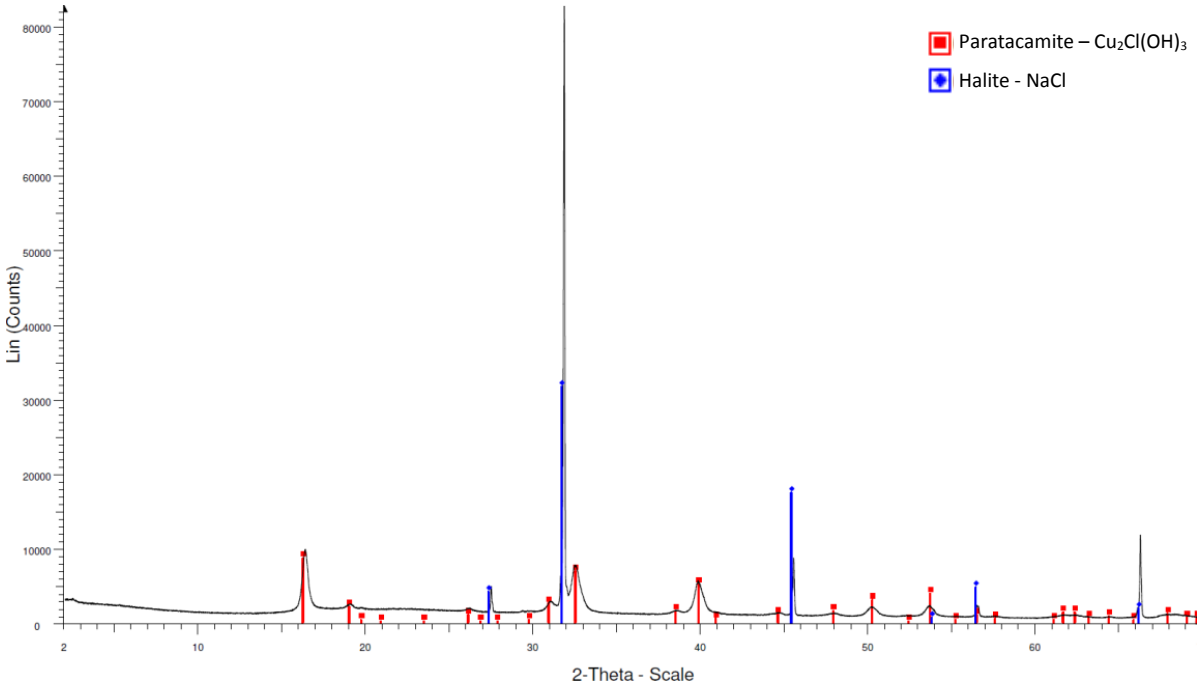

Fig. 59 – XRD characterization of copper (II) oxo-hydroxide particles modified with carnitine. The lines in red represent the XRD reference for Paratacamite ($Cu_2Cl(OH)_3$) and the blue ones for Halite (NaCl).

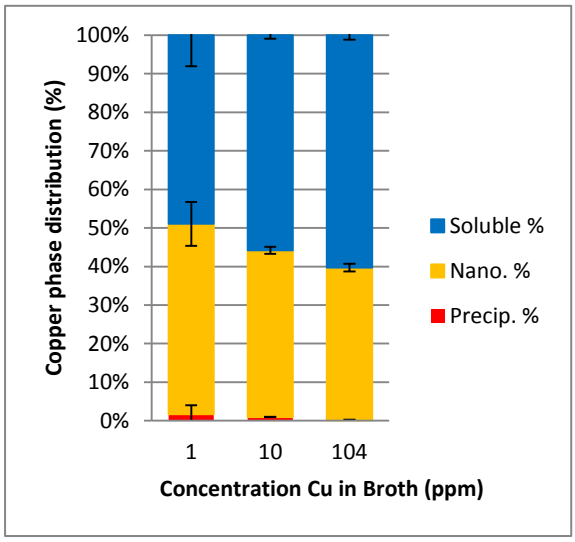

Fig. 60 - Copper phase distribution (%) of CuOH Car diluted in broth at concentrations 1, 10 and 104 ppm.

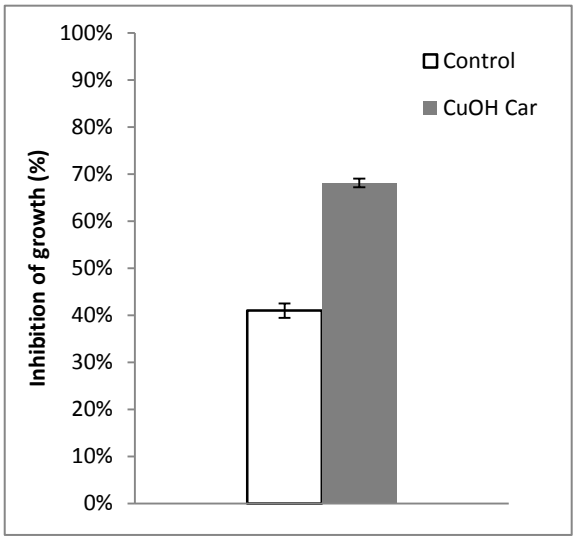

Fig. 61 – Inhibition of growth of *E. coli* by CuOH Car nanoparticles at 6h, 100 ppm of copper, and 10^{-2} bacterial dilution. The white column represents the results for control (40 mM solution of copper chloride) and the grey one for the suspension.

Next, in order to try to further disperse the copper particles with carnitine, a higher concentration of carnitine was tested. Thus, 40 mM of copper (II) and 120 mM of carnitine were used, following the same method. However, a polydisperse population of large particles was still obtained (Fig. 62), and it was concluded that with this method the use of this ligand alone is not a good option for the production of copper nanoparticles in water.

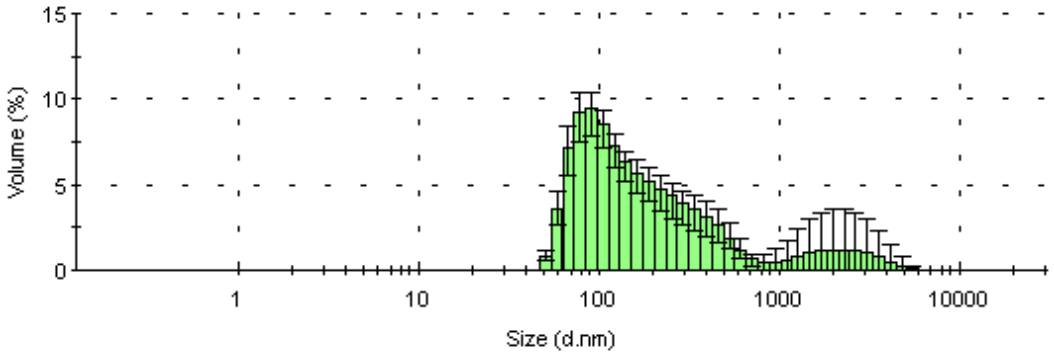

Fig. 62 - Particle size distribution at pH 7 during the synthesis of copper oxo-hydroxide ([Cu]=40 mM) in the presence of carnitine (120 mM).

Tartaric acid used previously shown to be a good dispersive ligand for copper oxo-hydroxides [77]. Therefore, this ligand was used in combination with carnitine. Here a solution of 40 mM of copper (II), 20 mM of carnitine, and 20 mM of tartaric acid was prepared and NaOH was added to it. At pH 5 the average particle size of is 0.7 nm

(Fig. 63A). At pH 6, there was a substantial precipitation and all particles had a size higher than 1000 nm (Fig. 63B). This agglomeration was probably due to charge neutralization.

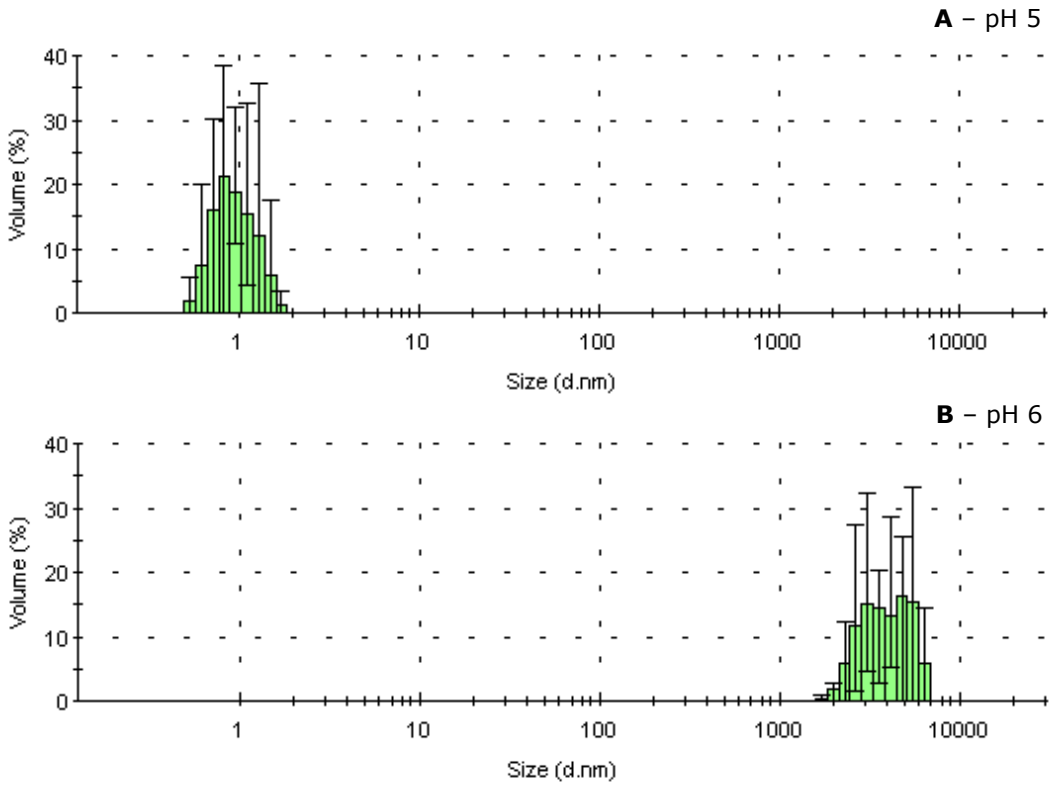

Fig. 63 - Particle size distribution at various pH's during the synthesis of copper oxo-hydroxide ([Cu]=40 mM) in the presence of carnitine (20 mM) and tartaric acid (20 mM). (A) pH 5; (B) pH 6.

4.2. ZINC

Zinc, like copper, acts as a Lewis acid, being an electron pair acceptor. Thus, when zinc (II) chloride ($ZnCl_2$) is dissolved in water the resulting solution has a low pH:

$$ZnCl_2\ (s) \rightarrow Zn^{2+}(aq) + 2Cl^{-}(aq) + 2H_2O\ (l) \quad (5)$$

$$Zn(H_2O)_n^{2+} + H_2O \rightarrow Zn(H_2O)_{n-1}(OH)^{1+} + H_3O^{+} \quad (6)$$

As a control experiment for the production of unmodified zinc oxo-hydroxides, the pH of a zinc solution (40 mM) was gradually increased with NaOH. Initially, zinc remained soluble but as the pH was raised (>pH7), a white precipitate started to form (Fig. 64). This precipitation is due to the formation of unmodified zinc oxo-hydroxide particles, which are insoluble. These particles were characterized by XRD (Fig. 65). The identified peaks matched the XRD pattern for halite (NaCl). The remaining peaks were also compared to the

pattern for several zinc hydroxide mineral phases (ashoverite, sweetite, and wulfingite), but they did not match any of those. Thus, it was not possible to determine the mineral phase of these particles. In comparison to the curve of the synthesis of unmodified copper oxo-hydroxide particles (Fig. 14), the precipitation of zinc occurs for a much higher pH. This may result on the production of nanoparticles for only high pHs.

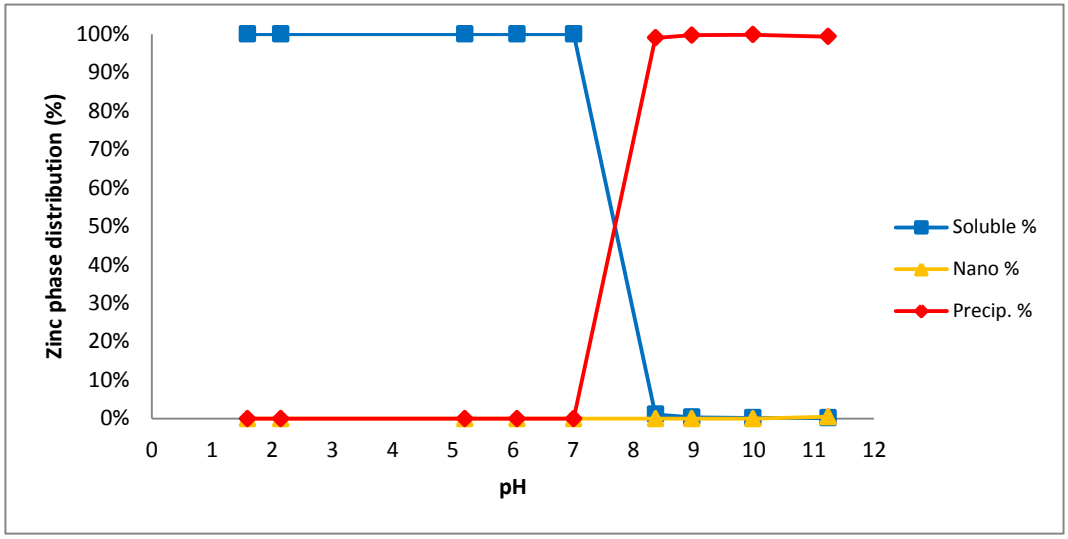

Fig. 64 – Zinc phase distribution (%) with varying pH during the synthesis of zinc oxo-hydroxide ([Zn]=40 mM).

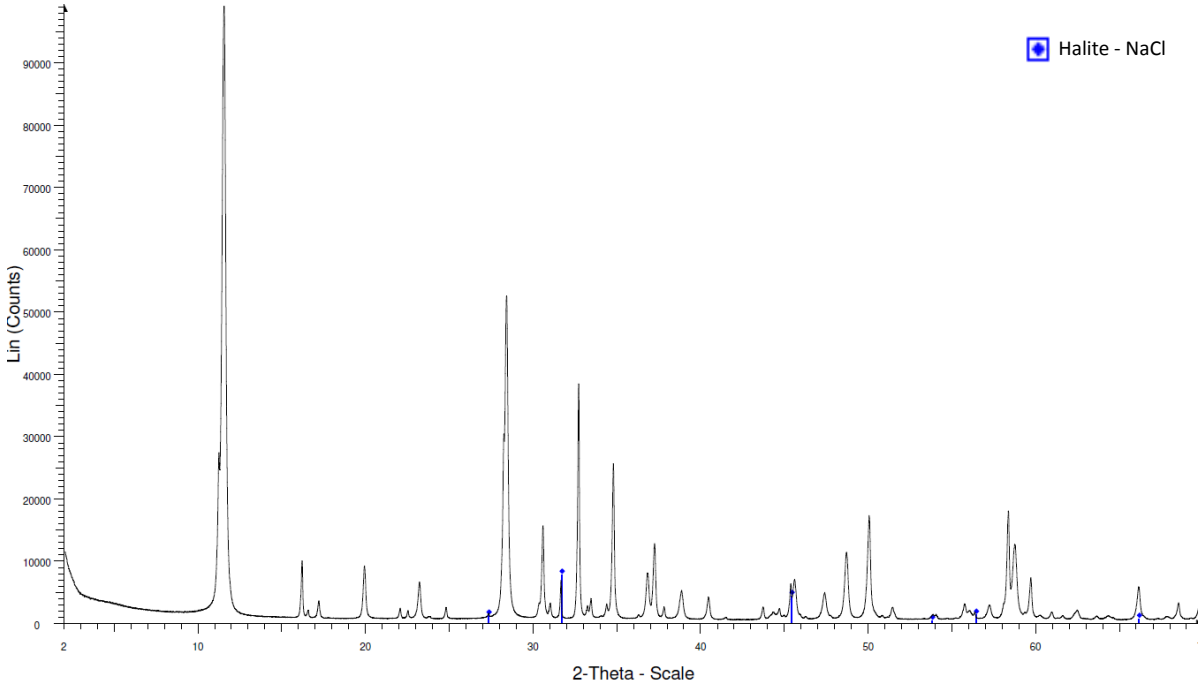

Fig. 65 – XRD characterization of unmodified zinc oxo-hydroxide particles. The peaks in blue represent the XRD pattern for Halite (NaCl).

4.2.1. Zinc nanoparticles

Cysteine allowed the production of copper nanoparticles at higher pH and has also affinity for zinc. This amino acid was used for the production of zinc nanoparticles. Firstly the pH of an equimolar (40 mM) solution of zinc (II) and cysteine was gradually increased. The zinc phase distribution during the synthesis is shown in Fig. 66. There was substancial precipitation at pH 5. The agglomeration occurred for a lower pH than for unmodified zinc oxo-hydroxide (Fig. 64). Only a small amount of nanoparticles was obtained and the highest amount was obtained for pH 10.2 (30.1%). In this case, the cysteine did not have enough dispersive power and did not lead to a major production of nanoparticles. The use of a higher concentration of cysteine could lead to higher yield on the production of nanoparticles.

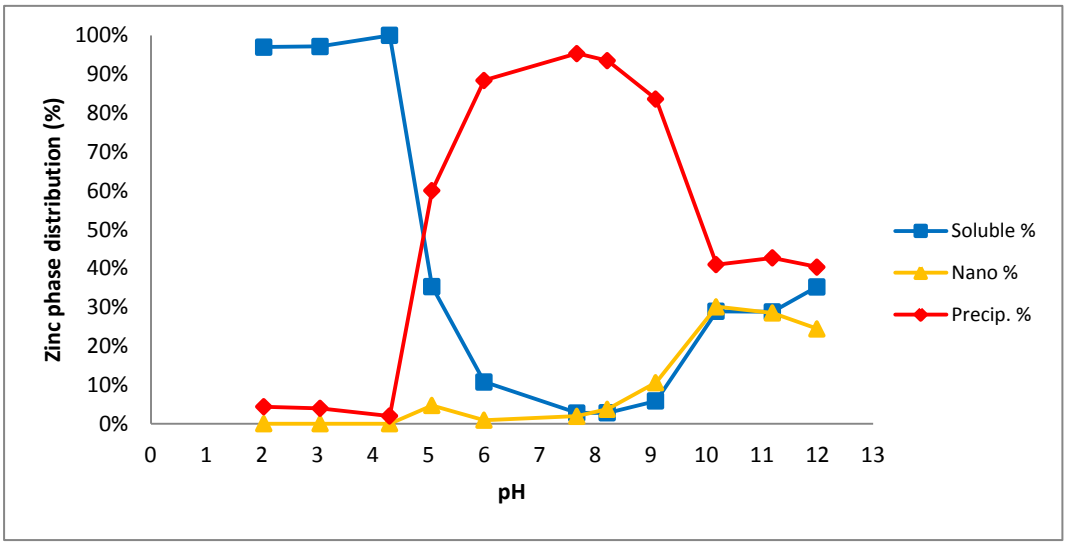

Fig. 66 – Zinc phase distribution (%) with varying pH during the synthesis of zinc (II) oxo-hydroxide ([Zn]=40 mM) in the presence of cysteine (40 mM).

Thus, a higher concentration of cysteine was used. A solution containing 40 mM of zinc (II) and 60 mM of cysteine was prepared and the synthesis was carried out. From pH 4 nanoparticles started to form (Fig. 67). The highest amount of nanoparticles was obtained at pH 6 (93.0%) The mean particle size of the particles at pH 7.6 was 0.9 nm (Fig. 68). These nanoparticles were further characterized by XRD (Fig. 69). Also in this case, only halite was identified. The remaining peaks were also compared to the XRD pattern for several zinc hydroxide mineral phases (ashoverite, sweetite, and wulfingite), but they did not match any of those. However, there is a difference when comparing to the spectrum obtained for the unmodified particles (Fig. 65); the unidentified peaks are more defined than for the naniparticulate ones. Perhaps also in this case an amorphous material was obtained. When tested against *E. coli*, these nanoparticles showed not to have antimicrobial activity. Instead

of inhibiting the bacterial growth, these nanoparticles led to an increase of 7.7% of the bacterial growth (Fig. 70).

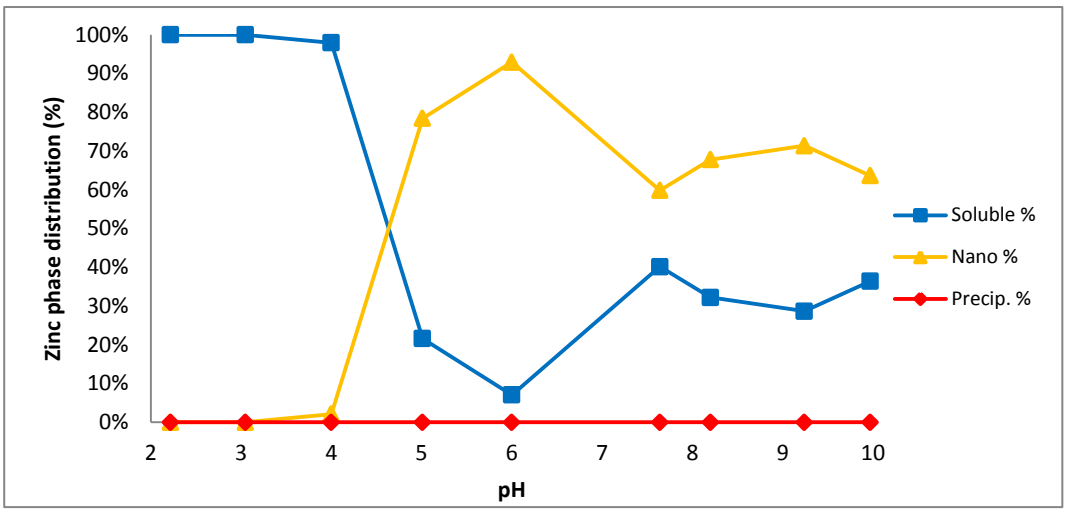

Fig. 67 – Zinc phase distribution (%) with varying pH during the synthesis of zinc (II) oxo-hydroxide nanoparticles ([Zn]=40 mM) in the presence of cysteine (60mM).

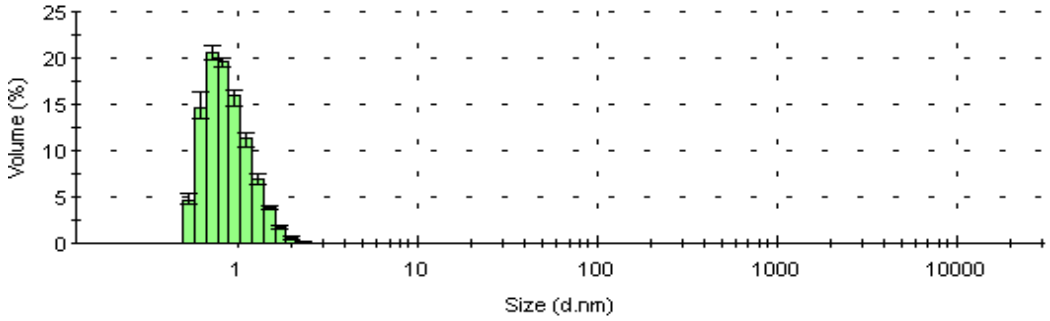

Fig. 68 - Particle size distribution at pH 7.6 during the synthesis of zinc (II) oxo-hydroxide ([Cu]=40 mM) in the presence of cysteine (60 mM).

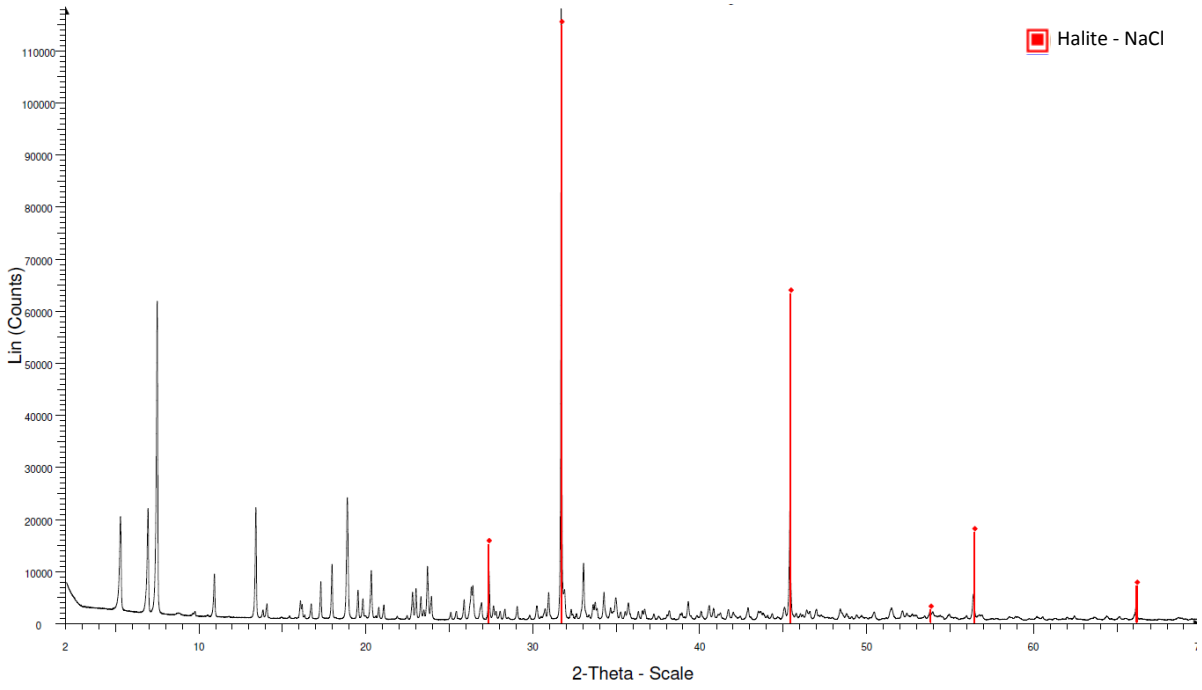

Fig. 69 – XRD characterization of ZnOH Cys nanoparticles. The lines in red represent the XRD reference for Halite (NaCl).

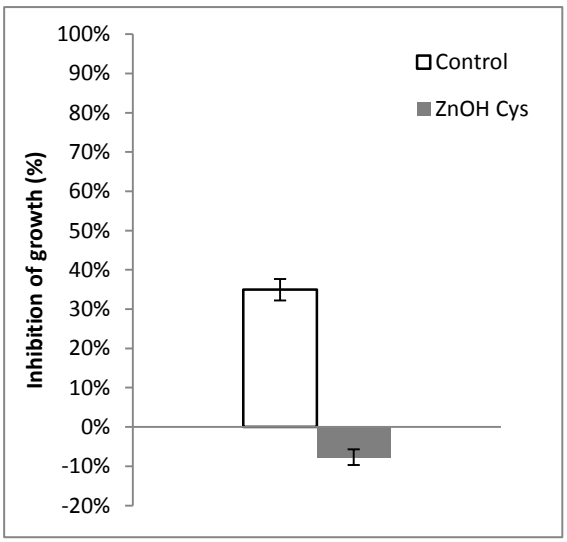

Fig. 70 – Inhibition of growth of *E. coli* by ZnOH Cys nanoparticles at 6h, 100 ppm of copper, and 10^{-2} bacterial dilution. The white column represents the results for control (40 mM solution of zinc chloride) and the grey one for the suspension.

Tartaric acid was also used again to further disperse the particles produced with an equimolar solution of zinc and cysteine. Therefore, part of the cysteine used before was substituted by tartaric acid and a solution containing 40 mM of zinc (II) and 20 mM of cysteine and tartaric acid was used for this synthesis. The agglomeration started at pH 5.0 and from this pH on it kept rising until pH 7.0 (Fig. 71). At pH 8.1, nanoparticles were produced and the precipitated zinc decreased. The highest amount of nanoparticles was obtained at pH (33.5%). Even at this pH, there was still a high amount of precipitate. Thus, this synthesis did not result in satisfactory yield of production of nanoparticles.

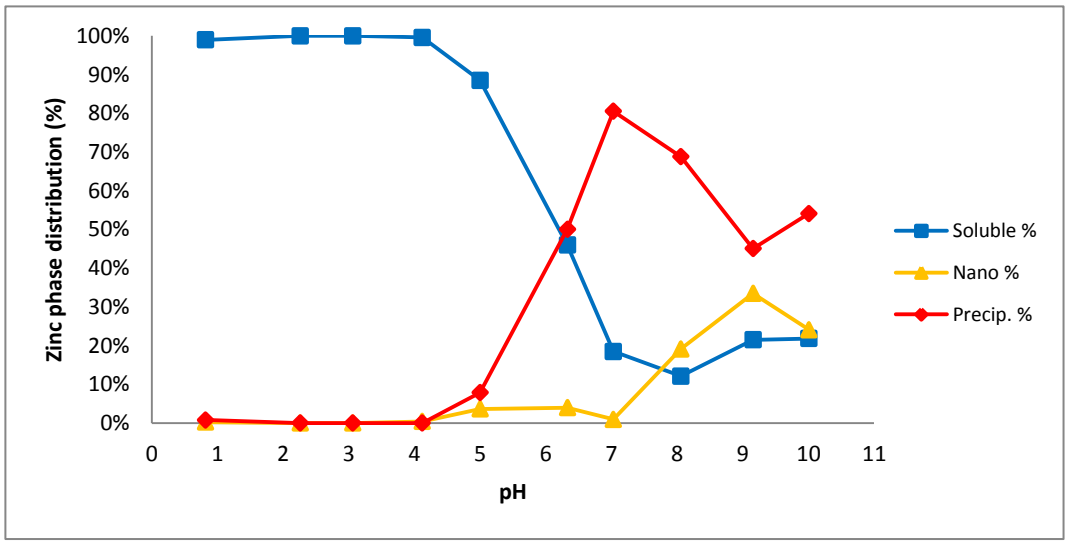

Fig. 71 – Zinc phase distribution (%) with varying pH during the synthesis of zinc (II) oxo-hydroxide nanoparticles ([Zn]=40 mM) in the presence of cysteine (20mM) and tartaric acid (20mM).

4.3. EFFECT OF AQUEOUS RESUSPENSION OF NANOPARTICLES

Throughout this project, a major problem has been the partial dissolution of the nanoparticles when diluted in broth, the bacterial culture medium used in the antibacterial activity tests. However, it was not known if this dissolution was due to the dilution of the suspension, i.e. to a lower concentration of the particles. So, in order to clarify this, a powder obtained from a sub-micron suspension was resuspended at around the same concentration in water and in broth (4 mM). This should show whether the dissolution of particles is due to dilution or to the composition of the broth. The resulting copper phase distribution is shown in Fig. 72. Whilst the suspension remained mostly agglomerated in water, the same was not verified in broth. In fact, in broth most of the copper solubilised (59.6%) and a part of it turned nanoparticulate (40.4%). This shows that the solubilisation of the particles in broth is not due to the dilution factor, but it is probably due to the presence of certain ligands which further disperse the particles.

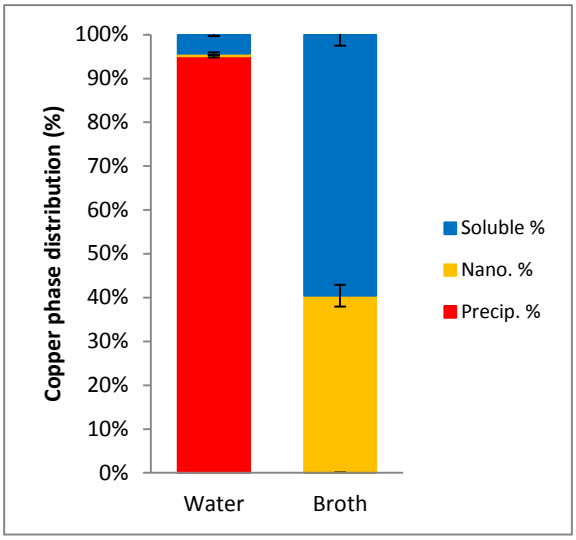

Fig. 72 - Copper phase distribution (%) resulted from the resuspension of a material obtained from a sub-micron particle containing suspension in water and broth at 4 mM.

5. Conclusion

A summary of the most important results obtained during this project is present in Table 1.

Copper oxo-hydroxide nanoparticles were produced using a different ligand, glucuronic acid, in combination with a ligand previously used, tartaric acid. The obtained nanoparticles presented the same limitations as in previous work as they partly solubilised when diluted in broth. So, in order to increase the stability of the nanoparticles, a different salt was used. The aim of this synthesis was to produce copper oxo-hydroxide nanoparticles of a different mineral phase other than paratacamite, using tartaric acid and adipic acid as ligands. This strategy proved successful and the mineral phase of the unmodified particles was copper (II) hydroxide. The mineral phase of the nanoparticles was not identified but most likely consisted of an amorphous phase related to the parent mineral, i.e. copper (II) hydroxide. However, there was not an improvement in antimicrobial activity and the nanoparticles showed to have limited action in the inhibition of the bacterial growth. Next, synthesis methods for copper oxides, which should be more stable than copper oxo-hydroxides, were developed. The method used displayed efficacy on the production of copper oxides. Although a higher stability seems to have been achieved, the nanoparticles showed to have even less antibacterial activity than the control. Nanoparticles of a different mineral phase, i.e. copper phosphates, were also obtained using citric acid as ligand. The stability of these nanoparticles was not improved but they did show higher antibacterial activity (68.6%), the best one obtained so far. However, these results are still not ideal. Next, attempts were made to produce copper nanoparticles using micelles, but only large particles were obtained. For a higher interaction between nanoparticle and the bacterium cell wall, positively charged sub-micron particles were produced using carnitine. The mineral phase of these particles was paratacamite, which may indicate that the ligand forms a coating instead of intercalate in the structure of the particles. The positive charge seems to have indeed resulted in a higher interaction between the particles and the bacterium, since that a higher antibacterial activity was also obtained (68%). However, improvements have still to be made, since that this inhibition of bacterial growth is still not completely satisfactory.

Zinc nanoparticles were produced using cysteine as ligand. It was already expected that these nanoparticles would show less antibacterial activity than copper nanoparticles, but instead of inhibiting the bacterial growth they stimulated it. Perhaps this was due to cysteine leading to a lower interaction between nanoparticle and bacterium cell wall, since that the same problem was verified for the copper oxide nanoparticles produced with cysteine. Thus, further attempts should be made on the production of zinc nanoparticles.

Throughout this project, a major problem has been the instability of the nanoparticles when diluted in broth, the bacterial culture medium used. However, it was not known if this was due to the effect of dilution or to the composition of the broth. It was possibly to clarify this by resuspending a material obtained from a sub-micron suspension in both water and broth at the same concentration. The resulting phase distribution was completely different; in water, the particles remained sub-micron, whilst in broth a fraction was further dispersed and nanoparticles were formed and there was also partial dissolution. The instability of the particles in broth may be due to the presence of certain ligands that further disperse them.

Table 1 – Summary of key results.

Suspension[2]	**Nano.**	**Mineral phase**	**Hydrodynamic size (nm)**	**Nano. fraction in broth**	**Bacterial growth inhibition**
CuOH	No	Paratacamite	-	-	-
CuOH Glr	No	-	-	-	-
CuOH TartGlr	Yes	-	1.4 ± 0.3 (pH 6) 2.6 ± 0.2 (pH 10)	46%	57.8%
CuOH (acetate)	No	Copper (II) hydroxide ($Cu(OH)_2$)	-	-	-
CuOH TartAd (acetate)	Yes	Sodium acetate hydrate ($C_2H_3NaO_2 \cdot 3H_2O$) and unidentified peaks	1.9 ± 0.4 (pH 7) 3.6 ± 0.3 (pH 8)	-	56.1%
CuO	No	Tenorite	-	-	-
CuO Tart	No	Tenorite	-	-	-
CuO Cys	Yes	-	-	61%	16.3%
$CuPO_4$	No	Copper hydrogen phosphate hydrate ($Cu_4H(PO_4)_3 \cdot 3H_2O$ and $CuHPO_4 \cdot H_2O$)	-	-	-
$CuPO_4$ Cit	Yes	Unidentified	1.0 ± 0.3 (pH 6)	49%	68.5%
CuOH SDS	No	-	>100	-	-
CuOH SDSC_{18}TAB	No	-	>>100	-	-
CuOH TartC_{18}TAB	No	-	>>100	-	-
CuOH Car	No	Paratacamite	124 ± 1.5	40%	68.1%
ZnOH	No	Unidentified	-	-	-
ZnOH Cys	Yes	Unidentified	0.90 ± 0.01	-	-7.7%

[2] This is an internal nomenclature, as the exact compositional formula was not determined.

6. Future work

Copper (II) carbonates nanoparticles were synthesised. However, they were still not tested due to the lack of time. Thus, for future work, the antibacterial activity of these nanoparticles should be tested and further characterisation should be carried out, namely, XRD characterisation.

A different approach to the general method used in this project should also be made, since that all the nanoparticles so far partly dissolve when diluted in broth. This medium can be seen as a model for what happens in physiological conditions, since its composition is more similar to the one of physiological liquids than water. Thus, this dissolution can also occur once these nanoparticles are biologically applied. In order to obtain more stable nanoparticles in broth, modifications to some of the best results obtained during this project can be made (to produce carnitine coated oxides, other oxo-phophates, etc.). Another possible strategy is to produce large particles in water and then study them when diluted in broth. Also, particles that were excluded during this project due to their large size should be further tested, since they can became nanoparticulate when diluted in broth.

Further attempts should be made on the synthesis of zinc nanoparticles and, if a satisfactory antimicrobial activity is obtained, they could be used in a mixture of copper and zinc nanoparticles, in order to obtain even higher antimicrobial activity.

To further characterize the composition of the nanoparticles that presented the best results, using other techniques, such as scanning transmission electron microscopy (STEM) and Fourier transform infra-red (FTIR).

The nanoparticles should also be tested in other strains of bacteria, since that some nanoparticles may not have great effect on *E. coli* but can have a better one in other strains. This could be done by starting to test them also on a gram-positive bacterium, such as *Pseudomonas aeruginosa*, since that till now only a gram-negative bacterium was tested. If possible, they should also be tested against bacteria with resistance to antibiotics. Subsequently, these nanoparticles could also be tested against other microorganisms.

The aim of this project is to produce safe nanoparticles that present antimicrobial activity. Thus, in case a suspension has an effective antimicrobial activity, the cytotoxicity for human cells of the nanoparticles should also be tested. This is an important step, since that the nanoparticles can be effective as antimicrobials but also prejudicial for human cells, not making them suitable for application.

7. References

1. Levy, S.B., *The challenge of antibiotic resistance.* Sci Am., 1998. **278**(3): p. 46-53.
2. Lara, H.H., et al., *Silver nanoparticles are broad-spectrum bactericidal and virucidal compounds.* Journal of Nanobiotechnology, 2011. **9**.
3. Grass, G., Rensing, C., and Solioz, M., *Metallic Copper as an Antimicrobial Surface.* Applied and Environmental Microbiology, 2011. **77**(5): p. 1541-1547.
4. Phan, T.N., et al., *Physiologic actions of zinc related to inhibition of acid and alkali production by oral streptococci in suspensions and biofilms.* Oral Microbiology and Immunology, 2004. **19**(1): p. 31-38.
5. Cooper, G.M. and Hausman, R.E., *The Cell: A Molecular Approach*2007: ASM Press.
6. Forbes, B.A., et al., *Bailey & Scott's diagnostic microbiology*2007: Elsevier Mosby.
7. Madigan, M.T., et al., *Brock biology of microorganisms*. 13 ed2010, San Francisco: Benjamin Cummings. 1152.
8. Lansing, M.P., Harley, J.P., and Klein, D.A., *Microbiology*2002: McGraw-Hill.
9. Mozes, N., Leonard, A.J. and Rouxhet, P.G., *On the Relations Between the Elemental Surface-Composition of Yeast and Bacteria and Their Charge and Hydrophobicity.* Biochimica Et Biophysica Acta, 1988. **945**(2): p. 324-334.
10. Kolter, R., Siegele, D.A., and Tormo, A., *The stationary phase of the bacterial life cycle*, in *Annual Review of Microbiology*1993, Annual Reviews Inc. {a}, P.O. Box 10139, 4139 El Camino Way, Palo Alto, California 94306, USA. p. 855-874.
11. Tortora, G.J., Funke, B.R., and Case, C.L., *Microbiology: an introduction*. 10th ed2010, San Francisco: Pearson Benjamin Cummings. 812.
12. Finkel, S.E., *Long-term survival during stationary phase: evolution and the GASP phenotype.* Nature Reviews Microbiology, 2006. **4**(2): p. 113-120.
13. Tenover, F.C., *Mechanisms of antimicrobial resistance in bacteria.* American Journal of Infection Control, 2006. **34**(5): p. S3-S10.
14. Neu, H.C., *The crisis in antibiotic resistance.* Science, 1992. **257**(5073): p. 1064-1073.
15. Alanis, A.J., *Resistance to antibiotics: Are we in the post-antibiotic era?* Archives of Medical Research, 2005. **36**(6): p. 697-705.
16. Hawkey, P.M., *The origins and molecular basis of antibiotic resistance.* British Medical Journal, 1998. **317**(7159): p. 657-660.
17. Morones, J.R., et al., *The bactericidal effect of silver nanoparticles.* Nanotechnology, 2005. **16**(10): p. 2346-2353.

18. Kim, J.S., et al., *Antimicrobial effects of silver nanoparticles.* Nanomedicine-Nanotechnology Biology and Medicine, 2007. **3**(1): p. 95-101.

19. Neal, A.L., *What can be inferred from bacterium-nanoparticle interactions about the potential consequences of environmental exposure to nanoparticles?* Ecotoxicology, 2008. **17**(5): p. 362-371.

20. Gurunathana, S., et al., *Biosynthesis, purification and characterization of silver nanoparticles using Escherichia coli.* Colloids Surf B Biointerfaces, 2009. **74**(1): p. 328-35.

21. Lok, C.N., et al., *Proteomic analysis of the mode of antibacterial action of silver nanoparticles.* Journal of Proteome Research, 2006. **5**(4): p. 916-924.

22. Jain, J., et al., *Silver Nanoparticles in Therapeutics: Development of an Antimicrobial Gel Formulation for Topical Use.* Molecular Pharmaceutics, 2009. **6**(5): p. 1388-1401.

23. Guo, T., et al., *Antibacterial effects of the Cu(II)-exchanged montmorillonite on Escherichia coli K88 and Salmonella choleraesuis.* Veterinary Microbiology, 2005. **105**(2): p. 113-122.

24. Asha Rani, P.V., et al., *Cytotoxicity and Genotoxicity of Silver Nanoparticles in Human Cells.* Acs Nano, 2009. **3**(2): p. 279-290.

25. HSE, *EH40/2005 Workplace exposure limits*. 2 ed2011, London: Health and Safety Executive.

26. Frausto Da Silva, J.J.R. and Williams, R.J.P., *The Biological Chemistry of the Elements: the Inorganic Chemistry of Life*1991, Oxford: Oxford University Press.

27. Osman, D. and Cavet, J.S., *Copper Homeostasis in Bacteria*, in *Advances in Applied Microbiology, Vol 65*2008. p. 217-247.

28. Xue, Y., et al., *Cu(I) recognition via cation-pi and methionine interactions in CusF.* Nature Chemical Biology, 2008. **4**(2): p. 107-109.

29. Borkow, G. and Gabbay, J., *Copper, An Ancient Remedy Returning to Fight Microbial, Fungal and Viral Infections.* Current Chemical Biology, 2009. **3**: p. 272-278.

30. van Hoof, N., et al., *Enhanced copper tolerance in Silene vulgaris (Moench) Garcke populations from copper mines is associated with increased transcript levels of a 2b-type metallothionein gene.* Plant Physiology, 2001. **126**(4): p. 1519-1526.

31. Capdevila, M. and Atrian, S., *Metallothionein protein evolution: a miniassay.* Journal of Biological Inorganic Chemistry, 2011. **16**(7): p. 977-989.

32. Rensing, C. and Grass, G., *Escherichia coli mechanisms of copper homeostasis in a changing environment.* Fems Microbiology Reviews, 2003. **27**(2-3): p. 197-213.

33. Kim, E.-H., et al., *Switch or Funnel: How RND-Type Transport Systems Control Periplasmic Metal Homeostasis.* Journal of Bacteriology, 2011. **193**(10): p. 2381-2387.

34. Aggett, P.J. and Harries, J.T., *Current status of zinc in health and disease states.* Archives of Disease in Childhood, 1979. **54**(12): p. 909-917.

35. Arora, P.N., et al., *Serum zinc levels in cutaneous disorders.* Medical Journal Armed Forces India, 2002. **58**(4): p. 304-306.

36. Blencowe, D.K. and Morby, A.P., *Zn(II) metabolism in prokaryotes.* Fems Microbiology Reviews, 2003. **27**(2-3): p. 291-311.

37. Dintilhac, A., et al., *Competence and virulence of Streptococcus pneumoniae: Adc and PsaA mutants exhibit a requirement for Zn and Mn resulting from inactivation of putative ABC metal permeases.* Molecular Microbiology, 1997. **25**(4): p. 727-739.

38. Outten, C.E. and O'Halloran, T.V., *Femtomolar sensitivity of metalloregulatory proteins controlling zinc homeostasis.* Science, 2001. **292**(5526): p. 2488-2492.

39. Patzer, S.I. and Hantke, K., *The zinc-responsive regulator Zur and its control of the znu gene cluster encoding the ZnuABC zinc uptake system in Escherichia coli.* Journal of Biological Chemistry, 2000. **275**(32): p. 24321-24332.

40. Elvin, C.M., Dixon, N.E., and Rosenberg, H., *Molecular cloning of the phosphate (inorganic) transport (pit) gene of Escherichia coli K12. Identification of the pit$^+$ gene product and physical mapping of the pit-gor region of the chromosome.* Molecular & General Genetics, 1986. **204**(3): p. 477-484.

41. Choudhury, R. and Srivastava, S., *Zinc resistance mechanisms in bacteria.* Current Science, 2001. **81**(7): p. 768-775.

42. O'Halloran, T.V. and Culotta, V.C., *Metallochaperones, an intracellular shuttle service for metal ions.* Journal of Biological Chemistry, 2000. **275**(33): p. 25057-25060.

43. Mergeay, M., et al., *Alcaligenes eutrophus CH34 is a facultative chemolithotroph with plasmid-bound resistance to heavy metals.* Journal of Bacteriology, 1985. **162**(1): p. 328-334.

44. Claverys, J.P., *A new family of high-affinity ABC manganese and zinc permeases.* Research in Microbiology, 2001. **152**(3-4): p. 231-243.

45. Patzer, S.I. and Hantke, K., *The ZnuABC high-affinity zinc uptake system and its regulator zur in Escherichia coli.* Molecular Microbiology, 1998. **28**(6): p. 1199-1210.

46. Liu, W.-T., *Nanoparticles and Their Biological and Environmental Applications.* Journal of Bioscience and Bioengineering, 2006. **102**(1): p. 1-7.

47. Sayes, C.M. and Warheit, D.B., *Characterization of nanomaterials for toxicity assessment.* WIREs Nanomed Nanobiotechnol 2009. **1**: p. 660-670.

48. Wuelfing, W.P., et al., *Taylor Dispersion Measurements of Monolayer Protected Clusters: A Physicochemical Determination of Nanoparticle Size.* Anal. Chem., 1999. **71**: p. 4069-4074.

49. Powers, K.W., et al., *Research Strategies for Safety Evaluation of Nanomaterials. Part VI. Characterization of Nanoscale Particles for Toxicological Evaluation.* Toxicological Sciences, 2006. **90**(2): p. 296-303.

50. Lu, A.-H., Salabas, E.L., and Schüth, F., *Magnetic Nanoparticles: Synthesis, Protection, Functionalization, and Application.* Angew. Chem. Int. Ed., 2007. **46**: p. 1222 - 1244.

51. Bailey, R.E. and Nie, S., *Alloyed Semiconductor Quantum Dots: Tuning the Optical Properties without Changing the Particle Size.* J. AM. CHEM. SOC., 2003. **125**: p. 7100-7106.

52. Thakkar, K.N., Mhatre, S.S., and Parikh, R.Y., *Biological synthesis of metallic nanoparticles.* Nanomedicine: Nanotechnology, Biology, and Medicine, 2010. **6** p. 257-262.

53. Sergeev, G.B., *Nanochemistry*2006: Elsevier.

54. Marahatta, A.B. *"Top Down" and "Bottom Up" approaches in chemistry*. 2011 [Accessed on 07/12/2011]; Available from: http://nepachem.blogspot.com/2011/01/top-down-and-bottom-up-approaches-in.html.

55. Granqvist, C.G. and Buhrman, R.A., *Ultrafine Metal Particles.* Journal of Applied Physics, 1976. **47**(5): p. 2200-2219.

56. Li, Y., et al., *Nanocrystalline Silver Particles: Synthesis, Agglomeration, and Sputtering Induced by Electron Beam.* Journal of Colloid and Interface Science, 1999. **209**(2): p. 347-349.

57. Jadhav, S., et al., *Copper Oxide Nanoparticles: Synthesis, Characterization and Their Antibacterial Activity.* J Clust Sci, 2011. **22**: p. 121-129.

58. Raffi, M., et al., *Investigations into the antibacterial behavior of copper nanoparticles against Escherichia coli.* Annals of Microbiology. **60**(1): p. 75-80.

59. Dan, Z.G., et al., *Microstructure and antibacterial properties of AISI 420 stainless steel implanted by copper ions.* Thin Solid Films, 2005. **492**(1-2): p. 93-100.

60. Hoshino, N., et al., *Bactericidal activity of catechin-copper (II) complexes against Staphylococcus aureus compared with Escherichia coli.* Letters in Applied Microbiology, 2000. **31**(3): p. 213-217.

61. Zhang, L., et al., *Investigation into the antibacterial behaviour of suspensions of ZnO nanoparticles (ZnO nanofluids).* Journal of Nanoparticle Research, 2007. **9**(3): p. 479-489.

62. Brayner, R., et al., *Toxicological impact studies based on Escherichia coli bacteria in ultrafine ZnO nanoparticles colloidal medium.* Nano Letters, 2006. **6**(4): p. 866-870.

63. Xie, Y., et al., *Antibacterial Activity and Mechanism of Action of Zinc Oxide Nanoparticles against Campylobacter jejuni.* Applied and Environmental Microbiology, 2011. **77**(7): p. 2325-2331.

64. Utamapanya, S., Klabunde, K.J., and Schlup, J.R., *Nanosclae metl-oxide particles clusters as chemical reagents - synthesis and properties of ultrahigh surface-area*

magnesium-hydroxide and magnesium-oxide. Chemistry of Materials, 1991. **3**(1): p. 175-181.

65. Alexander, M. and Dalgleish, D.G., *Dynamic light scattering techniques and their applications in food science.* Food Biophysics, 2006. **1**(1): p. 2-13.

66. *Colloidal Dynamics tutorial, The Zeta Potential.* Electroacoustics Turorials, 1999: p. 1-4.

67. Das, S.K., Das, A.R., and Guha, A.K., *Gold Nanoparticles: Microbial Synthesis and Application in Water Hygiene Management.* Langmuir, 2009. **25**(14): p. 8192-8199.

68. Butcher, D.J., *Advances in Inductively Coupled Plasma Optical Emission Spectrometry for environmental analysis.* Instrumentation Science & Technology, 2010. **38**(6): p. 458-469.

69. Manning, T.J. and Grow, W.R., *Inductively Coupled Plasma - Atomic Emission Spectrometry.* The Chemical Educator, 1997. **2**(1): p. 1-19.

70. Stanjek, H. and Hausler, W., *Basics of X-ray diffraction.* Hyperfine Interactions, 2004. **154**(1-4): p. 107-119.

71. He, B.B., *Two-dimensional X-Ray Diffraction*. 1st ed2009, New Jersey: Wiley. 426.

72. *Scintag, Inc.: Chapter 7: Basics of X-ray Diffraction.* Scintag, Inc, 1999.

73. Hasselmann, C., *Determination of minimum inhibitory concentrations (MICs) of antibacterial agents by broth dilution.* Clinical Microbiology and Infection, 2003. **9**(8): p. 7.

74. Baek, Y.W. and An, Y.J., *Microbial toxicity of metal oxide nanoparticles (CuO, NiO, ZnO, and Sb2O3) to Escherichia coli, Bacillus subtilis, and Streptococcus aureus.* Science of the Total Environment, 2011. **409**(8): p. 1603-1608.

75. Ansari, M.A., et al., *Synthesis and characterization of the antibacterial potential of ZnO nanoparticles against extended-spectrum beta-lactamases-producing Escherichia coli and Klebsiella pneumoniae isolated from a tertiary care hospital of North India.* Applied Microbiology and Biotechnology, 2012. **94**(2): p. 467-477.

76. Jones, N., et al., *Antibacterial activity of ZnO nanoparticle suspensions on a broad spectrum of microorganisms.* Fems Microbiology Letters, 2008. **279**(1): p. 71-76.

77. Bastos, C., *Master's thesis: Study of $Cu(OH)_2$ nanoparticles with antibacterial properties*, in *Department of Chemistry* 2011, University of Aveiro: Aveiro. p. 84.

78. Dawson, R.M.C., et al., *Data For Biochemical Research*, in *Dawson, R. M. C., D. C. Elliott, W. H. Elliott and K. M. Jones. Data for Biochemical Research, Third Edition. Xii+580p. Oxford University Press: New York, N.Y., USA; Oxford, England; Clarendon Press: Oxford, England. Illus*1986, Oxford Science Publications: Oxford. p. 38.

79. Gyurcsik, B. and Nagy, L., *Carbohydrates as ligands: coordination equilibria and structure of the metal complexes.* Coordination Chemistry Reviews, 2000. **203**: p. 81-149.

80. Ren, G., et al., *Characterisation of copper oxide nanoparticles for antimicrobial applications.* International Journal of Antimicrobial Agents, 2009. **33**(6): p. 587-590.

81. Studer, A.M., et al., *Nanoparticle cytotoxicity depends on intracellular solubility: Comparison of stabilized copper metal and degradable copper oxide nanoparticles.* Toxicology Letters, 2010. **197**(3): p. 169-174.

82. Singh, D.P., Ojha, A.K., and Srivastava, O.N., *Synthesis of Different Cu(OH)(2) and CuO (Nanowires, Rectangles, Seed-, Belt-, and Sheetlike) Nanostructures by Simple Wet Chemical Route.* Journal of Physical Chemistry C, 2009. **113**(9): p. 3409-3418.

83. Anthony, J.W., et al. *Handbook of Mineralogy*. 2012; Available from: http://www.handbookofmineralogy.org/.

84. Dokken, K.M., et al., *Synthesis and structural analysis of copper(II) cysteine complexes.* Inorganica Chimica Acta, 2009. **362**(2): p. 395-401.

85. Singh, I. and Bedi, R.K., *Surfactant-assisted synthesis, characterizations, and room temperature ammonia sensing mechanism of nanocrystalline CuO.* Solid State Sciences, 2011. **13**(11): p. 2011-2018.

86. Chen, Y.H. and Yeh, C.S., *Laser ablation method: use of surfactants to form the dispersed Ag nanoparticles.* Colloids and Surfaces a-Physicochemical and Engineering Aspects, 2002. **197**(1-3): p. 133-139.

87. Ahmed, A., Gajbhiye, N.S., and Joshi, A.G., *Shape controlled synthesis and characterization of Cu(2)O nanostructures assisted by composite surfactants system.* Materials Chemistry and Physics, 2011. **129**(3): p. 740-745.

88. Wilson, W.W., et al., *Status of methods for assessing bacterial cell surface charge properties based on zeta potential measurements.* Journal of Microbiological Methods, 2001. **43**(3): p. 153-164.

APPENDICES

1. ICP-OES CALIBRATION CURVE

This is an example of a calibration curve obtained during an ICP-OES analysis. The calibration consists of 8 different standards of copper or zinc, where the lowest has 0 ppm and the highest 100 ppm. In this case, during the analysis 4 calibrations were made: one at the beginning, another at the end and the other two in between.

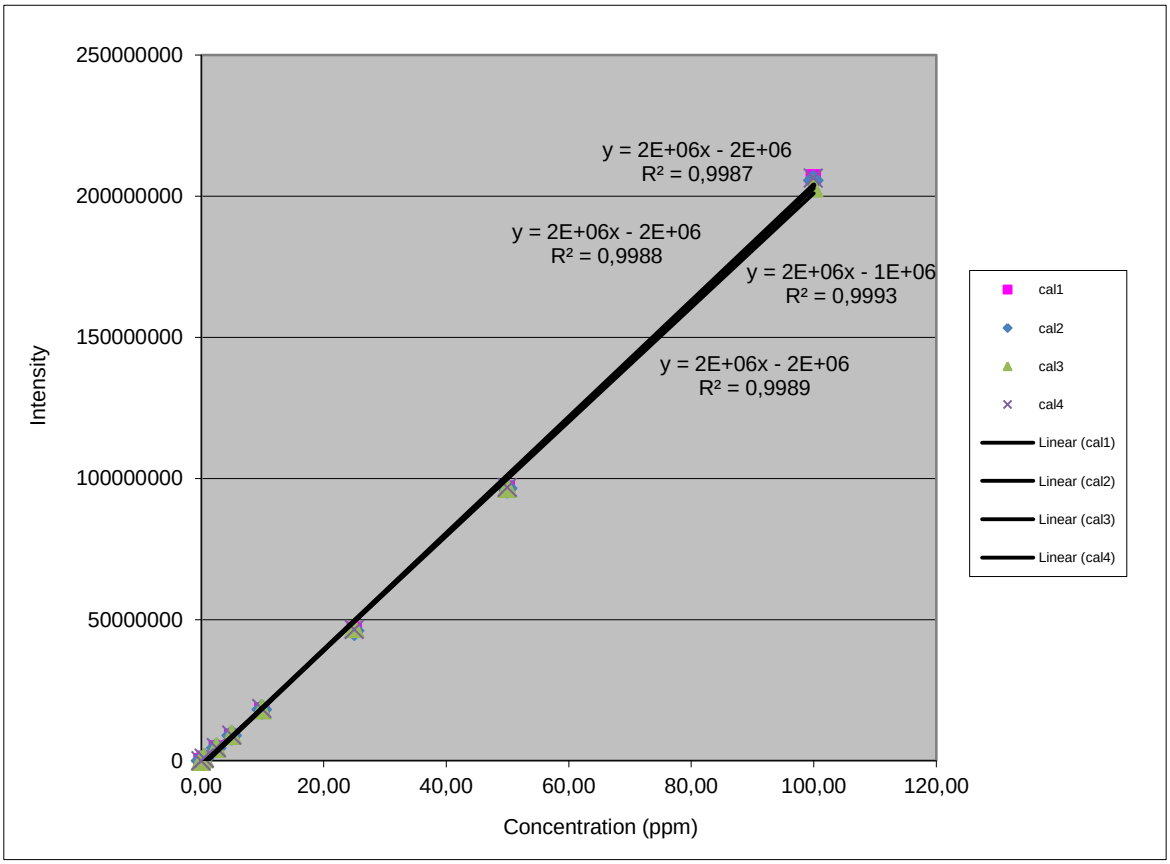

Fig. 73 – Calibration curves obtained during an analysis by ICP-OES. Four calibrations were made at different points.

2. GROWTH INHIBITION

Here an example of the results obtained for the OD variation with time for the different amounts of bacteria used is given.

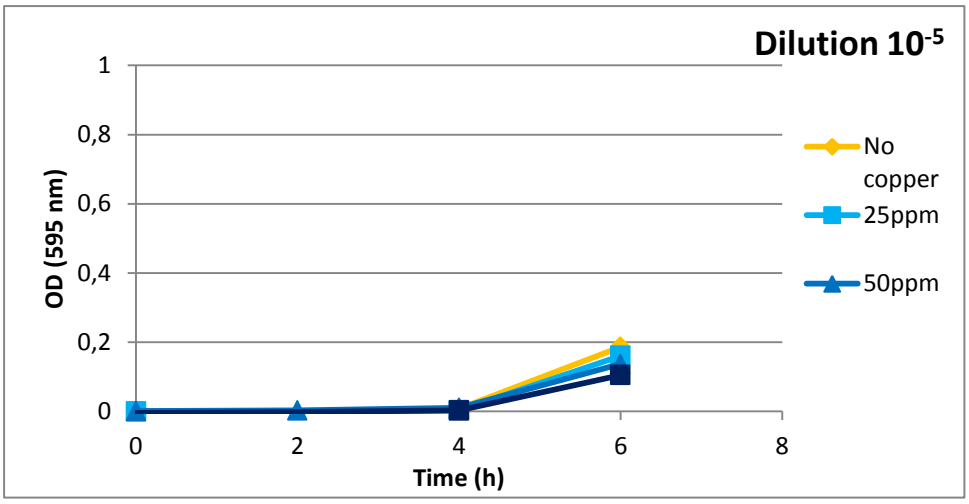

Fig. 74 – Evolution of optical density with time during a test for the determination of the antibacterial activity of copper nanoparticles with 10^{-5} bacterial dilution.

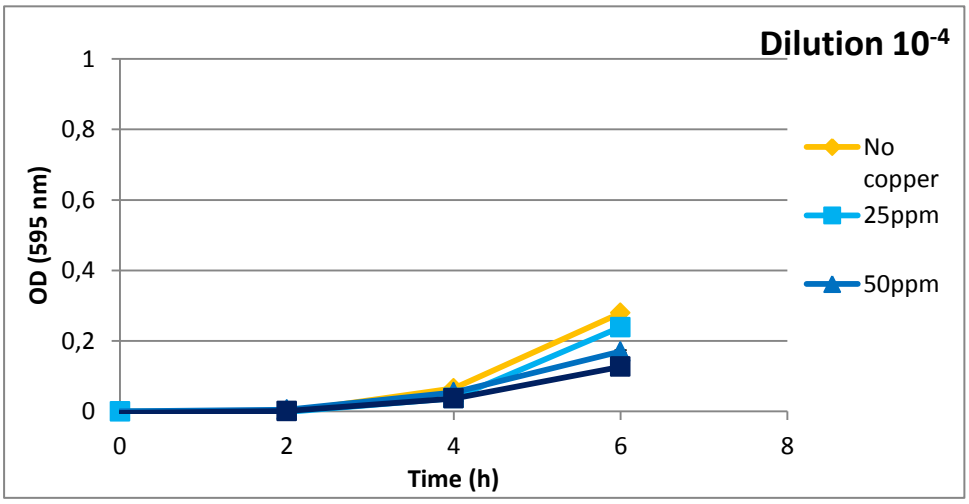

Fig. 75 - Evolution of optical density with time during a test for the determination of the antibacterial activity of copper nanoparticles with 10^{-4} bacterial dilution.

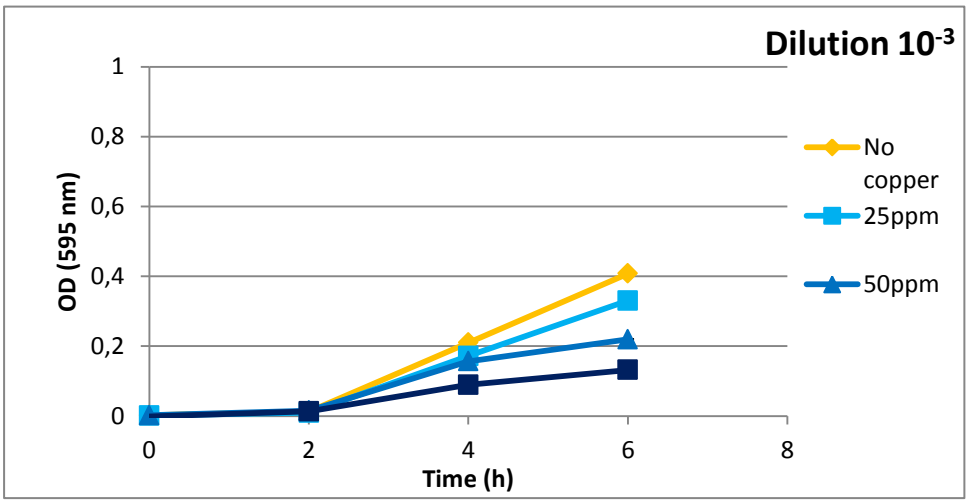

Fig. 76 - Evolution of optical density with time during a test for the determination of the antibacterial activity of copper nanoparticles with 10^{-3} bacterial dilution.

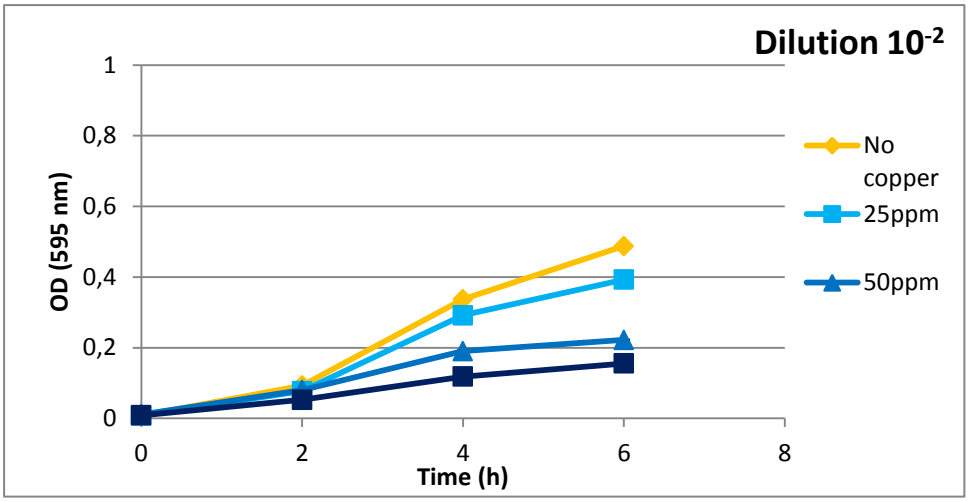

Fig. 77 - Evolution of optical density with time during a test for the determination of the antibacterial activity of copper nanoparticles with 10^{-2} bacterial dilution.

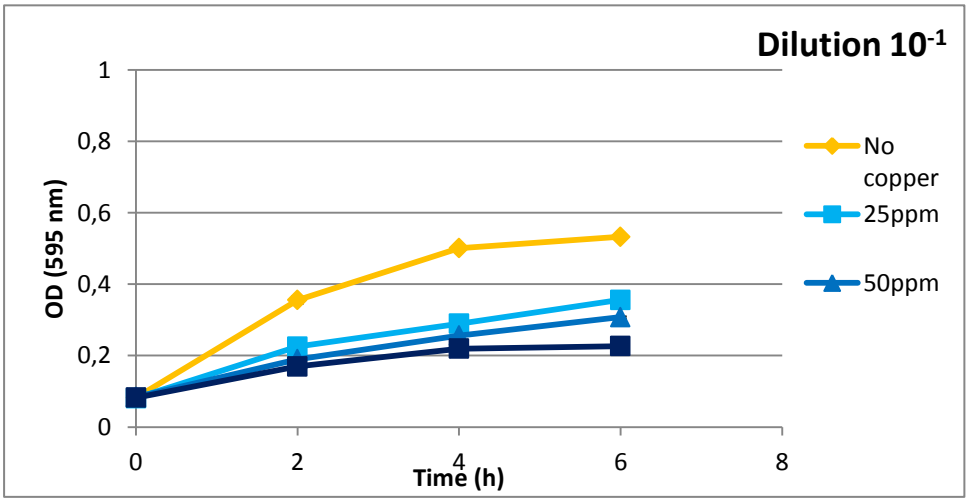

Fig. 78 - Evolution of optical density with time during a test for the determination of the antibacterial activity of copper nanoparticles with 10^{-1} bacterial dilution.